



EUROPEAN
COMMISSION

Community research

PAMINA

Performance Assessment Methodologies in Application to Guide the Development of the Safety Case

(Contract Number: **FP6-036404**)



Uncertainties Associated with Modelling the Consequences of Gas DELIVERABLE (D-N°: **D2.2.B.2**)

Author(s):

Simon Norris
Nuclear Decommissioning Authority

Date of issue of this report : **26/03/2008**

Start date of project : **01/10/2006**

Duration : **36 Months**

Project co-funded by the European Commission under the Euratom Research and Training Programme on Nuclear Energy within the Sixth Framework Programme (2002-2006)		
Dissemination Level		
PU	Public	X
RE	Restricted to a group specified by the partners of the [PAMINA] project	
CO	Confidential, only for partners of the [PAMINA] project	



Foreword

The work presented in this report was developed within the Integrated Project PAMINA: **P**erformance **A**ssessment **M**ethodologies **I**N **A**pplication to Guide the Development of the Safety Case. This project is part of the Sixth Framework Programme of the European Commission. It brings together 25 organisations from ten European countries and one EC Joint Research Centre in order to improve and harmonise methodologies and tools for demonstrating the safety of deep geological disposal of long-lived radioactive waste for different waste types, repository designs and geological environments. The results will be of interest to national waste management organisations, regulators and lay stakeholders.

The work is organised in four Research and Technology Development Components (RTDCs) and one additional component dealing with knowledge management and dissemination of knowledge:

- In RTDC 1 the aim is to evaluate the state of the art of methodologies and approaches needed for assessing the safety of deep geological disposal, on the basis of comprehensive review of international practice. This work includes the identification of any deficiencies in methods and tools.
- In RTDC 2 the aim is to establish a framework and methodology for the treatment of uncertainty during PA and safety case development. Guidance on, and examples of, good practice will be provided on the communication and treatment of different types of uncertainty, spatial variability, the development of probabilistic safety assessment tools, and techniques for sensitivity and uncertainty analysis.
- In RTDC 3 the aim is to develop methodologies and tools for integrated PA for various geological disposal concepts. This work includes the development of PA scenarios, of the PA approach to gas migration processes, of the PA approach to radionuclide source term modelling, and of safety and performance indicators.
- In RTDC 4 the aim is to conduct several benchmark exercises on specific processes, in which quantitative comparisons are made between approaches that rely on simplifying assumptions and models, and those that rely on complex models that take into account a more complete process conceptualization in space and time.

The work presented in this report was performed in the scope of RTDC 2.

All PAMINA reports can be downloaded from <http://www.ip-pamina.eu>.



PAMINA Task 2.2.B Model Uncertainty
Topic 2 Uncertainties Associated with Modelling the
Consequences of Gas

Simon Norris
Nuclear Decommissioning Authority
March 2008

Executive Summary

This report considers the generation of gases from waste emplaced in a deep geological disposal facility, and the consequences of such repository-derived gas. Uncertainty in gas generation and gas migration are scoped in a reference case and variant scenarios. It is noted that the treatment of uncertainty in groundwater pathway assessment studies is generally at a more mature position than the treatment of uncertainty in the assessment of the consequences of repository-derived gas. Studies such as this are therefore part of a staged approach to further develop understanding regarding the treatment of uncertainty for gas issues in the safety case, and to identify key aspects affecting the consequences of repository-derived gas to act as a focus both for further research activities, and in any future site characterisation programme.

The consequences of gas are considered for both a generic geology and a 'real' geology, allowing inferences to be drawn on how the representation of geology affects the outcome of the gas modelling undertaken.

For the generic fractured crystalline host rock studied, over-pressurisation effects are predicted to be insignificant. For the argillaceous host rock, on the other hand, the pressure builds up substantially. (There is, however, uncertainty in the mechanism of gas transport in low-permeability argillaceous media, and the applicability of porous-medium flow models for simulating gas migration in these materials.)

On the basis of work reported in this study, the following are recommended to be the key processes / key model parameters affecting the consequences of repository-derived gas that should be further investigated, and should be a significant focus of any future site characterisation programme. Note that these recommendations are made on the basis of this study, which itself has significant focus on the Sellafield dataset; such a study would therefore need to be repeated on a site-specific basis, as the site-specific key processes / key model parameters could differ from those noted in this study.

- The details of gas migration are very site-specific. The path followed by free gas depends on the geometry of the various rock units and on their hydrogeological properties (e.g. permeability and saturation functions). Migrating gas will dissolve in the groundwater, and the magnitude of the groundwater flows in the more permeable rock units is important in determining whether free gas breaks through at the surface. The repository design and generation rate of gas may also play a role in determining whether there is breakthrough. Breakthrough does not depend linearly on these factors, but there are threshold effects.
- Perhaps the most important of the assumptions affecting the behaviour of gas is the extent to which free gas will contact the groundwater within the rock volume represented by a grid block (i.e. the extent of 'viscous fingering'). If it is assumed that there is minimal contact (i.e. simulated by reducing the gas solubility to only 1% of its true value), then a free gas pathway forms. The effect of the geosphere is to introduce a time lag in, but not a reduction in the magnitude of, the initial release rate of gas compared with the release assuming instantaneous transport through the geosphere. Eventually, the free gas pathway collapses, to be replaced by dissolved gas migrating in the groundwater. If it is assumed that the free gas which migrates into a grid block contacts all of the groundwater within the grid block, then no free gas is released at the surface of the model. Only gas dissolved in the groundwater is discharged to the biosphere. The travel time for this case is longer than for the free gas pathway.
- Certain geosphere strata could affect gas migration, in a site-specific scenario, to a greater or lesser extent than other geosphere strata (this is relevant both to the geological disposal facility host rock and to the overburden). For strata that are considered key with regard to effects on gas migration, it is important that this is explicitly recognised in the development of a site-specific safety case, and that appropriate co-ordinated research, assessment and site characterisation studies focus on developing an enhanced understanding of the properties of such strata in order to better understand how associated gas migration could occur.

- Low permeability units may have a significant effect on site-specific gas migration. Key uncertainties to be addressed could consider the potential for gas migrating from depth to leak into this low permeability unit, the potential impact of capillary forces in retarding this migration, and the potential effects of a fault cutting this unit which can draw off a significant fraction of the migrating plume of free gas.
- The repository design and generation rate of gas may also play a role in determining whether there is breakthrough of free gas at the surface. Breakthrough does not depend linearly on these factors, but there are threshold effects.

Contents

1	Introduction	1
1.1	Treatment of Uncertainty	1
1.2	Consideration of Uncertainty in Assessment of Consequences of Repository-derived Gas	2
1.3	Acknowledgement	3
2	Gas Generation	4
2.1	Scenarios	4
2.1.1	Reference case	5
2.1.2	Varying Temperature case	5
2.1.3	Exclusion of Carbonation case	6
2.1.4	Small Organic Molecules case	6
2.1.5	Operational case	6
2.2	Results	7
2.2.1	Reference case	8
2.2.2	Varying Temperature case	13
2.2.3	Exclusion of Carbonation case	16
2.2.4	Small Organic Molecules case	19
2.2.5	Operational case	22
2.3	Solid-state Diffusion of Tritium from Steel Wastes	25
2.4	Summary of Gas Generation Calculations	26
3	Gas Migration	28
3.1	Gas Migration from a Repository in a Fractured Crystalline Host Rock	28
3.1.1	Model	28
3.1.2	Results	30
3.2	Gas Migration from a Repository in an Argillaceous Host Rock	33
3.2.1	Model	33
3.2.2	Results	35
3.3	Two-dimensional Model of Gas Migration from a Repository	36
3.3.1	Model domain	36
3.3.2	Hydrogeological properties	36
3.3.3	Two-phase flow properties	42
3.3.4	Miscellaneous properties	44
3.3.5	Results	47
3.4	Summary of Gas Migration Calculations	72
4	Conclusions	75
4.1	Gas Generation	75
4.2	Gas Migration	76
4.3	Identification of Key Processes and Model Parameters Affecting the Consequences of Repository-derived Gas	76
5	References	78

1 Introduction

1.1 Treatment of Uncertainty

A key driver for a deep geological repository as an option for the long-term management of radioactive waste, is to remove the large uncertainty associated with leaving the waste accessible to humans at the surface over very long timescales. There is considerable confidence that a well-chosen geological site will be relatively stable for a very long time into the future and provide effective containment of the radioactive material.

However, it is also important to recognise that there are substantial uncertainties associated with processes operating in a radioactive waste repository system on a timescale of hundreds of thousands of years, and these uncertainties require appropriate treatment in performance assessments in support of such a facility. In a repository system there are a number of different areas in which uncertainty may influence a performance assessment:

- uncertainty in data;
- uncertainty arising from the use of conceptual models;
- uncertainty in future states of the system; and
- uncertainty in future human behaviour.

For a post-closure performance assessment, there may be substantial uncertainty associated with the future of the repository system. The Nuclear Decommissioning Authority (NDA) has developed a methodology for addressing this uncertainty in a systematic way, based on the analysis of FEPs and development of scenarios which are then addressed in detail in a performance assessment.

For a given scenario, strategies for handling uncertainty tend to fall into the following broad categories:

1. Demonstrating that the uncertainty is not important to safety because, for example, safety is dominated by other processes.
2. Addressing the uncertainty explicitly, usually using probabilistic techniques, and showing that the expected situation is acceptable.
3. Bounding the uncertainty and showing that even the bounding case gives acceptable safety.
4. Ruling out the uncertainty, usually on the grounds of very low probability of occurrence, or because other consequences, were the uncertain event to happen, would far outweigh concerns over the repository performance.
5. Agreeing a stylised approach for handling a specific uncertainty.

When assessing the performance of a radioactive waste repository over very long timescales, there are acknowledged to be uncertainties in many areas. However, not all the uncertainties will be significant and, by using a combination of the above strategies for handling such uncertainties, it is possible to build confidence in a safety case for a repository. A rigorous treatment of the uncertainty associated with performance assessment is essential to provide confidence in the validity of performance estimates and will be needed to satisfy regulatory scrutiny. The identification and analysis of those uncertainties to which the performance of the concept is most sensitive is essential and helps to identify areas where further data acquisition and development in scientific understanding are needed.

More detail about the uncertainties that arise in the post-closure performance assessment and the ways in which they are managed is given in Reference [1].

A combination of the strategies listed above has been used in NDA performance assessments. For the groundwater pathway a Probabilistic Safety Assessment (PSA) approach is adopted in which many simulations are carried out, each with many uncertain parameter values (for example solubilities and

sorption coefficients) sampled from probability density functions (PDFs) that represent the uncertainty in the parameters. (A PDF describes the relative likelihood that a parameter will have different values due to the uncertainty about its value.) The main performance measure is the mean risk from the simulations. The PDFs are elicited by suitably qualified and experienced experts on the basis of various data (see reference [2]). In certain cases, where there is a large degree of uncertainty, a cautious approach is taken in developing a conceptual model, such that the risk (or other performance measure) would be over- rather than under-estimated.

The PSA approach may be supplemented by other strategies such as deterministic sensitivity studies and 'what if' calculations, which are also of value in communicating a performance assessment. For example, in Nirex 97, in addition to the probabilistic modelling, deterministic calculations are also presented to explain certain processes. A section is also presented in which simple analytic expressions, rather than complex numerical models, are used to provide insight into the results of the complex models, and provide a simple understanding of which parameter values and processes have a key impact on risk. Confidence can be provided in the results of the complex numerical models by showing that similar results may be obtained on the basis of very simple models.

Some uncertainties cannot by their nature be treated within an assessment and this leads to potential biases. In the Nirex 97 assessment the following definition of bias was adopted:

'A bias is a significant systematic deviation from scientific expectation, introduced into the results of a performance assessment through decisions involved in the development of conceptual, mathematical or numerical models or data, or in the interpretation of results.' [3]

Examples might include bias resulting from using time-independent parameters and from not taking credit for physical containment by waste packages. It is important that in reporting a performance assessment, any such biases are acknowledged and their possible impact discussed. An audit of the most significant biases, based on this definition, was presented for each of the main areas of analysis in Nirex 97.

The issue of uncertainty is not unique to a deep geological repository option. To put the difficulties associated with evaluation of post-closure performance assessment into perspective, there are also significant uncertainties associated with other waste management options. For example, indefinite storage of waste under institutional control has large uncertainties associated with the possibility of societal breakdown and lack of financial provisions. These uncertainties will become larger the further into the future such institutional control is required.

1.2 Consideration of Uncertainty in Assessment of Consequences of Repository-derived Gas

This report considers the generation of gases from waste emplaced in a deep geological disposal facility, and the consequences of such repository-derived gas. The disposal concept considered has been developed in the UK, and is a reference concept for unshielded intermediate-level waste (UILW) and shielded intermediate-level / low-level waste (SILW / LLW) that can be used for demonstrating viability and to support the provision of waste packaging advice¹. In this concept, waste containers would be placed in underground disposal vaults. Eventually, a cement backfill would be placed around the disposed wastes, and the disposal facility would then be sealed off from the accessible environment and closed. The consequences of gas are considered for both a generic geology and a 'real' geology, allowing inferences to be drawn on how the representation of geology affects the outcome of the gas modelling undertaken.

¹ In the NDA forward programme, an evaluation of options as part of the geological disposal facility development programme will be undertaken; decisions regarding e.g. a preferred concept will only be made at appropriate points in time.

Uncertainty in gas generation and gas migration are scoped in reference case and variant scenarios, addressing some (but not all) of the strategies for handling uncertainty noted in Section 1.1. It is noted that the treatment of uncertainty in NDA groundwater pathway assessment studies is at a more mature position than the treatment of uncertainty in the assessment of the consequences of repository-derived gas. Studies such as this are therefore part of a staged approach by the NDA to further develop its level of understanding regarding the treatment of uncertainty for gas issues in the safety case, and to identify key aspects affecting the consequences of repository-derived gas to act as a focus both for further research activities, and in any future site characterisation programme.

Uncertainty in the rate of gas generation is scoped in Section 2 by the consideration of a reference case and four variant case scenarios designed to address a range of alternative assumptions that could affect gas generation in a 'real' repository environment. These scenarios all consider UK intermediate and some low-level wastes only.

In Section 3, the reference case gas generation rate from Section 2 is used as input to a series of geosphere gas migration calculations. Calculations of repository over-pressurisation and gas surface breakthrough time for two one-dimensional (generic) geologies – one corresponding to a hard fractured host rock, the other to an argillaceous host rock – are presented. Two-dimensional gas migration modelling is also reported, for an example site-specific study. This addresses both a reference case scenario, and variant scenarios to investigate the sensitivity of model output to selected variation of input parameter.

Section 4 discusses the outcome of Sections 2 and 3, and draws some simple conclusions that could inform future assessment, research and any site characterisation studies. Key aspects affecting gas migration are noted - further study of these could benefit NDA's understanding of the consequences of repository-derived gas by enhancing the level of understanding, and by reducing uncertainty in, for example, parameter ranges to be considered in subsequent assessment studies.

1.3 Acknowledgement

This report draws significant input from the following studies, which were produced under contract to the NDA:

Update of the GPA(03 Assessment of the Consequences of Gas, Serco report SA/ENV-0948 Issue 1, Andrew Hoch, Mike Thorne, Ben Swift and Fiona Bate, March 2007.

On Gas Migration Beneath a Dipping Low Permeability Horizon with Leakage, Andrew Woods & Adrian Farcas, BP Institute for Multiphase Flow, University of Cambridge, November 2007.

2 Gas Generation

In this section, uncertainty in the rate of gas generation is scoped by the consideration of a reference case and four variant case scenarios designed to address a range of alternative assumptions that could affect gas generation in a 'real' repository environment. These scenarios all consider UK intermediate and some low-level wastes only.

The calculations reported here were undertaken using Version 5 of the SMOGG program. Details of the SMOGG program are provided in References [4, 5], including the theoretical basis of the model and its mode of operation.

Five scenarios, which are described in Section 2.1, have been considered:

- A Reference case;
- A Varying Temperature case;
- An Exclusion of Carbonation case;
- A Small Organic Molecules case; and
- An Operational case.

For each scenario, there are two vault types, one for unshielded ILW and one for shielded ILW and LLW. There are therefore ten sets of basic results. Each of these consists of the evolution with time of the rates of production of the non-radioactive gases (hydrogen, carbon dioxide, and methane), and the rates of production of the radioactive gases ($^3\text{H}^1\text{H}$, $^{14}\text{CO}_2$, $^{14}\text{CH}_4$ and ^{222}Rn). Graphs of the results are reproduced in the following subsections.

2.1 Scenarios

In all scenarios the emplacement of wastes is assumed to occur over 50 years, from 2040 to 2090. In practice, the emplacement will continue on a more or less continuous basis. For computational purposes, it is assumed that the waste is emplaced in batches. One-fiftieth of each of the non-radioactive and the radioactive inventories is emplaced each year.

The radioactive component of the inventory is decay-corrected to 2040 (i.e. 2040 is assumed to be the time at which the waste is generated, with the inventory at 2040 calculated so that radioactive decay results in the correct inventory being present at later times, when the waste actually arises). For each emplacement, the radioactive content is reduced for the decay that would have occurred since 2040. It is assumed that no degradation of the non-radioactive wastes occurs prior to its emplacement in the repository.

Prior to repository closure, the gases that are generated will be released into the ventilated vault atmosphere. Hydrogen, including tritium, and methane, including any ^{14}C -labelled methane, will be released into the vault atmosphere at the rate at which they are being generated (although little methane is expected under the predominantly aerobic conditions assumed prior to closure). Carbon dioxide may be immobilised by reaction with the grout in some waste containers, but its release prior to closure is not an issue of concern. Radon has a short half-life, so it is expected that radioactive decay within waste packages will result in release at a lower rate than that at which it is being generated. This can be accounted for by the application of an empirical 'hold-up' factor.

The calculations of gas generation rates post-closure were carried out for five scenarios.

2.1.1 Reference case

The Reference case scenario is defined in Table 2.1.

Table 2.1 Reference Case Scenario

Stage	Time	Temperature (°C)	Water availability	Oxygen availability
Emplacement	2040 – 2090	35	Limited	Aerobic
Care and maintenance	2090 – 2140	35	Limited	Aerobic
Backfilling and closure	2140 – 2150	35	Limited	Aerobic
Post-closure	2150 – ∞	35	All pore space resaturates over 5 years	Oxygen present at closure is consumed (or is released after 5 years)

For this calculation, a temperature of 35°C is applied throughout the operational and post-closure phases. Metals are expected to experience a higher temperature (and therefore higher corrosion rates) during the backfilling period before closure, but the gas generated in consequence would not contribute to the post-closure risk.

Initially no water is associated with the waste. This restricts the gas generating reactions during the operational phase, and so maximizes the post-closure inventory of gas generating materials (mainly the Magnox and aluminium), which is conservative for calculating gas generation rates after repository closure. (The Generic Documents [6] assumed the waste packages were initially saturated. This assumption is not conservative for post-closure calculations as it allows additional corrosion of the reactive metals during the operational phase, leaving less remaining post-closure.)

It is assumed that gas can exchange with the atmosphere until the end of the backfilling period, and therefore the environment in the waste packages will remain aerobic until then. In practice, anaerobic niches are expected to form during this period, at least within some types of waste package. The scenario assumes that these niches occupy only a small fraction of the waste package volumes and thus have only a small effect on the overall gas generation. However, this is an assumption that warrants further examination.

As has already been mentioned, carbon dioxide, including ¹⁴C-labelled carbon dioxide, is expected to react with cement and not to escape from the repository post-closure. A variant (see Section 2.1.3) considers the possibility that this carbonation reaction does not occur.

2.1.2 Varying Temperature case

The Varying Temperature case scenario corresponds closely to the Base-case scenario and Variant 2001 inventory in the Generic Documents [6]. The temperatures assumed for each stage of repository evolution represent average vault temperatures, and are based on an interpretation by NDA of studies it had commissioned. The scenario is defined in Table 2.2.

Table 2.2 Varying Temperature Case Scenario

Stage	Time	Temperature (°C)	Water availability	Oxygen availability
Emplacement	2040 – 2090	35	Limited	Aerobic
Care and maintenance	2090 – 2140	35	Limited	Aerobic
Backfilling and closure	2140 – 2150	80 for 5 years, 50 for 5 years	Limited	Aerobic
Post-closure	2150 – ∞	50 for 100 years, 35 subsequently	All pore space resaturates over 5 years	Oxygen present at closure is consumed (or is released after 5 years)

2.1.3 Exclusion of Carbonation case

This variant of the Reference case allows carbon dioxide and hydrogen to combine forming methane, in contrast to the other variants in which this reaction is inhibited. Inhibition is assumed to be caused by the preferential reaction of the carbon dioxide with the cementitious materials present.

The preferential reaction of carbon dioxide with cement rather than with hydrogen (thereby preventing the formation of methane) is significant because any ¹⁴C-labelled methane that would otherwise be formed would not be trapped by the carbonation reaction. The effect of the carbonation reaction in preventing ¹⁴C release is a topic requiring further investigation, but the scenarios considered here provide a reasonable representation of the range of outcomes.

2.1.4 Small Organic Molecules case

GE Healthcare waste streams 1A07 and 1B05 include a significant inventory of ¹⁴C in small organic molecules. Current advice is that these waste streams will be processed to form inorganic materials, and so the Reference case did not model ¹⁴C release from these wastes.

This variant does include these waste streams, and in particular models ¹⁴C release from the small organic molecules.

2.1.5 Operational case

This variant was designed to be more realistic for the operational phase.

In the Operational case, the initial mass of water is calculated from the amount of water that would fill the pore space of the conditioned wastes. However, to ensure correct accounting of this water, the UILW wastes and the SILW/LLW wastes are split into Magnox, aluminium and other wastes. Splitting the wastes in this way means that the consumption of water by the reactive metals can be modelled more correctly and will not impact on the generation of gas by the other wastes. For the Magnox and aluminium wastes, the pore space of the conditioned waste and its associated water are calculated by assuming a conditioning factor of 4.

The scenario is defined in Table 2.3.

Table 2.3 Operational Case Scenario

Stage	Time	Temperature (°C)	Water availability	Oxygen availability
Emplacement	2040 – 2090	35	Pore space in waste packages initially water filled	Aerobic
Care and maintenance	2090 – 2140	35	Continues	Aerobic
Backfilling and closure	2140 – 2150	35	Continues	Aerobic
Post-closure	2150 – ∞	35	All pore space resaturates over 5 years	Oxygen present at closure is consumed (or is released after 5 years)

2.2 Results

The main results of the gas generation calculations are shown in Figures 2.1–10. For each of the five scenarios, there are two figures: one showing gas generation from the UILW vaults, and the other showing gas generation from the SILW/LLW vaults. Each figure comprises three graphs, which are plots of the gas generation on three different timescales.

Some general comments on these graphs are as follows:

- Each graph shows the generation rate of the significant bulk gases (i.e. hydrogen, carbon dioxide and methane).
- In all cases except the Exclusion of Carbonation case, any carbon dioxide produced is assumed to react with the grout or backfill and so is not released as a gas.
- The scale used to plot the generation rate of the bulk gases is generally $10^{-2} - 10^6 \text{ m}^3$ at $\text{STP}^2 \text{ a}^{-1}$ for the UILW vaults, and is $10^{-4} - 10^3 \text{ m}^3$ at $\text{STP} \text{ a}^{-1}$ for the SILW/LLW vaults.
- In addition, each graph shows the release rate of the active gases (i.e. tritium, ^{14}C -labelled carbon dioxide and methane, and ^{222}Rn).
- The release rate of tritium has a declining trend due to radioactive decay. The half-life of tritium is 12.33 years, and therefore at 2240 AD the tritium inventory will have decayed by nearly five orders of magnitude.
- The release rate of ^{14}C also decreases due to radioactive decay. The half-life of ^{14}C is 5730 years, and therefore at 100000 AD the ^{14}C inventory will have decayed by slightly more than five orders of magnitude.

² Standard Temperature and Pressure, defined as 10^5 Pa and 273.15K .

- The evolution of the release rate of ^{222}Rn (half-life 3.825 days) is complex. ^{222}Rn is produced by the radioactive decay of ^{226}Ra . Because the half-life of ^{226}Ra is 1600 years, ^{222}Rn will continue to be produced well beyond the operational phase of the disposal facility. In the longer term, ^{222}Rn will be generated also by ^{226}Ra that arises from the decay of ^{238}U (half-life $4.47 \cdot 10^9$ years) either disposed of in the repository or occurring naturally in the surrounding rock. The time required to achieve secular equilibrium between the parent and the ^{226}Ra progeny is determined by the half-lives of the various radionuclides in the chain, and is very long. Hence, waste materials, such as fuel residues from which ^{226}Ra will have been separated, typically are not at secular equilibrium. As a result, the maximum ^{226}Ra inventory, and therefore the maximum release rate of ^{222}Rn , is predicted to occur about 100000 years after closure of the disposal facility.
- The release rate of ^{222}Rn should be scaled by a 'hold-up' factor, which is just the ratio of ^{222}Rn escaping from the container to that produced by decay of ^{226}Ra . A substantial hold-up factor of 0.002 was used in the Generic Documents [6]. Recent research [7] suggests it could be difficult to justify this value, and a more likely value might be about 0.1.
- The scale used to plot the generation rate of the active gases is $10^{-4} - 10^4 \text{ TBq a}^{-1}$ for the UILW vaults, and is $10^{-6} - 10^1 \text{ TBq a}^{-1}$ for the SILW/LLW vaults.

The subsections below discuss the individual results for each of the scenarios.

2.2.1 Reference case

The results for the Reference case are shown in Figures 2.1–2.

Consider the gas production rates from the UILW vaults. The following sequence of main events explains the way that the gas production rates vary with time:

- The inventory peaks at 2090 AD, when all of the wastes have been emplaced.
- Before closure, hydrogen is formed from radiolysis of polymers, cellulose and oils in the inventory. Uranium and the steels corrode aerobically releasing both tritium and ^{14}C in methane. ^{14}C in methane is formed also from radiolysis of small organic molecules and from degradation of graphite. Uranium is the major contributor to the generation rate of the active gases.
- The repository is closed at 2150 AD and starts to resaturate. As a result, aluminium and Magnox start to corrode at a high rate generating hydrogen and tritium, and also tritium from the tritiated water that is present in this vault type. The latter process is the biggest contributor to the generation rate of tritium. In the case of Magnox, corrosion also produces ^{14}C in methane, and this is the dominant process for forming this active gas.
- At about 2155 AD the facility is calculated to resaturate and conditions become anaerobic. As a result, uranium, steels and Zircaloy start to corrode anaerobically producing hydrogen and tritium; tritium is also produced from the tritiated water. Mild steel and Zircaloy experience a short period of rapid (acute) corrosion, which causes a spike in the generation rate of hydrogen. Uranium corrodes more rapidly anaerobically than aerobically, and so this metal's contribution to the generation rate of the active gases increases. However, corrosion of the Magnox plates continues to dominate the generation rate of ^{14}C in methane.
- The uranium corrodes so quickly that it is consumed within a few years of repository closure (i.e. by 2159 AD).
- The Magnox plates are all corroded at 2164 AD, closely followed by the Magnox spheres at 2166 AD. As a result, the production rates of hydrogen and tritium decrease. In the case of tritium, this is actually because the consumption rate of water, including tritiated water, falls. There is also a dramatic decrease in the generation rate of ^{14}C in methane. From this point on stainless steel

becomes the dominant source of ^{14}C in methane; corrosion of mild steel, radiolysis of small organic molecules and degradation of graphite are minor contributors.

- The aluminium plates are all corroded at 2174 AD, causing another decrease in the production rates of hydrogen and tritium. The consumption rate of tritiated water falls as well, and as a result radiolysis of water becomes the biggest contributor to the generation rate of tritium.
- Thereafter, the various gas generating processes (i.e. corrosion of steels and Zircaloy, degradation of organic materials and radiolysis) continue at a slow rate until the end of the calculation.
- The only other noteworthy feature of the plots is at 4940 AD, when methane starts to be generated. This corresponds to the point when sulphate runs out (nitrate was all consumed by 4240 AD), and so methane can start to form. Initially methane is generated at a high rate from the small organic molecules (iso-saccharinic acid, ISA) that are present, and ^{14}C in methane is generated at a rate that is just less than that from corrosion of stainless steel. When these small organic molecules have been consumed, the new rate-limiting step for the formation of methane is the mid-chain scission of stopped cellulose. Methane continues to form, but at a much slower rate.

The behaviour seen for the gas production rate from the SILW/LLW vaults is analogous to that discussed above for the UILW vaults, except that there is no inventory of readily degradable small molecules (and only a small inventory of cellulose), so the contribution from methane production to the overall gas generation rate is much less significant for this vault type.

- The repository inventory peaks at 2090 AD, when all of the wastes have been emplaced.
- Before closure, hydrogen is formed from radiolysis of polymers, cellulose and oils in the inventory. The steels corrode aerobically releasing both tritium and ^{14}C in methane. ^{14}C in methane is formed also from degradation of graphite, and this is the dominant process for forming this active gas.
- The repository is closed at 2150 AD and starts to resaturate. As a result, aluminium and Magnox start to corrode at a high rate generating hydrogen.
- At about 2155 AD, the repository resaturates and goes anaerobic. As a result, the steels and Zircaloy start to corrode anaerobically producing hydrogen. Mild steel and Zircaloy experience a short period of rapid (acute) corrosion, which causes a spike in the generation rate of hydrogen. In the case of the steels, corrosion also generates tritium and ^{14}C in methane. The anaerobic corrosion rate of the steels is less than the aerobic corrosion rate, and so the production rate of tritium decreases.
- The Magnox plates are all corroded at 2164 AD. As a result the production rate of hydrogen decreases.
- The aluminium plates are all corroded at 2176 AD, causing another decrease in the production rate of hydrogen.
- Thereafter the various gas generating processes (i.e. corrosion of steels and Zircaloy, degradation of organic materials and radiolysis) continue at a slow rate until the end of the calculation.
- The only other noteworthy feature of the plots is at 2740 AD, when methane starts to be generated. This corresponds to the point when sulphate runs out (nitrate was all consumed by 2440 AD), and so methane can start to form. Initially methane is generated at a high rate from the small organic molecules (ISA) that have been produced. When these small organic molecules have been consumed, the new rate-limiting step for the formation of methane is the mid-chain scission of stopped cellulose. Methane continues to form, but at a much slower rate.

- Finally, at 13040 AD degradation of graphite becomes less important than corrosion of the steels for forming ^{14}C in methane.

Similar remarks can be made for all the other scenarios. The following subsections explain only the differences between the results for the relevant scenario and for the Reference case.

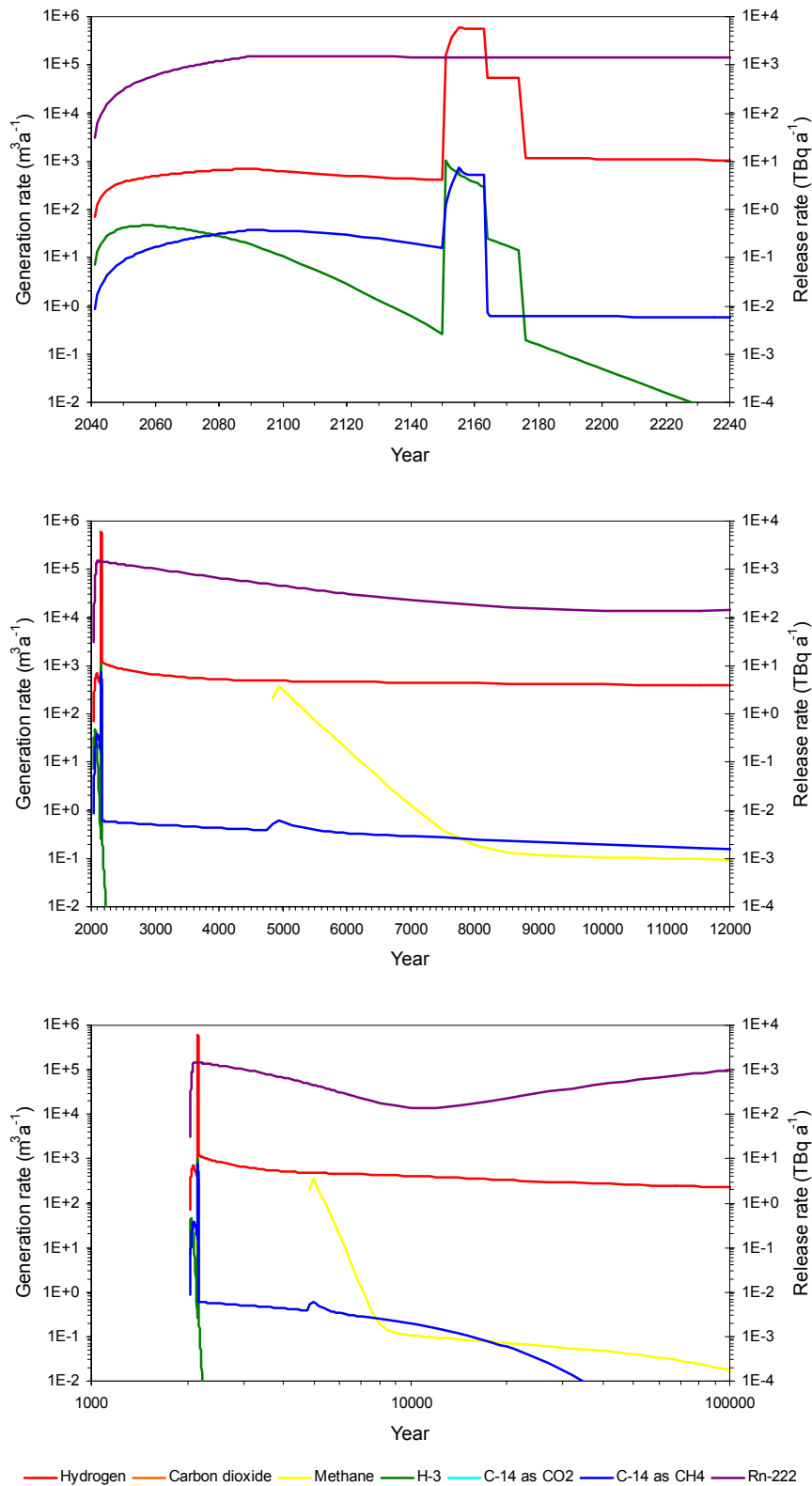


Figure 2.1 Gas generation from the 2004 UILW inventory for the Reference case – plotted on various time scales. The bulk gases (i.e. H₂, CO₂ and CH₄) are plotted against the left-hand axis, and the active gases (i.e. ³HH, ¹⁴CO₂, ¹⁴CH₄ and ²²²Rn) are plotted against the right-hand axis.

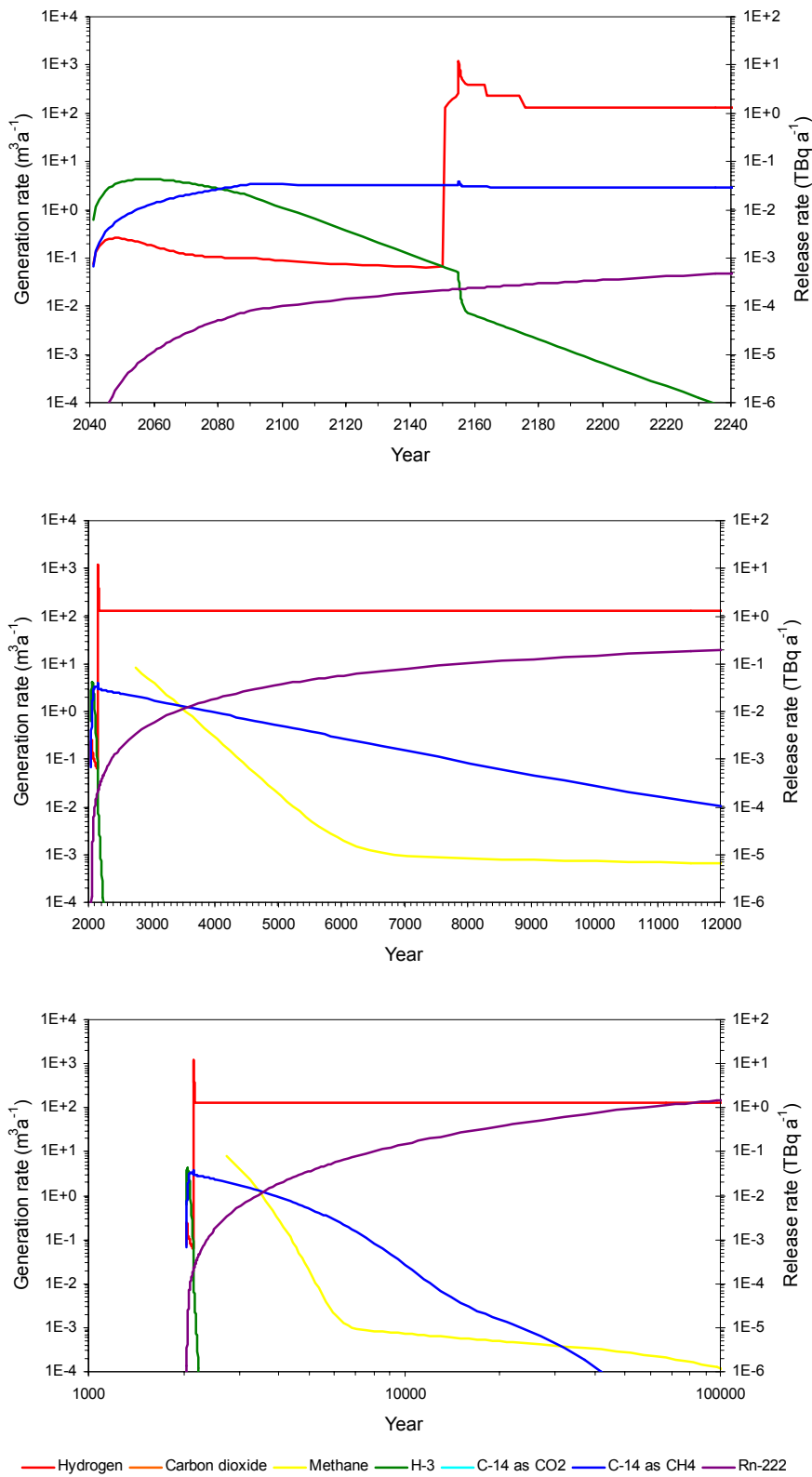


Figure 2.2 Gas generation from the 2004 SILW/LLW inventory for the Reference case – plotted on various time scales. The bulk gases (i.e. H_2 , CO_2 and CH_4) are plotted against the left-hand axis, and the active gases (i.e. ^3H , $^{14}\text{CO}_2$, $^{14}\text{CH}_4$ and ^{222}Rn) are plotted against the right-hand axis.

2.2.2 Varying Temperature case

The results for the Varying Temperature case are shown in Figures 2.3–4.

In this scenario the temperature is higher than in the Reference case for a period of 10 years before closure and 100 years after closure. During this period some of the metals, in particular Magnox and uranium, corrode more rapidly. As a result, these metals give a higher generation rate of gas, but also are all consumed sooner.

For the UILW vaults:

- The uranium corrodes so quickly that it is consumed before repository closure (i.e. by 2144 AD).
- The Magnox plates are all corroded at 2154.6 AD, closely followed by the Magnox spheres at 2154.8 AD. This is just before the system goes anaerobic, so there is a short period during which the only metal producing hydrogen is aluminium.
- At about 2155 AD, the repository resaturates and goes anaerobic. As a result, the steels and Zircaloy start to corrode anaerobically producing hydrogen gas. Mild steel and Zircaloy experience a short period of rapid (acute) corrosion, which causes a spike in the generation rate of hydrogen.

For the SILW vaults, there is no inventory of uranium and so:

- The Magnox plates are all corroded at 2154.6 AD. As a result, the production rate of hydrogen gas decreases. This is just before the system goes anaerobic, so there is a short period during which the only metal producing hydrogen is aluminium.
- At about 2155 AD, the repository resaturates and goes anaerobic. As a result, the steels and Zircaloy start to corrode anaerobically producing hydrogen gas. Mild steel and Zircaloy experience a short period of rapid (acute) corrosion, which causes a spike in the generation rate of hydrogen.

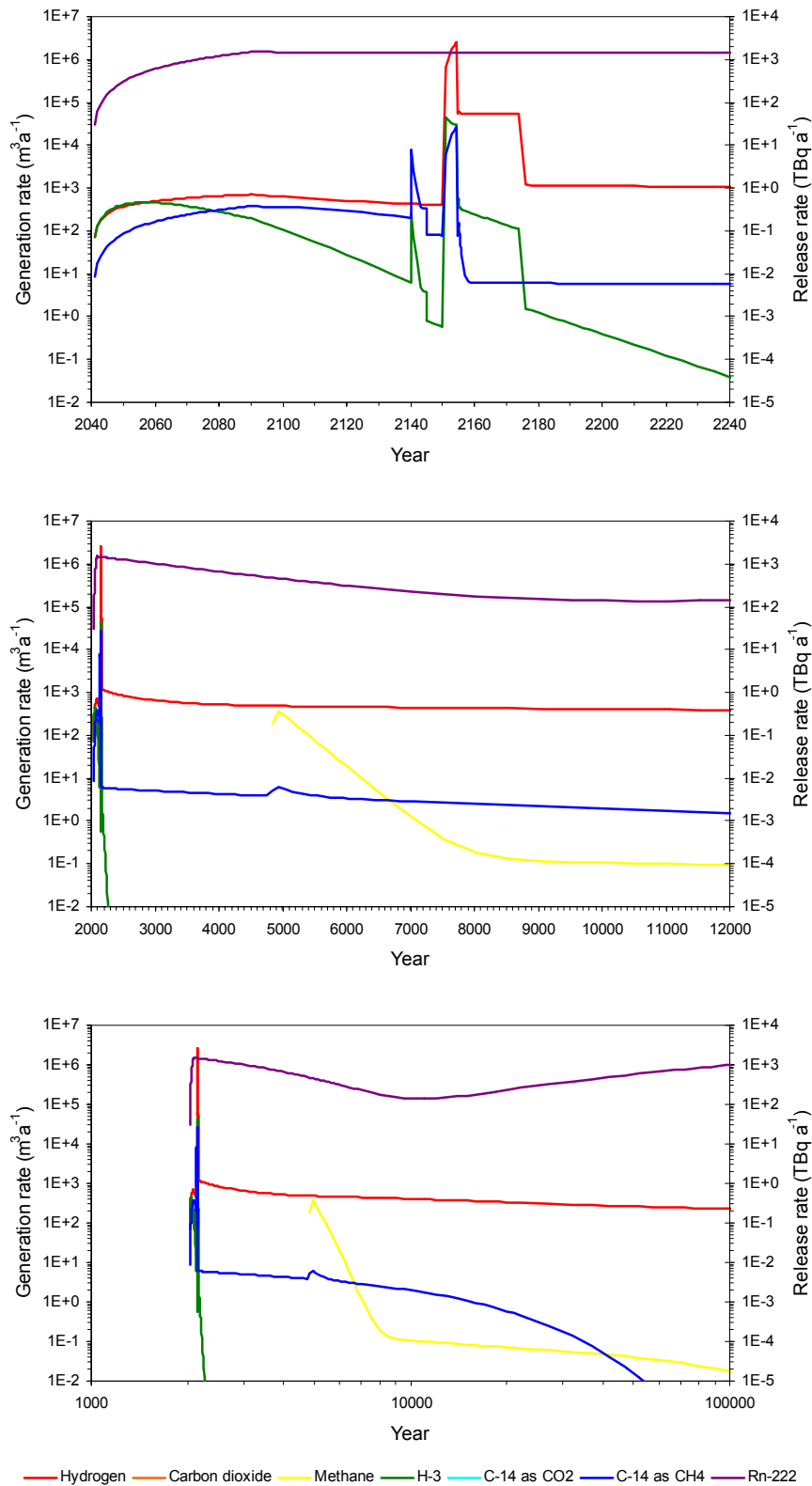


Figure 2.3 Gas generation from the 2004 UILW inventory for the Varying Temperature case – plotted on various time scales. The bulk gases (i.e. H₂, CO₂ and CH₄) are plotted against the left-hand axis, and the active gases (i.e. ³H, ¹⁴CO₂, ¹⁴CH₄ and ²²²Rn) are plotted against the right-hand axis.

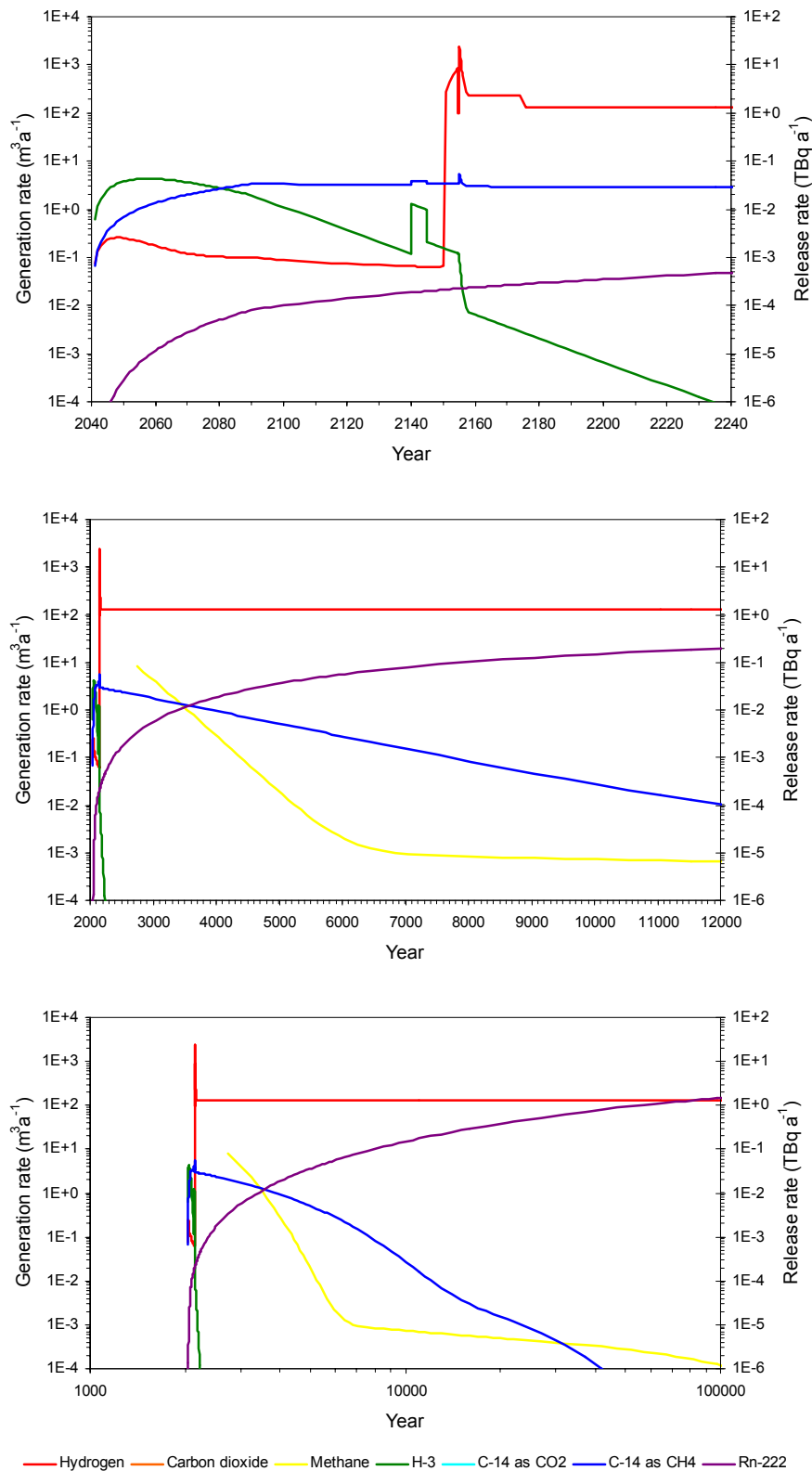


Figure 2.4 Gas generation from the 2004 SILW/LLW inventory for the Varying Temperature case – plotted on various time scales. The bulk gases (i.e. H_2 , CO_2 and CH_4) are plotted against the left-hand axis, and the active gases (i.e. ^3H , $^{14}\text{CO}_2$, $^{14}\text{CH}_4$ and ^{222}Rn) are plotted against the right-hand axis.

2.2.3 Exclusion of Carbonation case

The results for the Exclusion of Carbonation case are shown in Figures 2.5–6.

This scenario allows carbon dioxide and hydrogen to combine forming methane, in contrast to the other variants in which this reaction is inhibited. The activity of the methanogenic bacteria which mediate this reaction is inhibited by the presence of oxygen, nitrate and sulphate, so if any of these species are present the reaction can not occur.

The results show carbon dioxide that is produced from organic degradation. When the oxygen, nitrate and sulphate have run out:

- Methane and carbon dioxide are produced; and
- Carbon dioxide and hydrogen can combine to form methane.

Either carbon dioxide is produced sufficiently rapidly to consume all the hydrogen produced during a time step, or it is not.

For the UILW vaults:

- Sulphate is all consumed at 4940 AD (nitrate was all consumed by 4240 AD), and so methane can start to form. Initially carbon dioxide and methane are generated at a high rate from the small organic molecules (ISA) that are present. This rate is sufficiently high that all the hydrogen produced during a time step can react with carbon dioxide to form methane.
- When the small organic molecules have been consumed, the new rate-limiting step for the formation of carbon dioxide and methane is the mid-chain scission of stopped cellulose. Carbon dioxide continues to form, but at a much slower rate. This rate is so low that even if all the carbon dioxide produced during a time step reacts with hydrogen, there is only a small effect on the generation rate of hydrogen.
- The switch from complete consumption of hydrogen to complete consumption of carbon dioxide occurs at 5340 AD.

For the SILW vaults, there is no inventory of readily degradable small molecules and only a small inventory of cellulose, and so:

- Sulphate is all consumed at 2740 AD (nitrate was all consumed by 2440 AD), and so methane can start to form. Initially carbon dioxide and methane are generated at a high rate from the small organic molecules (ISA) that have been produced. This rate is so low that even if all the carbon dioxide produced during a time step reacts with hydrogen, there is only a small effect on the generation rate of hydrogen.
- When the small organic molecules have been consumed, the new rate-limiting step for the formation of carbon dioxide and methane is the mid-chain scission of stopped cellulose. Carbon dioxide continues to form, but at an even slower rate.

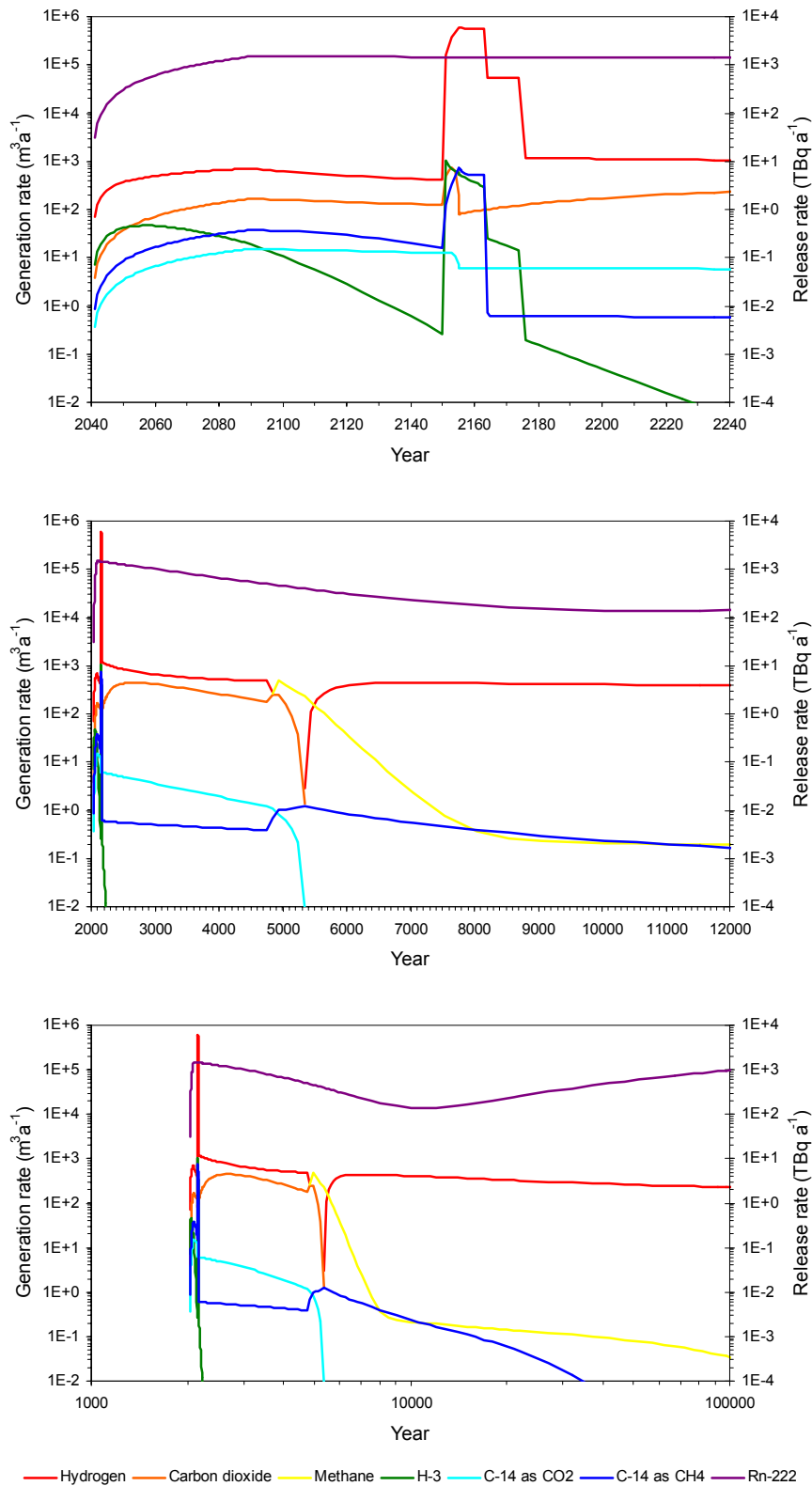


Figure 2.5 Gas generation from the 2004 UILW inventory for the Exclusion of Carbonation case – plotted on various time scales. The bulk gases (i.e. H₂, CO₂ and CH₄) are plotted against the left-hand axis, and the active gases (i.e. ³H, ¹⁴CO₂, ¹⁴CH₄ and ²²²Rn) are plotted against the right-hand axis.

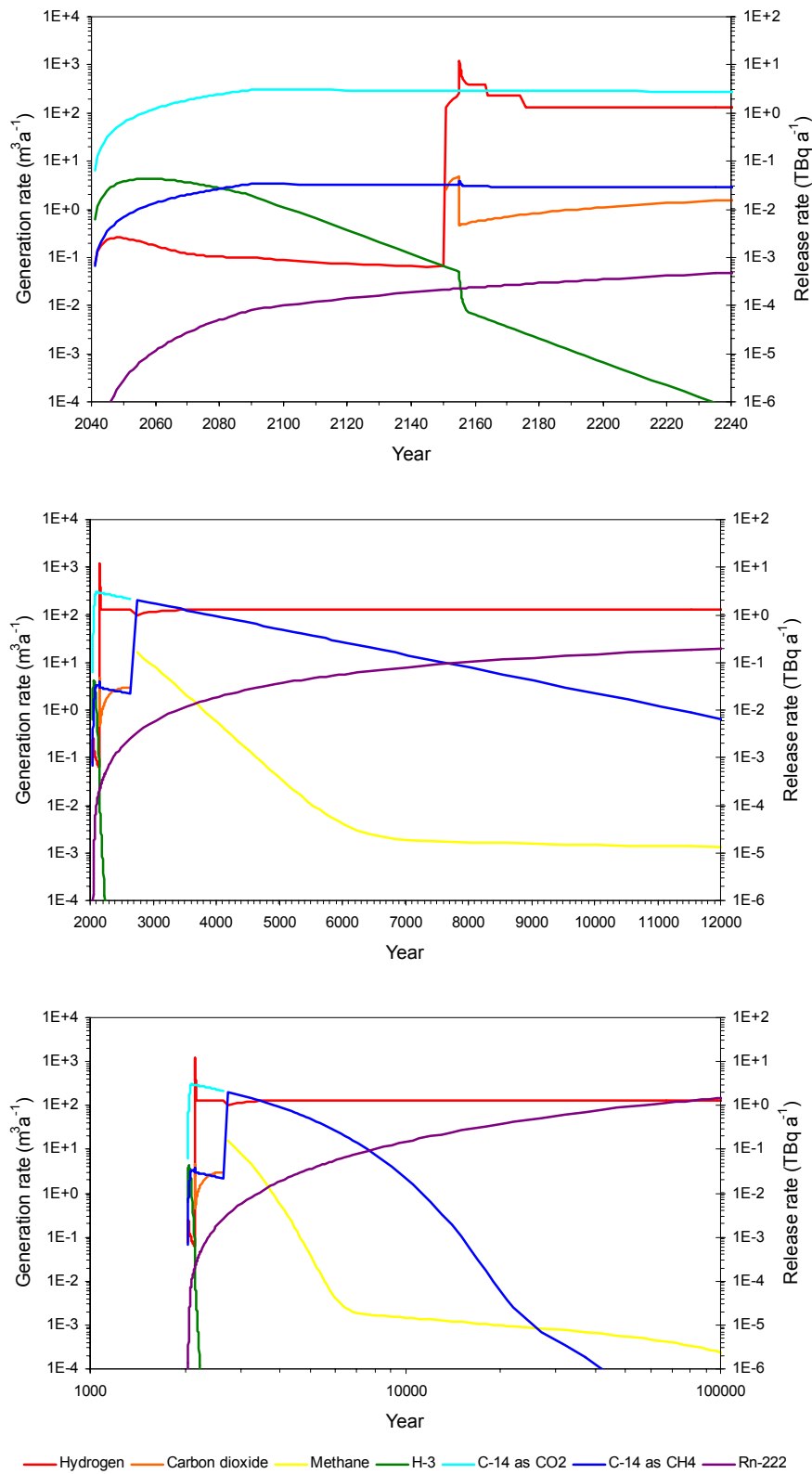


Figure 2.6 Gas generation from the 2004 SILW/LLW inventory for the Exclusion of Carbonation case – plotted on various time scales. The bulk gases (i.e. H₂, CO₂ and CH₄) are plotted against the left-hand axis, and the active gases (i.e. ³HH, ¹⁴CO₂, ¹⁴CH₄ and ²²²Rn) are plotted against the right-hand axis.

2.2.4 Small Organic Molecules case

The results for the Small Organic Molecules case are shown in Figures 2.7–8.

This scenario takes account of GE Healthcare waste streams 1A07 and 1B05, which include a significant inventory of ^{14}C in small organic molecules. This inventory is all in the UILW vaults. For these vaults:

- Sulphate is all consumed by 4940 AD (nitrate was all consumed by 4240 AD), and so methane can start to form. Initially methane is generated at a high rate from the small organic molecules (ISA) that are present, and ^{14}C in methane is generated at a higher rate than in the Reference case because of the extra inventory of ^{14}C . After the small organic molecules have been consumed, ^{14}C in methane is produced at essentially the same rate as in the Reference case.

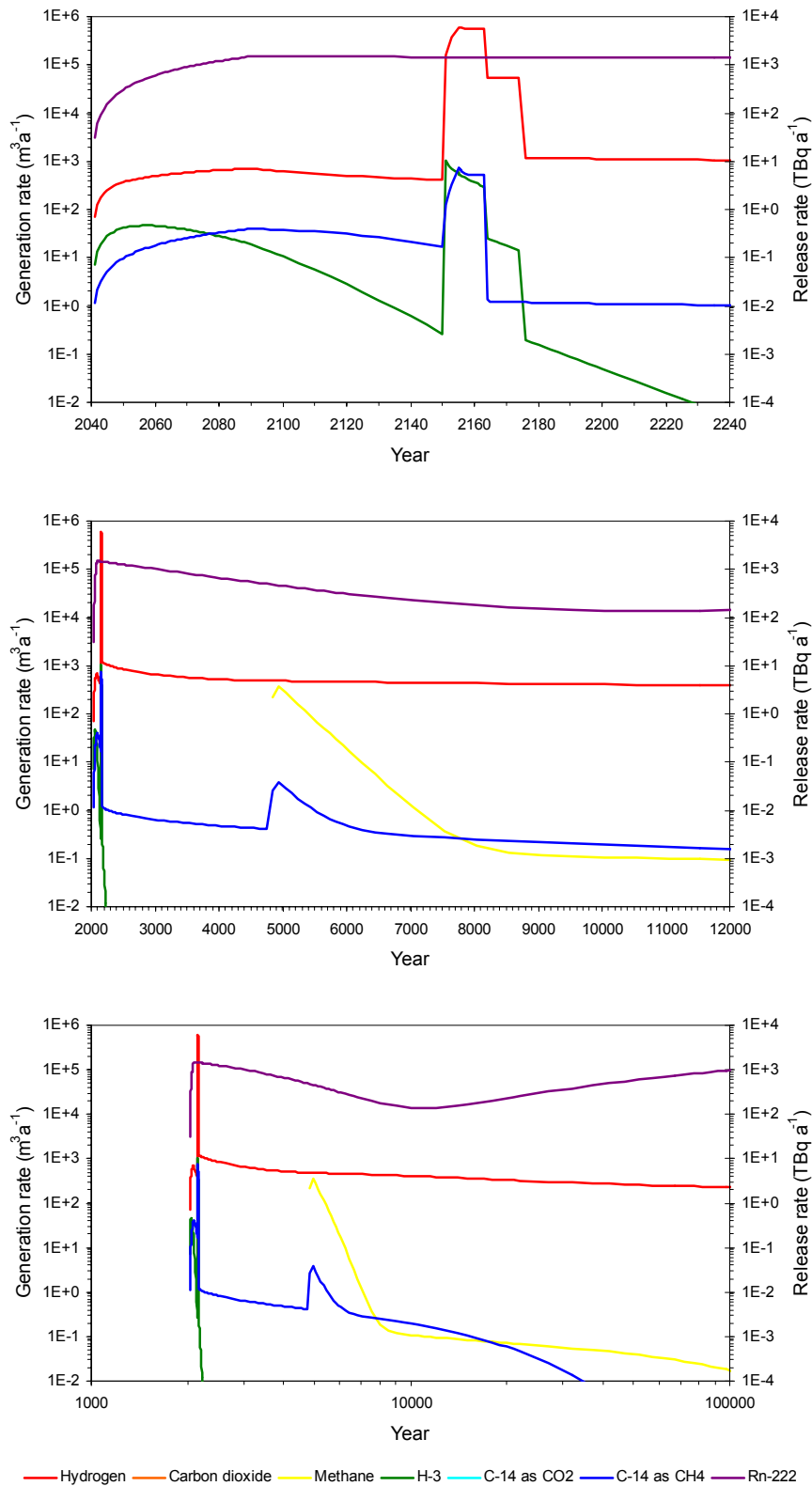


Figure 2.7 Gas generation from the 2004 UILW inventory for the Small Organics case – plotted on various time scales. The bulk gases (i.e. H₂, CO₂ and CH₄) are plotted against the left-hand axis, and the active gases (i.e. ³H, ¹⁴CO₂, ¹⁴CH₄ and ²²²Rn) are plotted against the right-hand axis.

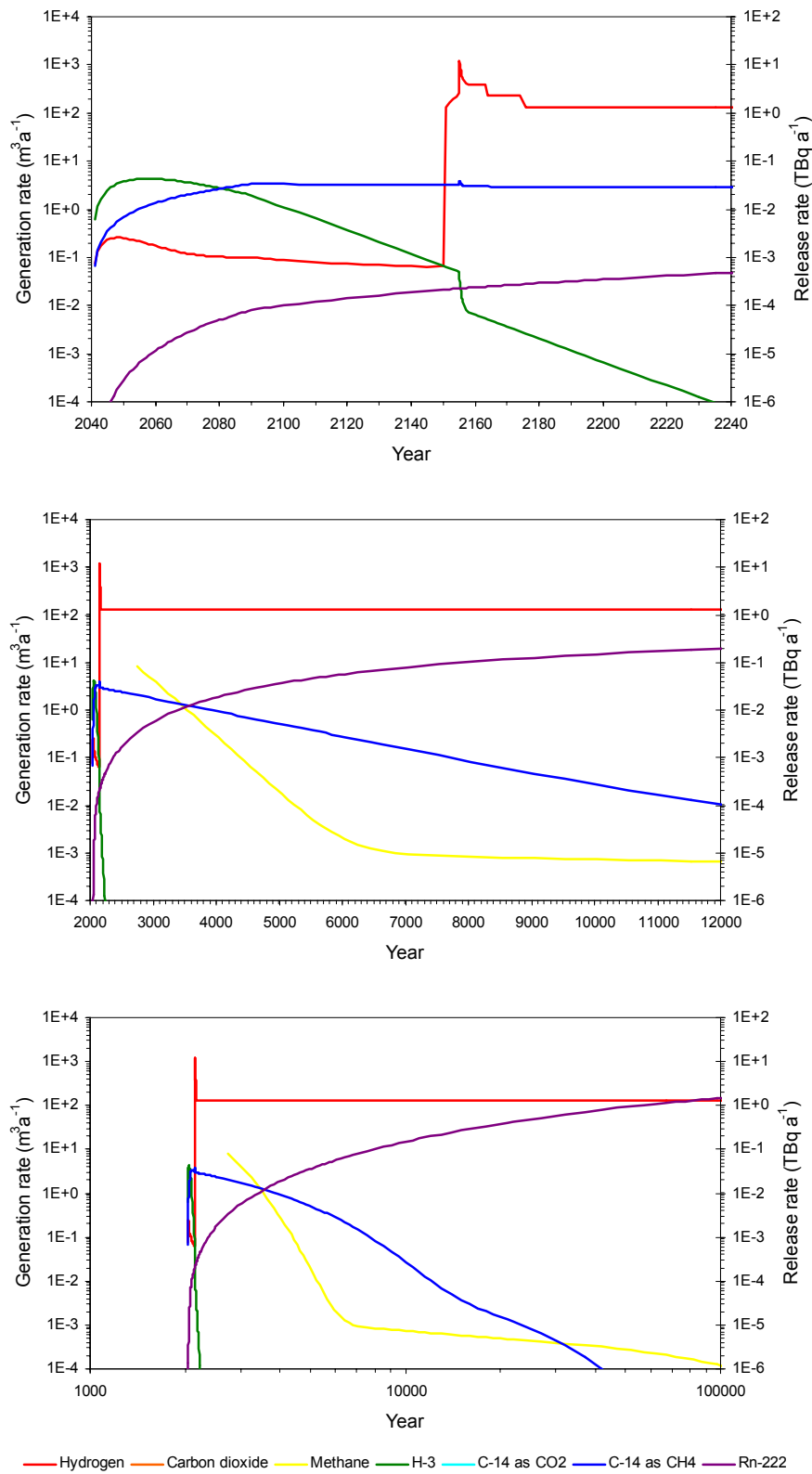


Figure 2.8 Gas generation from the 2004 SILW/LLW inventory for the Small Organics case – plotted on various time scales. The bulk gases (i.e. H₂, CO₂ and CH₄) are plotted against the left-hand axis, and the active gases (i.e. ³H, ¹⁴CO₂, ¹⁴CH₄ and ²²²Rn) are plotted against the right-hand axis.

2.2.5 Operational case

The results for the Operational case are shown in Figures 2.9–10.

This scenario was designed to be more realistic for the operational phase. In particular:

- The initial mass of water is calculated from the amount of water that would fill the pore space of the conditioned wastes; and
- The UILW wastes and the SILW/LLW wastes are split into Magnox, aluminium and other wastes. (Splitting the wastes in this way means that the consumption of water by the reactive metals can be modelled more correctly and will not impact on the generation of gas by the other wastes.)

The main effect of this change in the initial inventory of water is to allow Magnox and aluminium to corrode before closure. Other effects include organic degradation starting immediately after packaging, changing the subsequent inventory of organic materials, and gas being generated from radiolysis of the water that is present.

For the UILW vaults:

- Aluminium and Magnox start to corrode immediately after packaging, generating hydrogen and tritium. Although the packages containing aluminium produce gas at a high rate, the water in these packages is consumed within 5 years and gas production stops until the packages resaturate post-closure. Before the Magnox runs out (the Magnox plates are all corroded at 2164 AD, closely followed by the Magnox spheres at 2165 AD), it is the major contributor to the generation rate of hydrogen. The next biggest contribution, apart from that of aluminium (the aluminium plates are all corroded at 2174 AD), is due to radiolysis of water.
- Radiolysis of water, except for a brief period after the repository has resaturated when the Magnox corrodes quickly, also dominates the production of tritium.
- Before closure, uranium is the major contributor to the generation rate of ^{14}C in methane. After the repository has resaturated, Magnox corrodes quickly and therefore becomes the dominant process for forming ^{14}C in methane. When the Magnox is consumed (the uranium has run out earlier), there is a dramatic decrease in the generation rate of this active gas. From this point on, stainless steel becomes the dominant source of ^{14}C in methane.

For the SILW vaults:

- Aluminium and Magnox start to corrode immediately after packaging, generating hydrogen. Although the packages containing aluminium produce gas at a high rate, the water in these packages is consumed within 5 years and gas production stops until the packages resaturate post-closure. Before the Magnox runs out (the Magnox plates are all corroded at 2164 AD), it is the major contributor to the generation rate of hydrogen. The next biggest contribution, apart from that of aluminium (the aluminium plates are all corroded at 2174 AD), is due to corrosion of the steels.

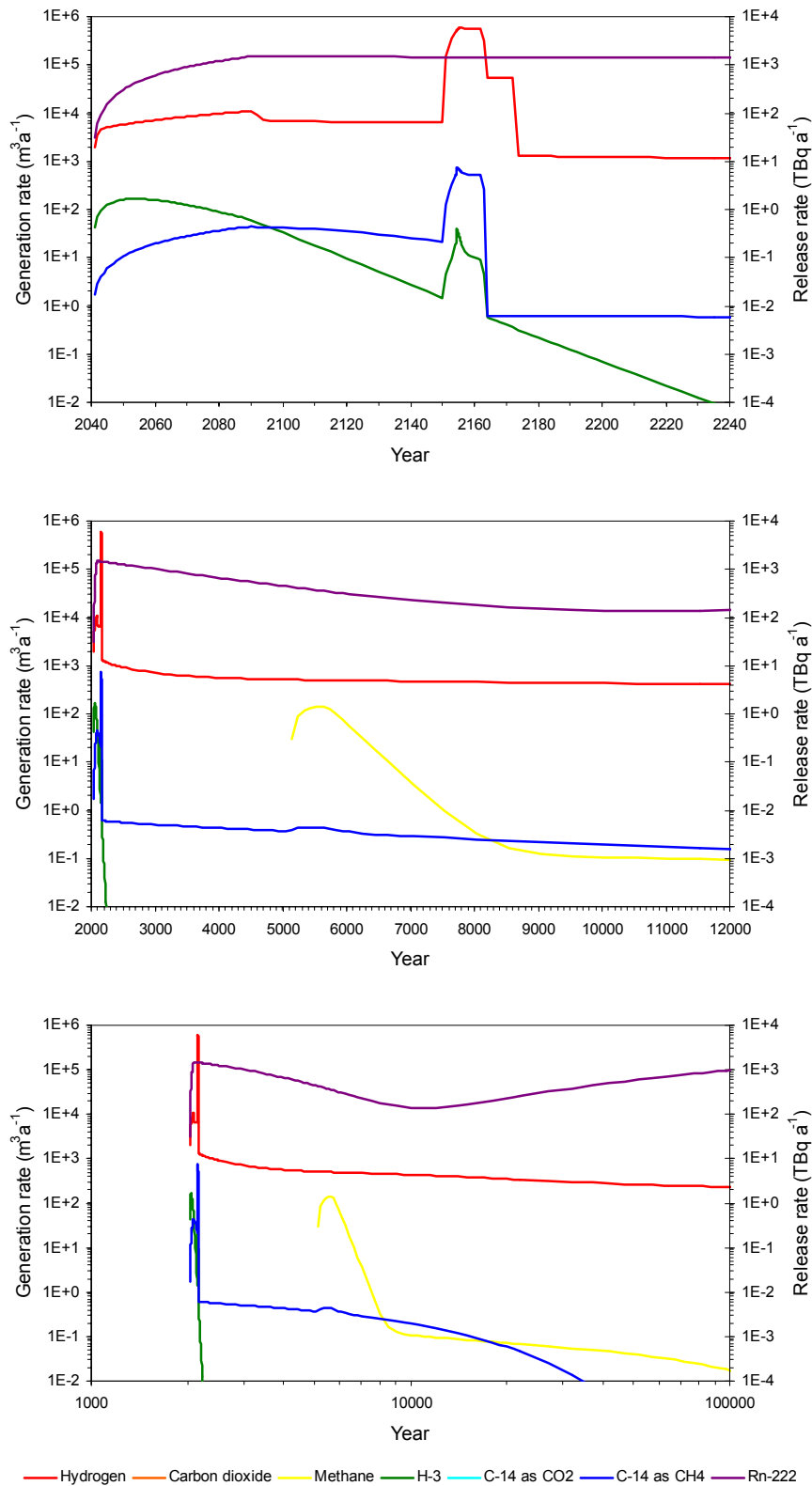


Figure 2.9 Gas generation from the 2004 UILW inventory for the Operational case – plotted on various time scales. The bulk gases (i.e. H₂, CO₂ and CH₄) are plotted against the left-hand axis, and the active gases (i.e. ³HH, ¹⁴CO₂, ¹⁴CH₄ and ²²²Rn) are plotted against the right-hand axis.

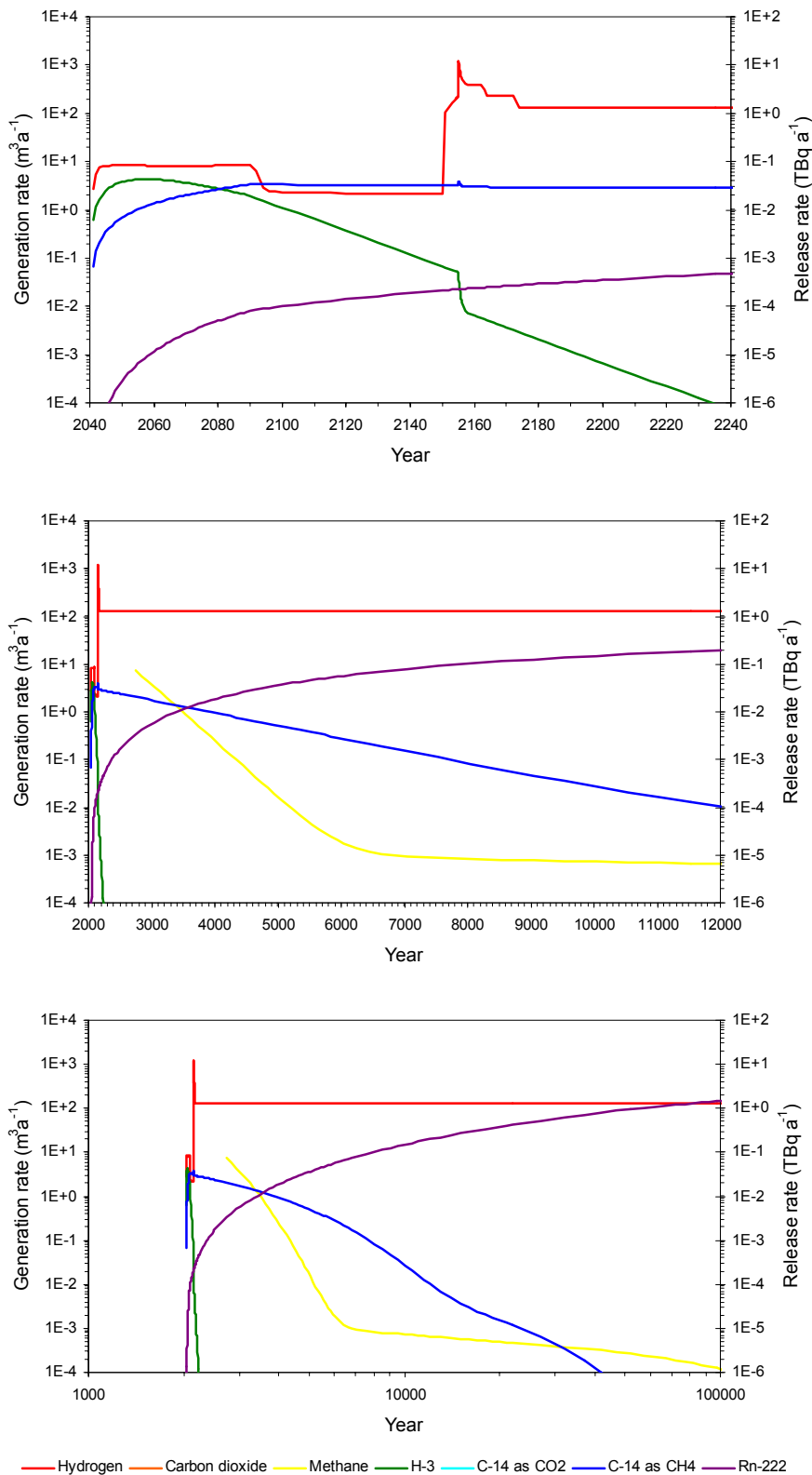


Figure 2.10 Gas generation from the 2004 SILW/LLW inventory for the Operational case – plotted on various time scales. The bulk gases (i.e. H₂, CO₂ and CH₄) are plotted against the left-hand axis, and the active gases (i.e. ³H, ¹⁴CO₂, ¹⁴CH₄ and ²²²Rn) are plotted against the right-hand axis.

2.3 Solid-state Diffusion of Tritium from Steel Wastes

SMOGG includes a model for solid-state diffusion of tritium from tritium-containing metal wastes. However, this simple model underestimates the release rate of tritium [8]. Therefore, semi-analytical solutions for diffusion out of a plate and out of a sphere [9, 10] have been used here.

Based on a limited review of the literature, a solid-state diffusion coefficient has been assumed for tritium in steels of $1.9 \cdot 10^{-16} \text{ m}^2\text{s}^{-1}$. The results of the calculations are shown in Figure 2.11–12.

In the case of the UILW vaults, if diffusion is neglected then the main processes leading to the release of tritium (see Section 2.2.1) are:

- Corrosion consuming tritiated water; and
- Radiolysis of tritiated water.

Figure 2.11 shows that except for a short period when aluminium (and, for part of that time, also Magnox) are corroding, diffusion of tritium from the steels in the waste is the dominant process for releasing this active gas.

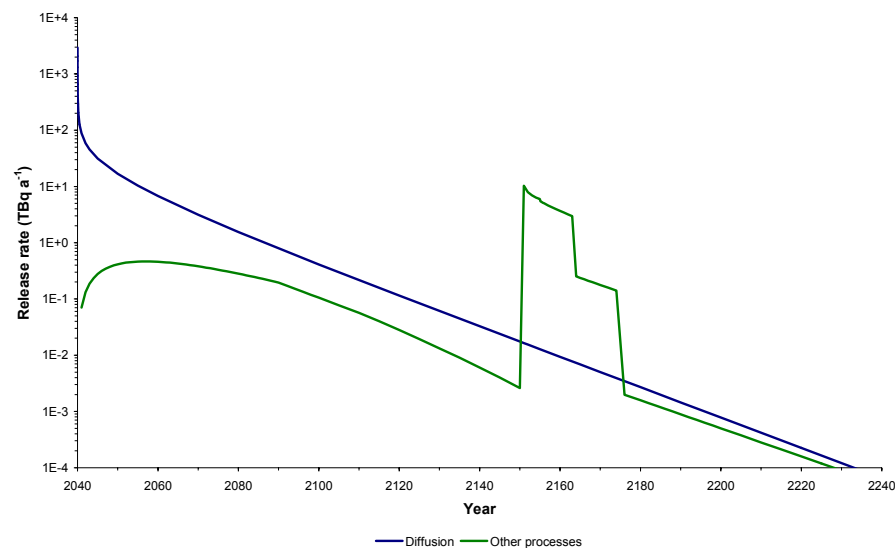


Figure 2.11 Diffusive release of ³H from steel wastes in the 2004 UILW inventory.

In the case of SILW/LLW vaults, corrosion of the steels in the waste releases tritium, but the diffusive release of tritium is a more significant process (see Figure 2.12).

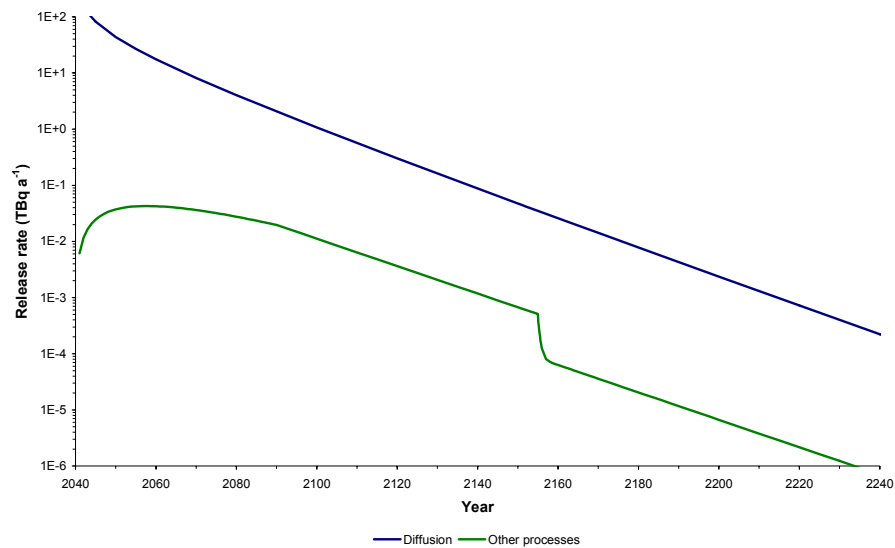


Figure 2.12 Diffusive release of ^3H from steel wastes in the 2004 SILW/LLW inventory.

2.4 Summary of Gas Generation Calculations

In this section, uncertainty in the rate of gas generation has been scoped by the consideration of a reference case and four variant case scenarios designed to address a range of alternative assumptions that could affect gas generation in a 'real' repository environment. These scenarios all consider UK intermediate and some low-level wastes only.

For the different variant calculations considered, typically:

- The generation rates of both bulk and active gases have short-lived peaks due to corrosion of the reactive metals (i.e. aluminium, Magnox and uranium).
- The peak generation rate of bulk gas is about $10^6 \text{ m}^3 \text{ a}^{-1}$ at STP.
- The peak generation rates of ^3H and $^{14}\text{CH}_4$ are about 10 TBq a^{-1} .
- The long-term generation rate of bulk gas is dominated by corrosion of steel in the repository, and is in the range $10^2 - 10^3 \text{ m}^3 \text{ a}^{-1}$ at STP. The generation rate from the UILW vaults is larger than the generation rate from the SILW vaults.
- Diffusion of tritium from the steels in the waste is the dominant process for releasing this active gas.
- After the reactive metals are all corroded, corrosion of steel becomes an important source of ^{14}C in methane. In the case of the SILW/LLW vaults, ^{14}C in methane is also released as a result of the degradation of graphite.

The rate of production of ^{222}Rn within the wasteform can be calculated readily from the activity of ^{226}Ra present. However, the radiological consequences arising from ^{222}Rn generated in the repository are insignificant because of the short half-life of this radionuclide. The dose from ^{222}Rn arises from radon that is 'stripped' from the Quaternary sediments rather than from radon that originates in the repository.

The reference case gas generation rate is further considered in Section 3, as input to a suite of gas migration calculations. As will be shown in this Section, gas migration is very site-specific. Any work as part of a future safety case will have to identify the relevant priority of further developing understanding in gas generation processes, and further developing understanding in gas migration processes, as part of

an overall programme to progress understanding of the consequences of repository-derived gas. This will be affected by any site-specific considerations that are prevalent at the relevant times.

3 Gas Migration

In this Section, the reference case gas generation rate from Section 2 is used as input to a series of geosphere gas migration calculations. Calculations of repository over-pressurisation and gas surface breakthrough time for two one-dimensional (generic) geologies – one corresponding to a hard fractured host rock, the other to an argillaceous host rock – are presented. Two-dimensional gas migration modelling is also reported, for an example site-specific study. This addresses both a reference case scenario, and variant scenarios to investigate the sensitivity of model output to selected variation of input parameter.

In the Generic Post-closure Performance Assessment [6, 11], gas migration from the repository was studied using simple one-dimensional TOUGH2 [12, 13, 14] calculations. These calculations were carried out for a generic fractured crystalline host rock and for a generic argillaceous host rock.

In the current assessment, these 1D models are updated using the Reference case gas generation rate determined in Section 2. The TOUGH2v2 calculations are run using the EOS7R fluid property module, instead of the EOS5 module used previously. The EOS7R module extends the EOS7 module (which has been customised to model water, brine and hydrogen) to include two additional mass components, which could be either bulk or active gases. The calculations and the results obtained for the two models are described in Sections 3.1 and 3.2 respectively.

It should be emphasised that these are simplistic calculations, undertaken, in the absence of an identified and characterised potential site, just to give an indication of the time that it might take for gas to reach the surface after repository closure, and of the degree of over-pressurisation of the repository that might occur. The basic properties of the formations in the generic host rocks were chosen originally to be consistent with those used in groundwater transport calculations as part of the 2001 generic assessment [15].

A two-dimensional TOUGH2v2 calculation is also presented. This model is based on the geology at Sellafield³, which has formed the basis for some recent work [16]. For this 2D geology, the fluxes of gas across the boundaries of the model were calculated as a function of time. The focus is mainly on the release of ¹⁴C, which is the active gas of most interest. Both the total flow of gas across the top surface of the model as a function of time, and the spatial distribution of the flux of gas are reported.

In practice, the occurrence of fingering and the presence of three-dimensional variability in the rock (including the presence of fractures) could modify the results obtained, in particular reducing the breakthrough times. A total of three variant 2D calculations which were designed to scope the effect of fingering were carried out. Only some of the variants led to the breakthrough of a free gas phase.

3.1 Gas Migration from a Repository in a Fractured Crystalline Host Rock

3.1.1 Model

The fractured generic host rock site consists of two hydrogeological formations: the fractured host rock (134 m thick above the vaults and a region also below the vaults) and a sedimentary cover rock (500 m thick). The one-dimensional model includes these two formations, and a representation of the vaults in which the gas is generated (including a vault crown space, assumed to be an open void at repository closure, but not an EDZ). The grid for the model is shown in Figure 3.1.

³ The use of Sellafield data is due entirely to the existence of an appropriate data set, and in no way pre-judges any future site selection programme in the UK.

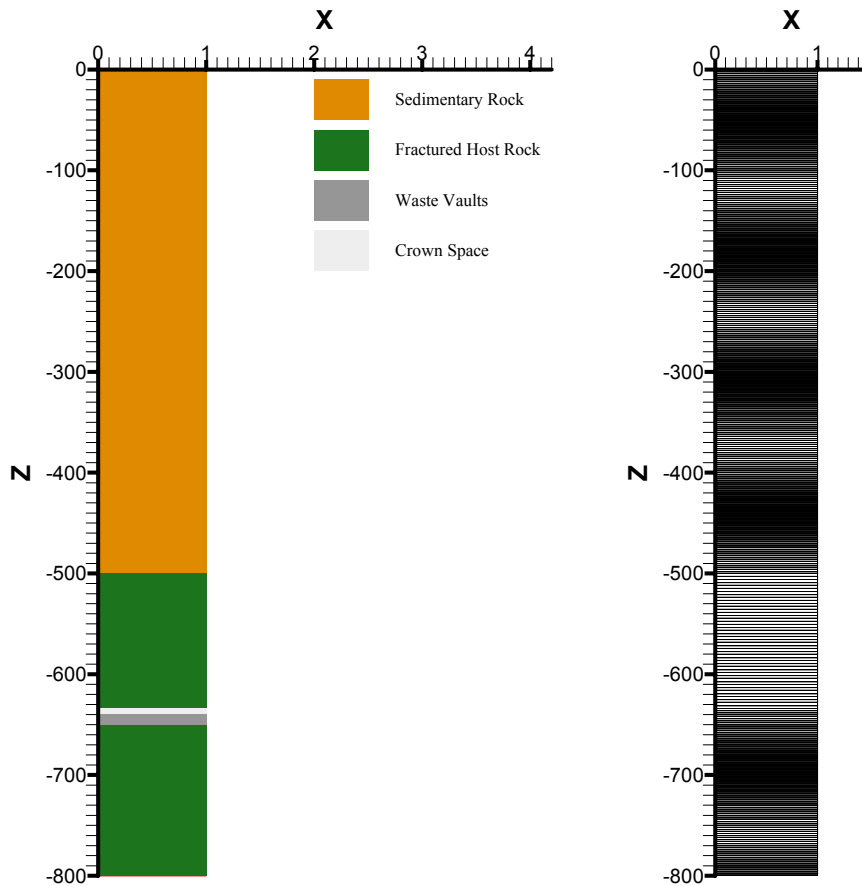


Figure 3.1 The grid for the fractured crystalline host rock one-dimensional model.

The hydrogeological properties of the different rock units are given in Table 3.1 (see [11]).

Table 3.1 Hydrogeological Properties Used in Fractured Crystalline Host Rock Model

Unit	Permeability (m ²)		Flow Type	Matrix Porosity	Fracture Porosity
	k_x	k_z			
Sedimentary rock	$5.0 \cdot 10^{-14}$	$5.0 \cdot 10^{-15}$	matrix	0.1	n/a
Fractured host rock	$2.0 \cdot 10^{-16}$	$2.0 \cdot 10^{-16}$	fracture	n/a	$9.0 \cdot 10^{-6}$
Waste vaults	$3.0 \cdot 10^{-16}$	$3.0 \cdot 10^{-16}$	matrix	0.08	n/a
Crown space	$1.0 \cdot 10^{-12}$	$1.0 \cdot 10^{-12}$	matrix	0.24	n/a

Only gas generation for the Reference case was considered.

Gas migration from the repository as a whole was considered, so the cross-sectional area of the model was chosen to represent the combined footprints of the two vault types. The areas covered by the two vault types and by the repository as a whole are shown in Table 3.2 (see also Table 2.1). The vault

footprints include the rock pillars; this makes some allowance for lateral movement of gas away from the area covered by the waste itself. The repository footprint is just the sum of the areas for the two vault types.

Table 3.2 Vault and Repository Areas

Vaults or Repository	Area (m ²)
SILW/LLW	143,700
UILW	279,600
Repository	423,300

3.1.2 Results

The results of the gas migration calculations for the generic fractured host rock are shown in Figures 3.2–4. Figure 3.2 shows the evolution of the gas pressure in the repository, and Figures 3.3–4 provide a comparison between the gas generation rates and gas flows from the repository and across the ground surface.

A drawdown phase was not modelled in this simple calculation, and so the repository is predicted to resaturate more quickly than it would. As in the previous generic assessment [6, 11], there is virtually no rise in pressure above hydrostatic (hydrostatic pressure is 6.332 MPa at the top of the backfill at 640 m). The maximum pressure is ~0.22 MPa above hydrostatic at 35.56 years after closure. The calculation shows, essentially, the restoration of the vault pressure to hydrostatic from the atmospheric pressure that prevailed in the gas-filled vaults at repository closure.

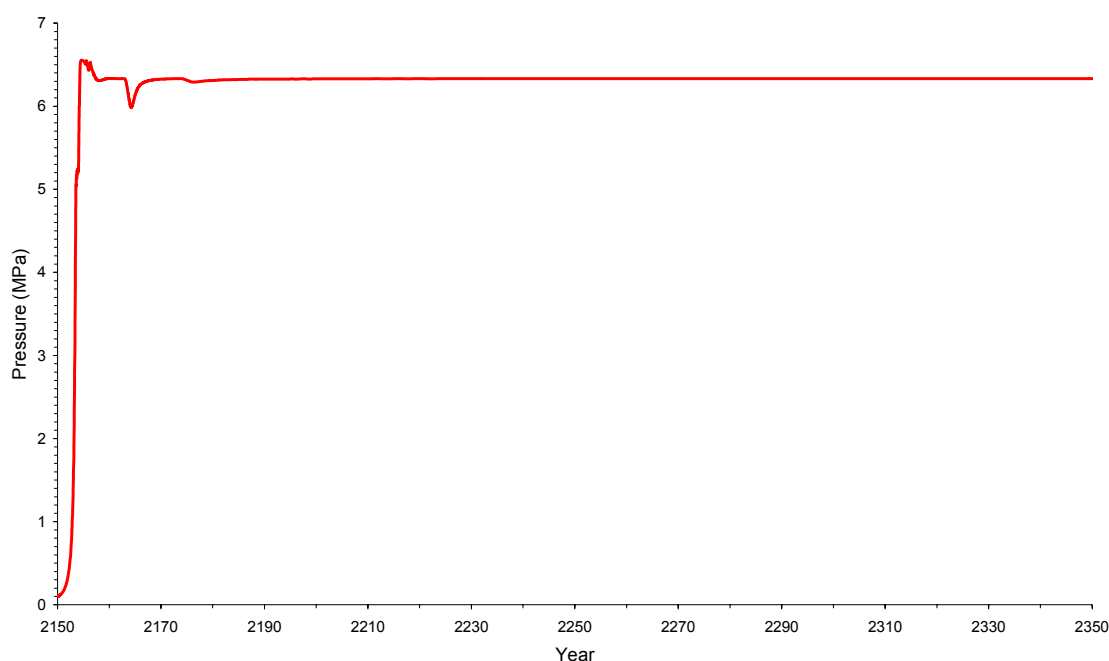


Figure 3.2 Pressure evolution in the repository for the Reference case rate of gas generation and the fractured host rock.

For the Reference case, a sharp pulse of gas is released from the repository between 3.5 and 4.2 years after closure, with a peak flow of $1.4 \times 10^6 \text{ m}^3 \text{ a}^{-1}$ (at STP); during this period gas is leaving the vaults to be

replaced by water until hydrostatic pressure is established. The pulse of gas that is released collects in a 'bubble' under the sedimentary cover. Then there is a gap in significant gas flow from the vaults, with gas displacing water, until ~6.5 years when the flow from the repository comes into equilibrium with the gas generation rate. Some of the details of this behaviour are a consequence of the one-dimensional nature of the model employed.

In this model, gas does not reach the surface until about 7,500 years after closure. There is a period while a gas bubble builds up below the overlying sedimentary cover, until the bubble is deep enough to overcome the capillary entry pressure for gas to move into the sediments. Subsequently the advance of gas through the sediments is slowed by its dissolution into the groundwater, and it is only when the advancing gas has saturated all the water between the repository and the surface that free gas can appear at the surface. The porosity of the sedimentary cover is 0.1 compared to 9×10^{-6} for the fractured host rock [6, 11], so much more gas can dissolve in the sediments than in the crystalline rock.

Gas breakthrough at the surface in this calculation takes a similar time as in the corresponding calculation for the previous generic assessment (7,500 years compared with 6,000 years) [6, 11]. This is because the generation rates of gas per unit area in the two calculations are comparable.

It is uncertain whether or not the migrating gas 'sees' all the water between the repository and the surface. Rock heterogeneities, including for example conducting fractures in the sedimentary cover, and viscous and gravitational instabilities, may cause the gas flow to 'finger' through the overlying rocks, leading to earlier appearance of the gas at the surface (see Reference [17] and references therein).

Figure 3.4 shows the contributions of methane and ^{14}C -labelled methane to the bulk gas flows.

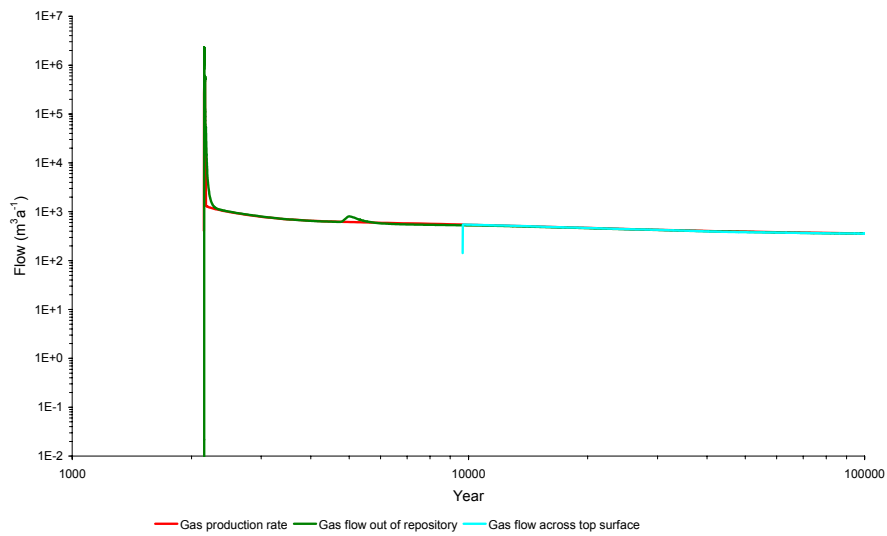
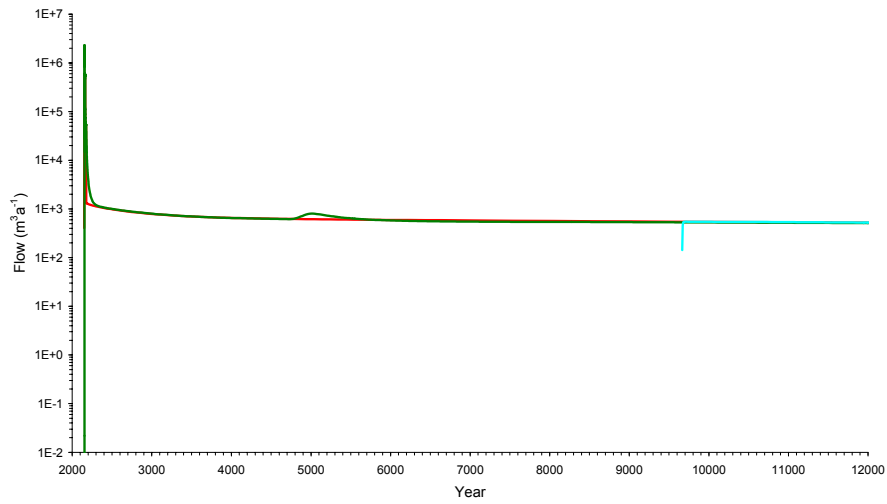
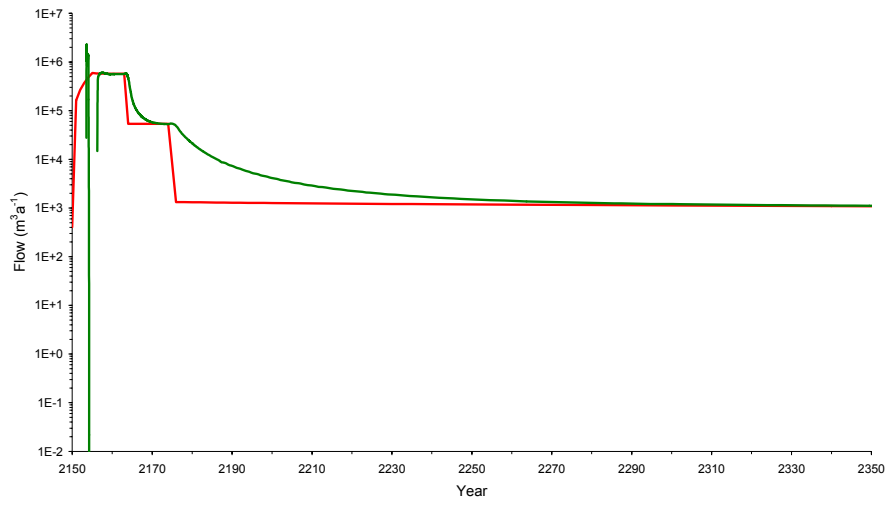


Figure 3.3 Flows of gas for the Reference case rate of gas generation and the fractured host rock.

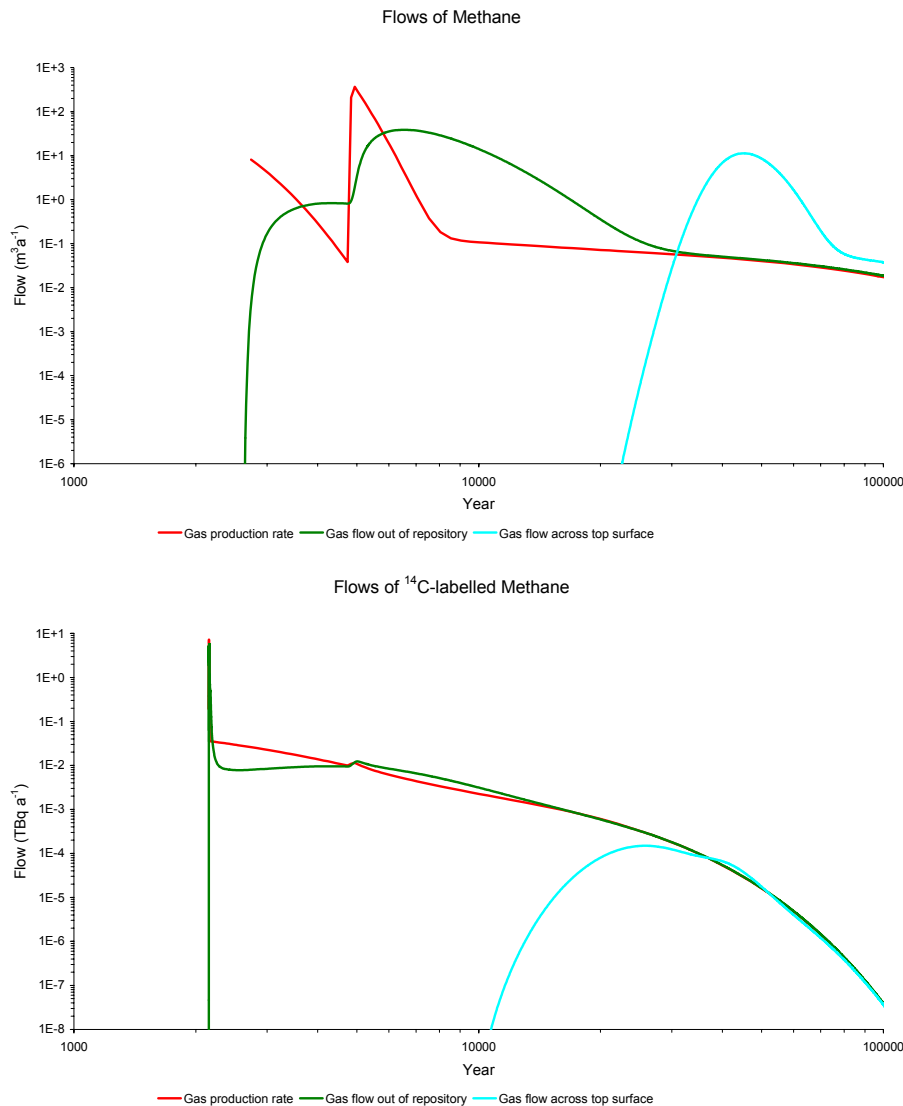


Figure 3.4 Flows of methane (top) and ¹⁴C-labelled methane (bottom) for the Reference case rate of gas generation and the fractured host rock.

3.2 Gas Migration from a Repository in an Argillaceous Host Rock

3.2.1 Model

The one-dimensional model of the site with an argillaceous host rock again contains two geological formations, the argillaceous host rock (142 m thick above the repository and a region also below the vaults) overlain by a sedimentary cover (500 m thick). However, in this case, only a single vault with its crown space is considered. This is because the gas does not penetrate very easily into the argillaceous host rock assumed, so it is not appropriate to assume that the gas advances on a front covering both the vaults and the spaces in between the vaults. The grid for this model is shown in Figure 3.5.

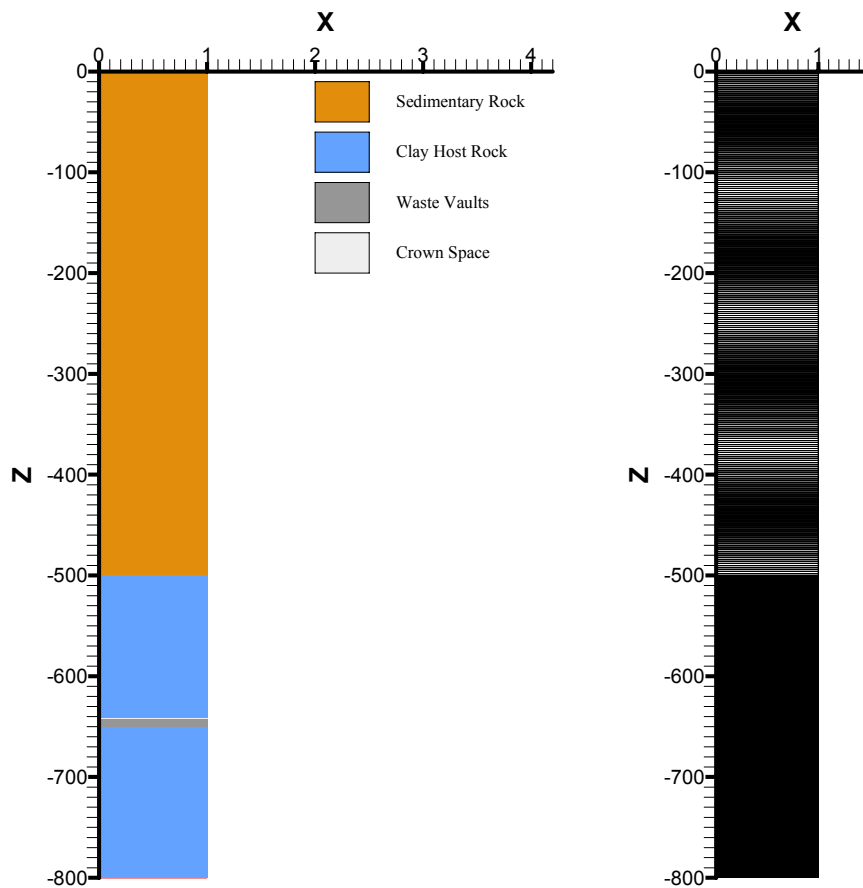


Figure 3.5 The grid for the argillaceous host rock one-dimensional model.

The hydrogeological properties of the different rock units are given in Table 3.3 (see [11]).

Table 3.3 Hydrogeological Properties Used in Argillaceous Host Rock Model

Unit	Permeability (m ²)		Flow Type	Matrix Porosity	Fracture Porosity
	k_x	k_z			
Sedimentary rock	$5.0 \cdot 10^{-14}$	$5.0 \cdot 10^{-15}$	matrix	0.1	n/a
Clay host rock	$5.0 \cdot 10^{-19}$	$2.0 \cdot 10^{-19}$	matrix	0.4	n/a
Waste	$5.0 \cdot 10^{-16}$	$5.0 \cdot 10^{-16}$	matrix	0.3	n/a
Crown	$1.0 \cdot 10^{-12}$	$1.0 \cdot 10^{-12}$	matrix	1.0	n/a

Only gas generation from the 2004 UILW inventory for the Reference case⁴ was considered.

Gas migration from a single UILW vault with its crown space was considered. It is likely that the design of this vault will differ from that for a fractured crystalline host rock. However design data specifically for an argillaceous host rock were not available, and therefore the vault data summarised in Table 3.4 were assumed.

Table 3.4 Vault Design Data used in Argillaceous Host Rock Model (cf. Table 3.1)

Repository parameter	Vaults for Unshielded ILW
Waste stack dimensions	
Height of backfill in vault, Hb	7 m
Nominal vault dimensions	
Average internal length, Li	300.00 m
Internal width, Wi	8 m
Internal height, Hi	8 m
Number of caverns, N	30

3.2.2 Results

The evolution of pressure in the vault is shown in Figure 3.6. The pressure rises substantially, reaching a pressure greater than 9 MPa before it starts to decline. This is similar to the pressure attained in this host rock for the previous generic assessment [6, 11], because the generation rates of gas per unit area in the two calculations are comparable.

There is uncertainty about the mechanism of gas migration in low-permeability argillaceous materials, but at present the general consensus is that it is likely to involve micro-fissuring of the clay and dilation of gas-filled pathways in response to the elevated gas pressures [17]. In some cases, if the gas pressure exceeds the minimum principal stress in the rock, macroscopic fracturing of the rock also might occur. This means that gas could migrate through an argillaceous host rock more easily than the calculations reported here would suggest. The appropriateness of using conventional multi-phase porous medium flow models for describing gas migration in clay materials is discussed in Reference [17]. The calculation carried out does not consider any contribution that diffusion might make to gas transport from the vault.

The feature in the gas pressure profile at ~12,000 years occurs when the backfill has become saturated with gas, and the gas in the vaults starts to enter the clay formation below the repository (as well as flowing into the host rock above the repository).

⁴ This is a worst case because the gas generation rate per unit volume of waste is higher for the UILW vaults than for the SILW/LLW vaults.

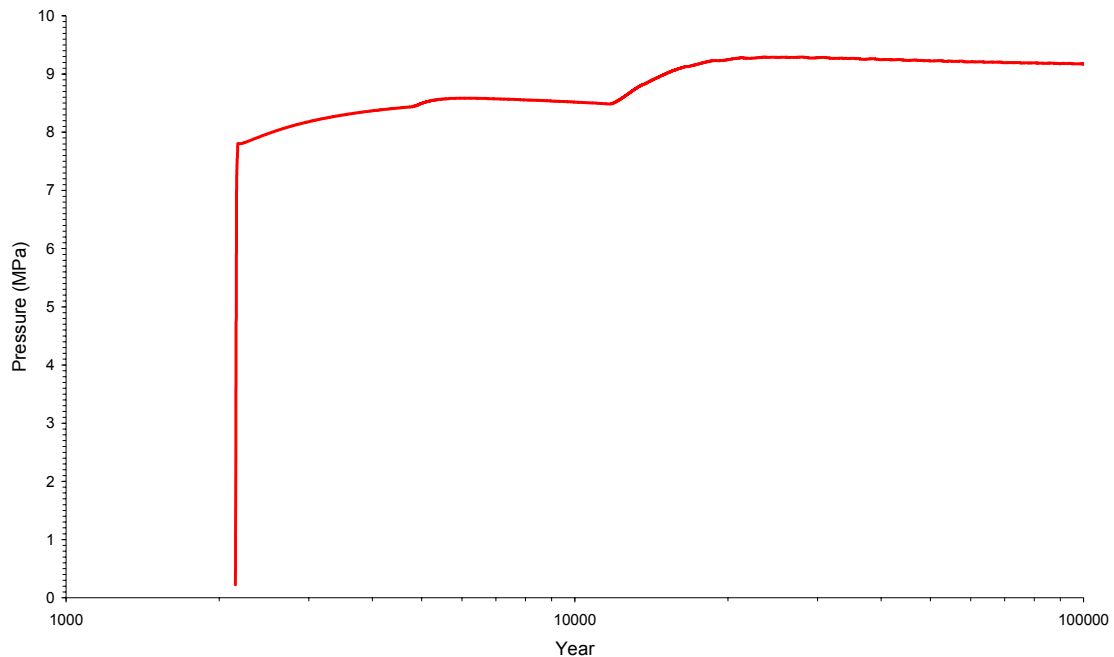


Figure 3.6 Pressure evolution in the repository for the Reference case rate of gas generation and the argillaceous host rock.

In this calculation, a free gas phase penetrates only a short distance from the vault and does not reach the surface during the period considered.

3.3 Two-dimensional Model of Gas Migration from a Repository

The model, which is effectively 2D, represents part of the geology of the Sellafield region in the vicinity of the potential repository that was considered in the *Nirex 97* assessment [18, 9]. The region is illustrated in Figure 3.7 and Figure 3.8. The details of the model and the parameters are discussed in the following Sections.

3.3.1 Model domain

As part of a previous gas migration study [16], an interface to the NAMMU model used to carry out the regional groundwater flow calculations in the *Nirex 97* assessment [18] was developed. This interface obtains the values of various quantities at the location of each TOUGH2v2 grid block (strictly at its centre) from the NAMMU model. The quantities obtained in this way are the rock units, and also the pressure, the salinity and the temperature calculated for the reference groundwater flow model in *Nirex 97* (see [18]).

The interface was used to set up the model for this study. The rock units were used to define the geometry of the model, and the pressure, the salinity and the temperature were used to provide the boundary and initial conditions for the TOUGH2v2 calculations.

3.3.2 Hydrogeological properties

The hydrogeological properties of the different rock units were based on those used for the reference groundwater flow model in *Nirex 97* [18]. These properties are listed in [18].

The hydrogeological properties (see Table 3.5) were not exactly the same as those used for the reference groundwater flow model in *Nirex 97*. In the hydrogeological model underlying *Nirex 97*, the principal axes

of the permeability tensors of many rock units were taken to be aligned with bedding and the principal axes of the permeability tensors of many fault rocks were taken to be aligned with the faults. This could be represented accurately in NAMMU, which can handle arbitrary orientations of the principal axes of the permeability tensor. However, in TOUGH2v2 the permeability tensor is taken to be aligned with a grid block. This required an approximation of the properties in *Nirex 97*. The error involved is small except in highly anisotropic rocks oriented at about 45° to the horizontal (or vertical).

In the region of the repository, care was taken to align the TOUGH2v2 grid blocks with the faults. However, using the interface to the NAMMU model has made some other faults in the TOUGH2v2 grid discontinuous (see Figure 3.7). This is a particular issue towards the left-hand edge of the grid. In this region the grid was extended towards the coast, so as to be able to represent the discharge of gas dissolved in groundwater to the sea, but a coarse discretisation had to be used to keep the problem computationally manageable.

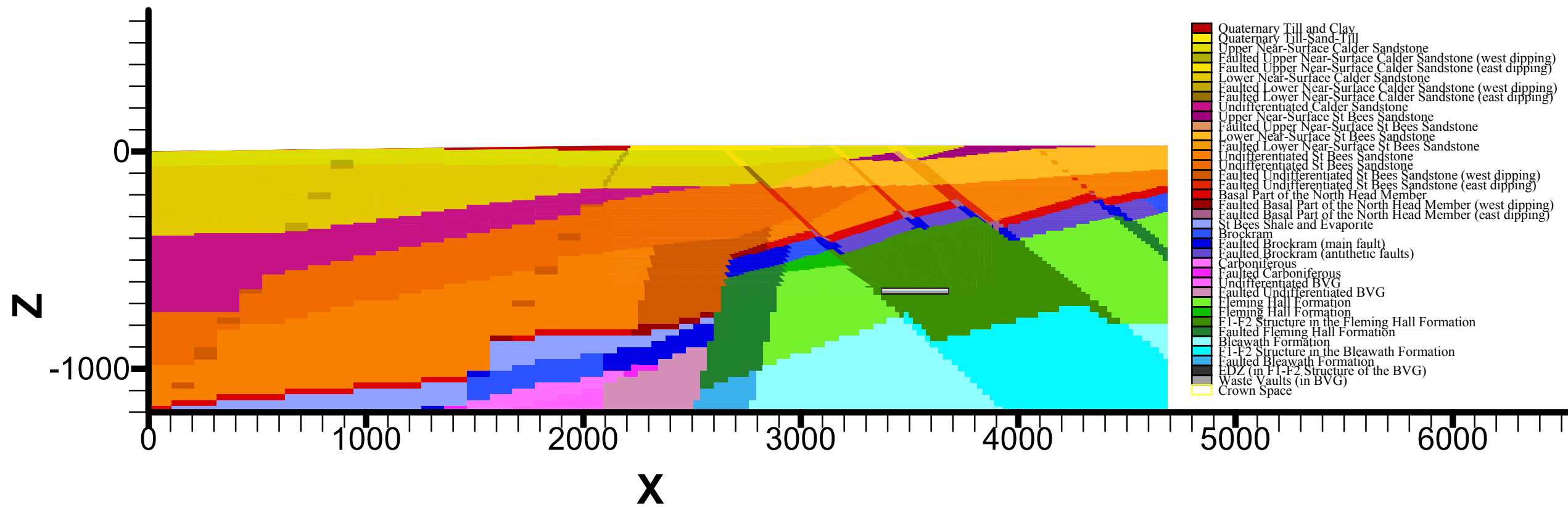


Figure 3.7 The 2D model region showing the repository and rock units.

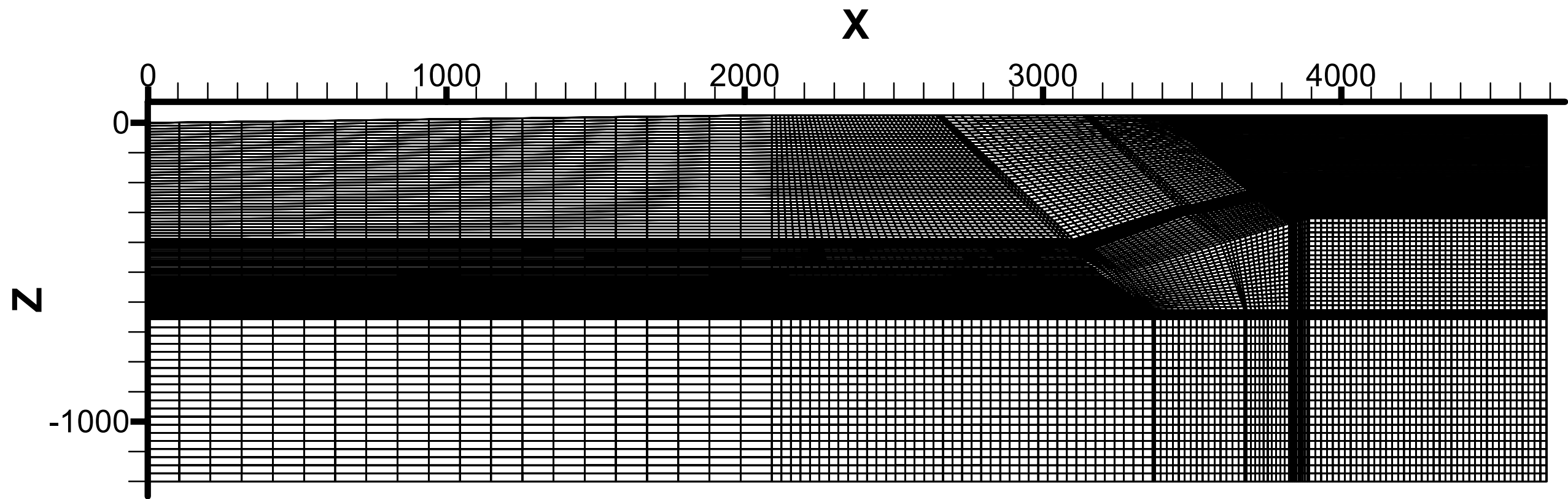


Figure 3.8 The 2D model grid.

Table 3.5 Table of Hydrogeological Properties Used in the Two-dimensional Model

Unit	Permeability (m ²)		Flow Type	Matrix Porosity	Fracture Porosity	$\frac{1}{\phi} \frac{d\phi}{dP}$
	k_x	k_z				
Quaternary Till and Clay	4.11 10 ⁻¹⁵	8.68 10 ⁻¹⁵	matrix	0.175	n/a	1.89 10 ⁻⁹
Quaternary Till-Sand-Till	1.20 10 ⁻¹³	1.04 10 ⁻¹⁴	matrix	0.175	n/a	6.81 10 ⁻⁸
Upper Near-Surface Calder Sandstone	2.34 10 ⁻¹²	1.17 10 ⁻¹³	matrix	0.187	n/a	1.25 10 ⁻⁶
Faulted Upper Near-Surface Calder Sandstone (west dipping)	2.34 10 ⁻¹²	1.17 10 ⁻¹³	fracture	n/a	2.29 10 ⁻³	1.02 10 ⁻⁴
Faulted Upper Near-Surface Calder Sandstone (east dipping)	6.58 10 ⁻¹³	3.70 10 ⁻¹³	fracture	n/a	1.50 10 ⁻³	4.39 10 ⁻⁵
Lower Near-Surface Calder Sandstone	9.00 10 ⁻¹⁴	4.50 10 ⁻¹⁴	matrix	0.187	n/a	4.77 10 ⁻⁸
Faulted Lower Near-Surface Calder Sandstone (west dipping)	9.00 10 ⁻¹⁴	4.50 10 ⁻¹⁴	fracture	n/a	7.73 10 ⁻⁴	1.16 10 ⁻⁵
Faulted Lower Near-Surface Calder Sandstone (east dipping)	6.58 10 ⁻¹³	3.70 10 ⁻¹³	fracture	n/a	1.50 10 ⁻³	4.39 10 ⁻⁵
Undifferentiated Calder Sandstone	1.08 10 ⁻¹⁴	2.74 10 ⁻¹⁵	matrix	0.201	n/a	4.92 10 ⁻⁹
Upper Near-Surface St Bees Sandstone	4.50 10 ⁻¹³	2.25 10 ⁻¹³	fracture	n/a	4.87 10 ⁻⁴	9.25 10 ⁻⁵
Faulted Upper Near-Surface St Bees Sandstone	3.28 10 ⁻¹³	1.85 10 ⁻¹³	fracture	n/a	1.19 10 ⁻³	2.76 10 ⁻⁵
Lower Near-Surface St Bees Sandstone	4.50 10 ⁻¹⁴	7.12 10 ⁻¹⁵	matrix	0.129	n/a	3.44 10 ⁻⁸
Faulted Lower Near-Surface St Bees Sandstone	3.28 10 ⁻¹³	1.85 10 ⁻¹³	fracture	n/a	1.19 10 ⁻³	2.76 10 ⁻⁵
Undifferentiated St Bees Sandstone	3.80 10 ⁻¹⁵	4.05 10 ⁻¹⁶	matrix	0.0951	n/a	3.54 10 ⁻⁹
Undifferentiated St Bees Sandstone	3.80 10 ⁻¹⁵	4.05 10 ⁻¹⁶	matrix	0.0951	n/a	3.54 10 ⁻⁹
Faulted Undifferentiated St Bees Sandstone (west dipping)	3.80 10 ⁻¹⁵	4.05 10 ⁻¹⁶	matrix	0.0951	n/a	3.54 10 ⁻⁹
Faulted Undifferentiated St Bees Sandstone (east dipping)	3.80 10 ⁻¹⁵	4.05 10 ⁻¹⁶	matrix	0.0951	n/a	3.54 10 ⁻⁹
Basal Part of the North Head Member	4.89 10 ⁻¹⁷	4.47 10 ⁻¹⁷	matrix	0.0822	n/a	5.95 10 ⁻¹¹
Faulted Basal Part of the North Head Member (west dipping)	4.89 10 ⁻¹⁷	4.47 10 ⁻¹⁷	matrix	0.0822	n/a	5.95 10 ⁻¹¹
Faulted Basal Part of the North Head Member (east dipping)	4.89 10 ⁻¹⁷	4.47 10 ⁻¹⁷	matrix	0.0822	n/a	5.95 10 ⁻¹¹
St Bees Shale and Evaporite	3.66 10 ⁻¹⁷	3.66 10 ⁻¹⁷	fracture	n/a	5.72 10 ⁻⁵	6.35 10 ⁻⁸
Brockram	4.74 10 ⁻¹⁸	4.74 10 ⁻¹⁸	matrix	0.0303	n/a	3.92 10 ⁻¹¹

Unit	Permeability (m ²)		Flow Type	Matrix Porosity	Fracture Porosity	$\frac{1}{\phi} \frac{d\phi}{dP}$
	k_x	k_z				
Faulted Brockram (main fault)	1.26 10 ⁻¹⁵	7.73 10 ⁻¹⁷	fracture	n/a	4.01 10 ⁻⁵	3.14 10 ⁻⁶
Faulted Brockram (antithetic faults)	1.26 10 ⁻¹⁵	7.73 10 ⁻¹⁷	fracture	n/a	4.01 10 ⁻⁵	3.14 10 ⁻⁶
Carboniferous	4.65 10 ⁻¹⁶	4.65 10 ⁻¹⁶	matrix	0.0133	n/a	3.04 10 ⁻⁹
Faulted Carboniferous	1.00 10 ⁻¹⁴	1.00 10 ⁻¹⁴	fracture	n/a	3.71 10 ⁻⁴	2.69 10 ⁻⁶
Undifferentiated BVG	1.26 10 ⁻¹⁷	1.26 10 ⁻¹⁷	fracture	n/a	1.51 10 ⁻⁵	8.29 10 ⁻⁸
Faulted undifferentiated BVG	1.26 10 ⁻¹⁷	1.26 10 ⁻¹⁷	fracture	n/a	1.51 10 ⁻⁵	8.29 10 ⁻⁸
Fleming Hall Formation	1.24 10 ⁻¹⁷	1.24 10 ⁻¹⁷	fracture	n/a	1.50 10 ⁻⁵	8.20 10 ⁻⁸
Fleming Hall Formation	1.24 10 ⁻¹⁷	1.24 10 ⁻¹⁷	fracture	n/a	1.50 10 ⁻⁵	8.20 10 ⁻⁸
F1-F2 Structure in the Fleming Hall Formation	6.93 10 ⁻¹⁷	6.93 10 ⁻¹⁷	fracture	n/a	2.67 10 ⁻⁵	2.59 10 ⁻⁷
Faulted Fleming Hall Formation	1.24 10 ⁻¹⁷	1.24 10 ⁻¹⁷	fracture	n/a	1.50 10 ⁻⁵	8.20 10 ⁻⁸
Bleawath Formation	2.79 10 ⁻¹⁸	2.79 10 ⁻¹⁸	fracture	n/a	9.14 10 ⁻⁶	3.01 10 ⁻⁸
F1-F2 Structure in the Bleawath Formation	8.71 10 ⁻¹⁸	8.71 10 ⁻¹⁸	fracture	n/a	1.34 10 ⁻⁵	6.47 10 ⁻⁸
Faulted Bleawath Formation	2.79 10 ⁻¹⁸	2.79 10 ⁻¹⁸	fracture	n/a	9.14 10 ⁻⁶	3.01 10 ⁻⁸
EDZ (in F1-F2 Structure of the BVG)	3.40 10 ⁻¹⁵	6.93 10 ⁻¹⁷	fracture	n/a	9.76 10 ⁻⁵	0.0
Waste Vaults (in F1-F2 Structure of the BVG)	2.03 10 ⁻¹⁶	2.03 10 ⁻¹⁶	matrix	0.0827	n/a	0.0
Crown Space †	1.00 10 ⁻¹²	1.00 10 ⁻¹²	matrix	0.245	n/a	0.0

† The crown space has a permeability that is not physical; it was chosen simply to be high enough to ensure that the calculated flow is accurate, but not so high that it leads to numerical problems.

In some of the units, as indicated, groundwater flow was considered to be predominantly through the rock matrix, and in these units the accessible porosity was taken to be the matrix porosity; whereas in other units, groundwater flow was considered to be predominantly through fractures, and for these units the accessible porosity was taken to be the fracture porosity.

This is another difference from the groundwater flow calculations carried out in *Nirex 97*. In the latter calculations, for those rocks in which flow was considered to be predominantly through fractures, this was taken into account in deriving the effective permeabilities of the rocks (listed in Table 3.5), but the groundwater travel times were nominal travel times calculated on the basis that the migrating solute would access all of the matrix porosity. The use of the fracture porosity in the gas migration calculations means that the travel times for dissolved gas in fractured rock units will not take rock-matrix diffusion into account, and will be much shorter than the groundwater travel times reported for the corresponding units in *Nirex 97*⁵.

In the direction normal to the plane of Figure 3.6, the model represents a length equal to the size of the repository. Thus the part of the model representing the repository includes the vaults (which conservatively were taken to lie along the line of the section) and the rock pillars between the vaults. In

⁵ In the calculations of radiological risk for *Nirex 97*, it was not assumed that all of the matrix porosity was accessed. Rather, the extent to which the matrix would be accessed as a result of rock-matrix diffusion was determined during the transport calculations that formed part of the risk calculations.

most cases, the permeabilities and porosities of the repository components are average values that represent the combined behaviour of the vaults and the rock pillars between them. The actual permeability of the crown space is extremely high, and use of this value would lead to numerical problems. However, the flow essentially is independent of the permeability of the crown space provided it is large, and the value of 10^{-12} m^2 used in the calculations is a value high enough to ensure that the calculated flow is accurate, but not so high that it leads to numerical problems.

In the TOUGH2v2 calculations, the compressibilities of the rocks and the groundwater were taken into account. These were represented in terms of the quantity

$$\frac{1}{\phi} \frac{d\phi}{dP}$$

where

ϕ is the porosity; and
 P is the pressure.

The values used were based on the results of the RCF3 Pump Test carried out at Sellafield [19]. This test examined the responses of different rock formations to pumping from borehole RCF3 over a period of about three months. Analysis of the results of this pump test gave typical values of the hydraulic diffusivity between about 0.01 and 0.08 m^2s^{-1} . The values of the compressibility therefore were taken to be such as to lead to a value of hydraulic diffusivity of 0.01 m^2s^{-1} . This prescription had to be modified slightly for some rock units because it led to a negative compressibility.

The prescription also had to be modified for the repository itself and for the Engineering Disturbed Zone (EDZ) immediately adjacent to the vaults and tunnel of the repository. In previous calculations [16] it was found that if the compressibilities derived from the above prescription were used, the porosities obtained in the repository and the EDZ could become unphysical. In order to avoid this problem, it was necessary to reduce the values of the compressibilities. For simplicity, the compressibilities were taken to be zero for the repository and the EDZ. The effect of this is that the modelled pressure changes propagate through these units faster than they would physically. However, the EDZ is only 8m thick in the model, and the errors introduced by the above treatment are considered small, and are conservative.

The 'compressibilities' used in the calculations are listed in Table 3.5.

It is worth noting that the compressibility is such that changes in the porosity (i.e. the fracture porosity) of the host rock are considerable during the drawdown phase. However, this was not considered to be a problem because the porosity of the host rock is very small and only a small fraction of the total gas is in the host rock. Similar problems would be encountered for some of the other rock units if there were large pressure changes in the units. However, in the calculations carried out, the pressure changes in these units were sufficiently small that problems did not arise.

3.3.3 Two-phase flow properties

Site-specific forms for the characteristic functions (or saturation functions) that characterise two-phase flow have not been measured for the rocks at Sellafield. The forms of the characteristic functions used here are realistic forms appropriate to real rocks, but are not site specific. This means that the results of the calculations, although helping to develop an understanding of how gas might migrate, should not be taken as an accurate prediction of the actual behaviour of gas migrating at Sellafield.

In the calculations, one set of characteristic functions was used for all the rock units in which groundwater flow was considered to be predominantly through the rock matrix (also described here as porous-medium flow), and a different set was used for all the rocks in which groundwater flow was considered to be predominantly through fractures.

Rock units with porous-medium flow

The characteristic functions for rock units in which groundwater flow was considered to be predominantly through the rock matrix were based on the Brooks and Corey formulation [20].

In this formulation, two different effective water saturations, S_e and S_e^* , are defined by:

$$S_e = \frac{S_w - S_r}{1 - S_r} \tag{3.1}$$

$$S_e^* = \frac{S_w - S_r}{(1 - S_{gc}) - S_r} \tag{3.2}$$

where

- S_w is the water saturation (fraction of the pore space occupied by water);
- S_r is the residual liquid saturation; and
- S_{gc} is the critical gas saturation.

The water relative permeability, k_{rw} , is given by

$$k_{rw} = S_e^{(2+3m)/m} \tag{3.3}$$

where m is a constant, and the gas phase relative permeability, k_{rg} , is given by

$$k_{rg} = (1 - S_e^*)^2 (1 - S_e^{*(2+m)/m}) \tag{3.4}$$

The capillary pressure, p_c , is given by

$$p_c = \frac{p_d}{S_e^{1/m}} \tag{3.5}$$

where

- p_d is the displacement pressure, which is a constant.

The parameter values used in the above equations are summarised in Table 3.6.

Table 3.6 Parameters for Brooks and Corey Characteristic Functions (Used for Rock Units in Which Groundwater Flow was Considered to be predominantly Through the Rock Matrix)

S_r	S_{gc}	m
0.273	0.0	0.85

The gas entry pressure (i.e. displacement pressure) of a hydrogeological unit was taken to be correlated with its permeability [17] according to

$$p_d = 5.874 \times 10^{-6} \left(\frac{1}{k} \right)^{0.33} \quad (3.6)$$

where

k is the permeability [m^2]; and
 p_d is the gas entry pressure [MPa].

The Brooks and Corey capillary pressure is discontinuous as the water saturation tends to 1, but TOUGH2v2, like most multi-phase codes, requires continuous characteristic functions. Therefore the discontinuity was 'smoothed' by modifying the capillary pressure as follows

$$p_c = \frac{p_d}{S_e^{1/m}} \tanh\left(\frac{1 - S_w}{\delta}\right) \quad (3.7)$$

where

δ is a constant, which was taken to be 0.01 in the calculations.

In addition, although a porous medium prescription was adopted for the repository, the capillary pressure in the repository was taken to be zero (as for rock units in which the flow is considered to be predominantly through fractures, see below). This was done in the original *techSIM* calculations for *Nirex 97* [9] in order 'to avoid spurious flows resulting purely from artificial differences in capillary pressure function between the repository and the host rock'. The same approach was used for the TOUGH2v2 calculations presented here. (However, it is noted that real differences between the capillary pressure of the cementitious backfill and the crown space are likely to cause the former to resaturate preferentially.)

Rock units with flow through fractures

For units where the predominant flow is considered to be through fractures, the relative permeabilities were taken to be linear functions of saturation and the capillary pressure was taken to be zero, as specified in Table 3.7 ($S_g = 1 - S_w$ is the gas saturation).

Table 3.7 Parameters for Linear Characteristic Functions (Used for Rock Units in Which Groundwater Flow was Considered to be predominantly Through Fractures)

S_g	k_{rg}	k_{rw}	p_c (MPa)
0.0	0.0	1.0	0.0
1.0	1.0	0.0	0.0

3.3.4 Miscellaneous properties

The gas phase was taken to behave as an ideal gas. The molar masses of the gases of interest are given in Table 3.8.

Table 3.8 Molar Masses of Gases

Gas	Molar Mass (g mol ⁻¹)
Hydrogen	2.01588
Methane	16.0428
Active methane	18.0

The Henry's constants for the gases of interest are listed in Table 3.9.

Table 3.9 Henry's Constants for Gases

Hydrogen	1.3985 10 ⁻¹⁰
Methane	2.3478 10 ⁻¹⁰
Active methane	2.3478 10 ⁻¹⁰

Although diffusion was not expected to be a significant process, it was included for completeness. The diffusion coefficients in the aqueous phase are listed in Table 3.10.

Table 3.10 Diffusion Coefficients in Aqueous Phase

Solute	Diffusion Coefficient at 25°C (m ² s ⁻¹)	Reference
Water (self diffusion coefficient)	2.2 10 ⁻⁹ (0.0 was used in the calculations for numerical reasons)	[21]
Hydrogen	4.50 10 ⁻⁹	[22]
Methane	1.49 10 ⁻⁹	[22]
Active methane	1.49 10 ⁻⁹	[22]

The diffusion coefficients in the bulk gas (i.e. hydrogen) phase are given in Table 3.11.

Table 3.11 Diffusion Coefficients in Gas Phase.

Solute	Diffusion coefficient at 25°C (m ² s ⁻¹)	Reference
Water vapour (in air, not hydrogen)	$D = 1.87 \cdot 10^{-10} T^{2.072} \frac{1}{P} = \frac{2.49 \cdot 10^{-5}}{P}$	[23]

Hydrogen (self diffusion coefficient)	$D = \frac{1.45 \cdot 10^{-5}}{P}$ (0.0 was used in the calculations for numerical reasons)	[24]
Methane	$D = 3.13 \cdot 10^{-9} T^{1.765} \frac{1}{P} = \frac{7.25 \cdot 10^{-5}}{P}$	[23]
Active methane	$D = 3.13 \cdot 10^{-9} T^{1.765} \frac{1}{P} = \frac{7.25 \cdot 10^{-5}}{P}$	[23]

In TOUGH2v2, the tortuosity (which is the inverse of the tortuosity defined in *Nirex 97*) of the crown space was taken to be 1.0. The tortuosity of the fractured rocks was taken to be 0.5. (It should be noted that the gas migration calculations considered only the fractures, and therefore the tortuosity is that of the fracture network and not the rock matrix.)

In TOUGH2v2, the tortuosity of the cementitious backfill (i.e. the NRVB) was taken to be 0.15. This value was derived from an analysis of data in [25]. In the NRVB, the intrinsic diffusion coefficient of tritiated water was measured to be about $6.0 \cdot 10^{-11} \text{ m}^2\text{s}^{-1}$, and the capacity factor was measured to be about 0.2. Hence, the tortuosity is

$$\frac{D_i}{\alpha D_m} = \frac{6 \cdot 10^{-11}}{0.2 \times 2 \cdot 10^{-9}} = 0.15 \quad (3.8)$$

where

- D_i is the intrinsic diffusion coefficient;
- D_m is the free-water or molecular diffusion coefficient; and
- α is the capacity factor.

In TOUGH2v2, the tortuosity values of the porous-medium rocks were obtained from the *Nirex 97* assessment [9]. The values are shown in Table 3.12.

Table 3.12 Tortuosity Values of the Porous-medium Rocks

Unit	Tortuosity in <i>Nirex 97</i> (τ)	Tortuosity in TOUGH2v2 ($\frac{1}{\tau}$)
Calder sandstone	7.76	0.13
St Bees sandstone	10.5	0.095
Shales / Evaporites / Brockram	16.6	0.060

As in the *Nirex 97* assessment [9], the Quaternary units took the tortuosity value of the Calder sandstone, and the carboniferous units took the tortuosity value of the St Bees sandstone.

3.3.5 Results

Calculations were carried out for a base case, and for a variant intended to explore the sensitivity of the results of the calculations to the value of a key parameter.

It was originally intended to carry out the TOUGH2v2 calculations with the EOS7R fluid property module. This module extends the EOS5 module used previously [16] to include brine and two additional mass components, which could be either bulk or active gases. EOS7R, for example, could be used to model hydrogen, methane and ^{14}C in methane. However, numerical difficulties, which could not be resolved during the course of this study, meant it was not practicable to carry out the gas migration calculations with the EOS7R module, and so the EOS5 module was used instead.

The use of the EOS5 module will give a realistic prediction of the migration of the bulk gas (i.e. hydrogen). Then in order to assess the consequences of the release of the active gases (in particular $^{14}\text{CH}_4$) from the repository, it is necessary to be able to relate the flows of these gases to the flows of the bulk gas.

Figure 3.9 demonstrates that the release rate of $^{14}\text{CH}_4$ is approximately related to the generation rate of hydrogen in the repository, i.e.

$$\text{release rate of } ^{14}\text{CH}_4 [\text{TBq a}^{-1}] \approx 2 \cdot 10^{-5} \exp(-\lambda t) \text{ generation rate of hydrogen } [\text{m}^3 \text{a}^{-1}] \quad (3.9)$$

where

- λ is the decay constant for ^{14}C [a]; and
- t is the time post-closure [a].

Since methane has relevant properties, and in particular Henry's constant (see Table 3.10), that are not very different to those of hydrogen, it is suggested that the outflows of ^{14}C in methane may be estimated by using Equation (3.9) to scale the outflows of bulk gas from the model.

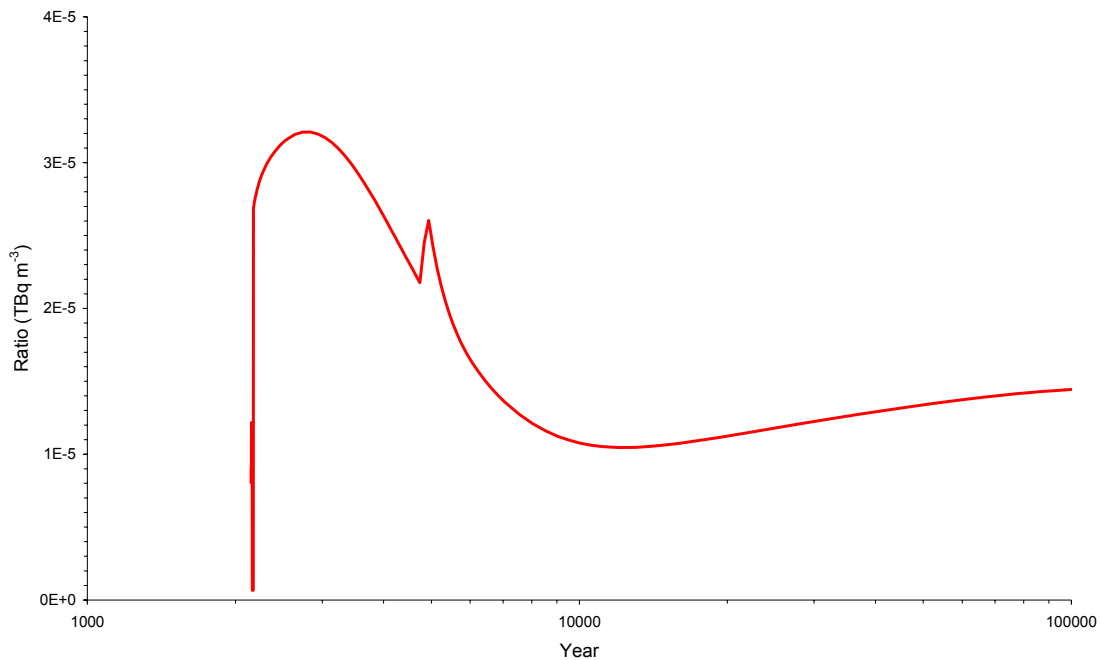


Figure 3.9 Ratio of the release rate of $^{14}\text{CH}_4$ to the generation rate of H_2 . The release rate of $^{14}\text{CH}_4$ has been adjusted so that it does not include radioactive decay.

The results of the various calculations are given below. Unlike the one-dimensional models, a drawdown phase is modelled in these calculations.

Base case

The results obtained from the TOUGH2v2 model are in accord with the expected evolution of the system [16].

The presence of the repository at atmospheric pressure before closure leads to a drawdown region around the repository where the pressure is reduced from hydrostatic and where groundwater flows towards the repository. For the parameter values considered, the drawdown region grows rapidly to a limiting size after repository construction.

After repository closure, the pressure in the drawdown region quickly returns to values close to hydrostatic (see Figure 3.10).

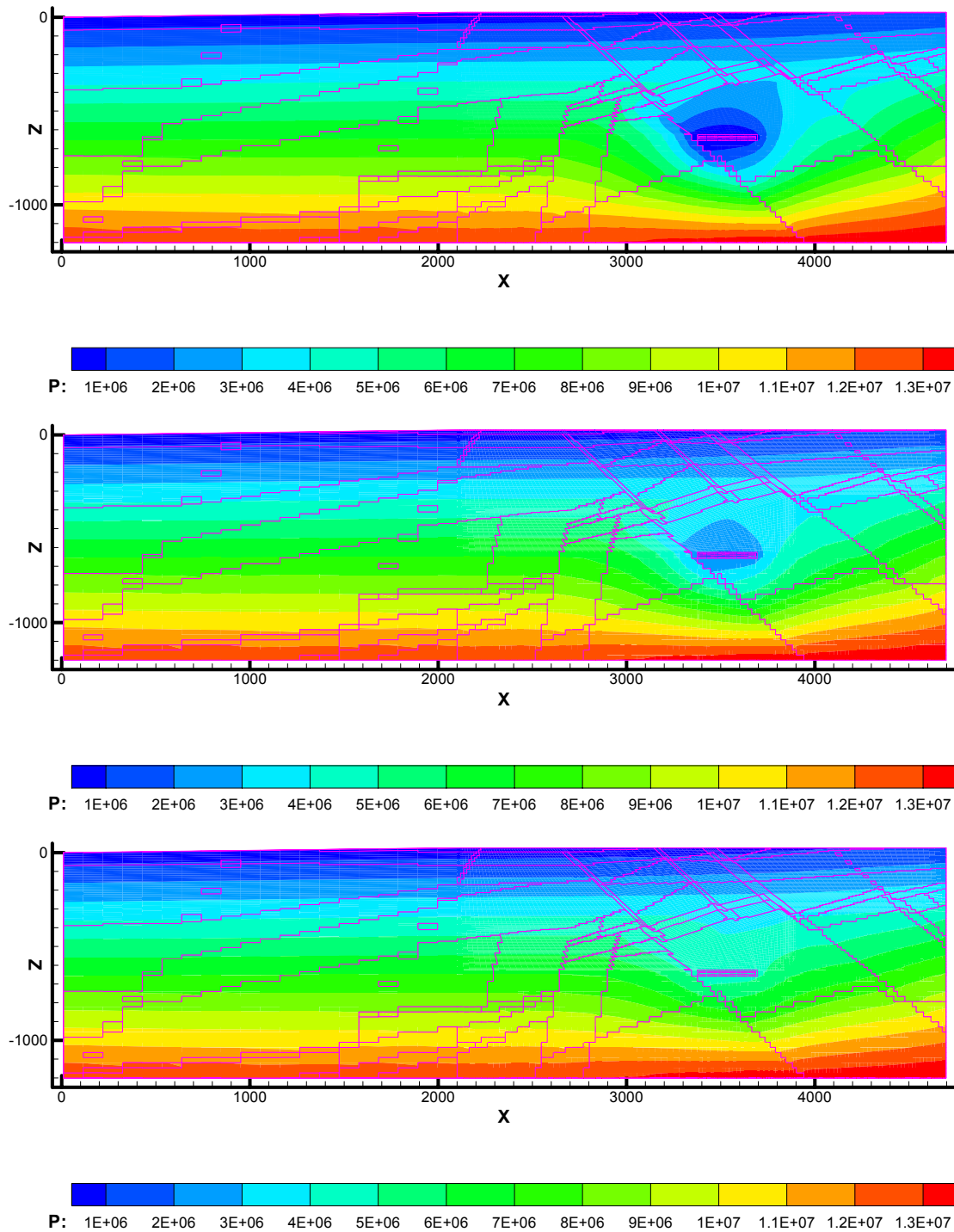


Figure 3.10 Pressure for the Reference case rate of gas generation and the 2D model. The top figure is at the end of the drawdown phase, 110 years after repository construction, the middle figure is 10 years post-closure, and the bottom figure is 14 years post-closure.

After closure, once the groundwater flowing into the repository is no longer drained and the generated gas is not removed, the pressure of the gas in the repository starts to build up and in a short time rises slightly over the hydrostatic pressure at the repository location. For the case considered, with a fractured

host rock, the amount by which the gas pressure in the repository overshoots hydrostatic pressure is small (see Section 3.1.2), and unlikely to lead to the rock fracturing.

Once the gas pressure in the repository has risen sufficiently (to a fraction of hydrostatic pressure), free gas is able to migrate out of the repository. It then moves upward through the host rock and overlying rocks until it comes to the Basal North Head Member (Figure 3.11). The gas moves in the Brockram beneath the Basal North Head Member up to the location where a major fault breaks the continuity of the Basal North Head Member. A gas pocket forms here (Figure 3.12). The pressure in the pocket increases, and ultimately the free gas moves from the pocket into the Faulted Undifferentiated St Bees Sandstone and then upward (Figure 3.13). As the gas migrates it dissolves in the groundwater (Figure 3.14). In fact, free gas did not break through at the surface, but all the gas dissolved (Figure 3.15).

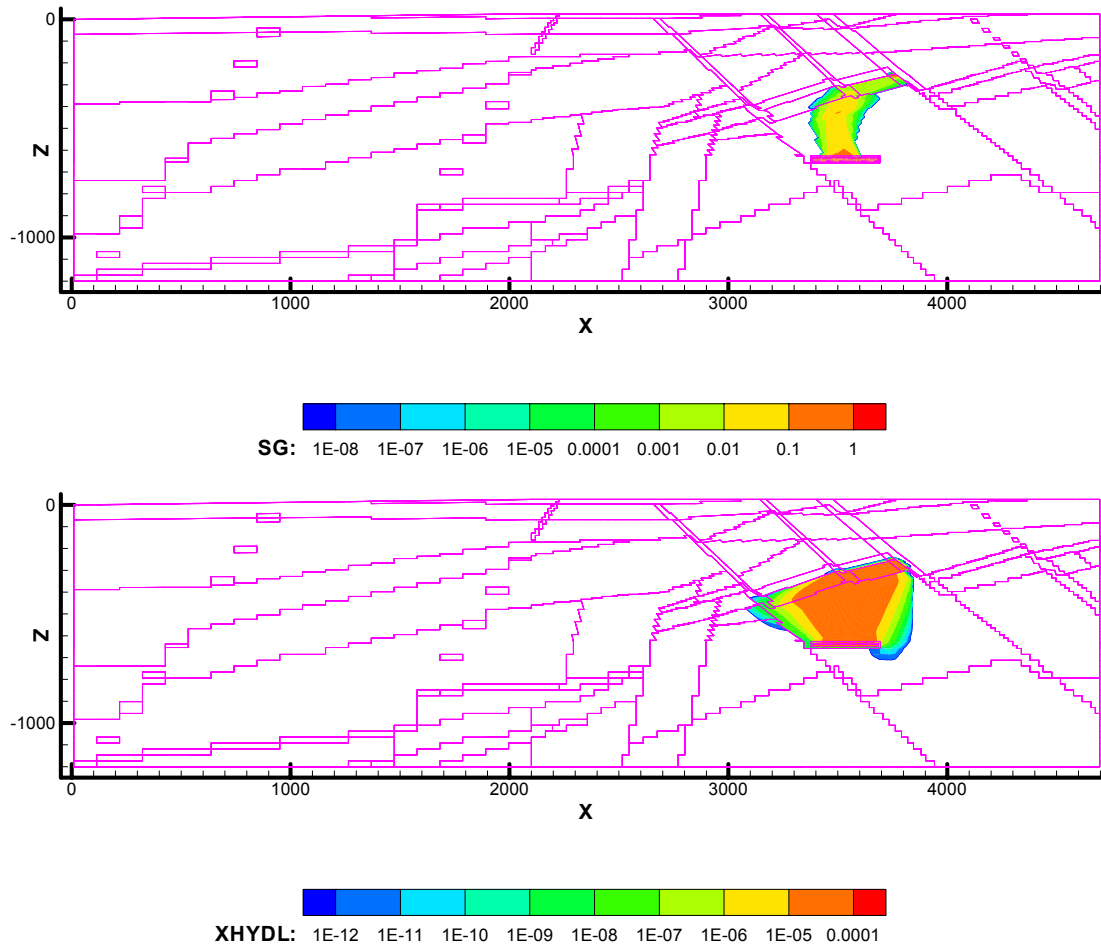


Figure 3.11 Gas saturation (top) and mass fraction of gas dissolved in liquid (bottom) 15 years post-closure.

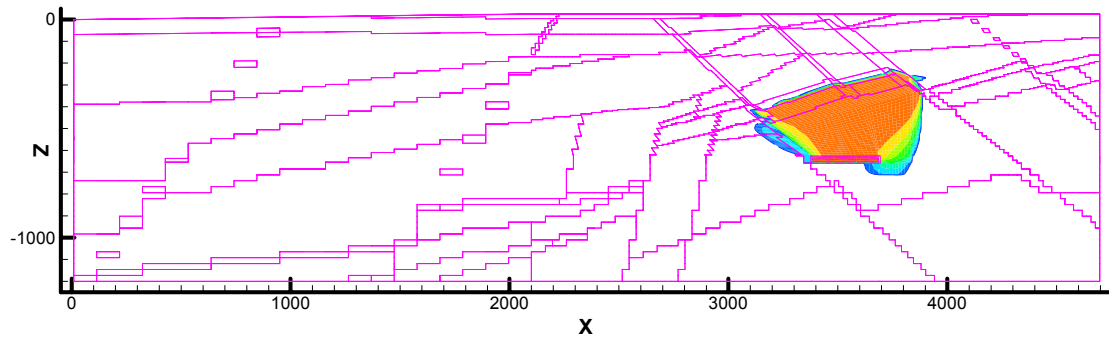
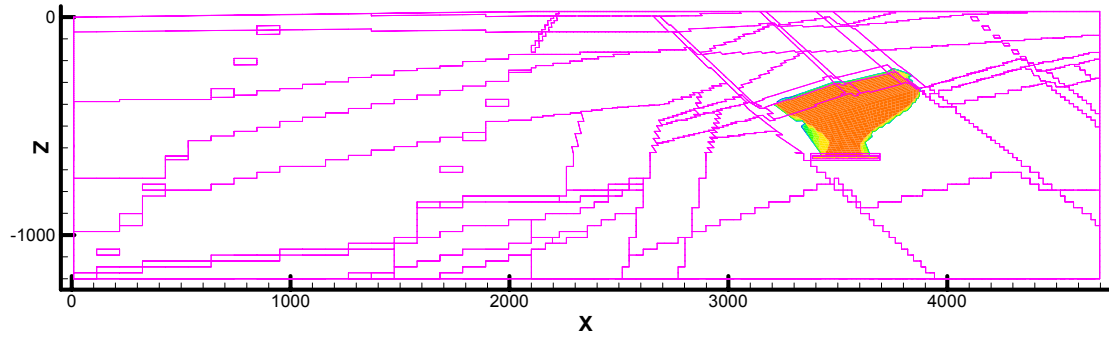


Figure 3.12 Gas saturation (top) and mass fraction of gas dissolved in liquid (bottom) 16 years post-closure.

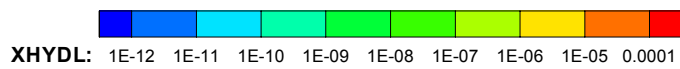
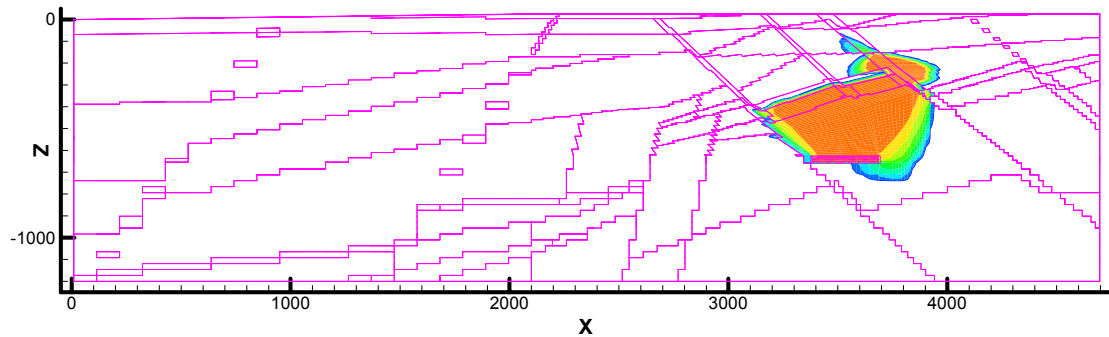
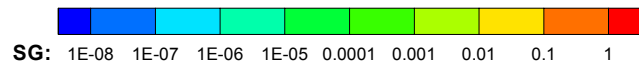
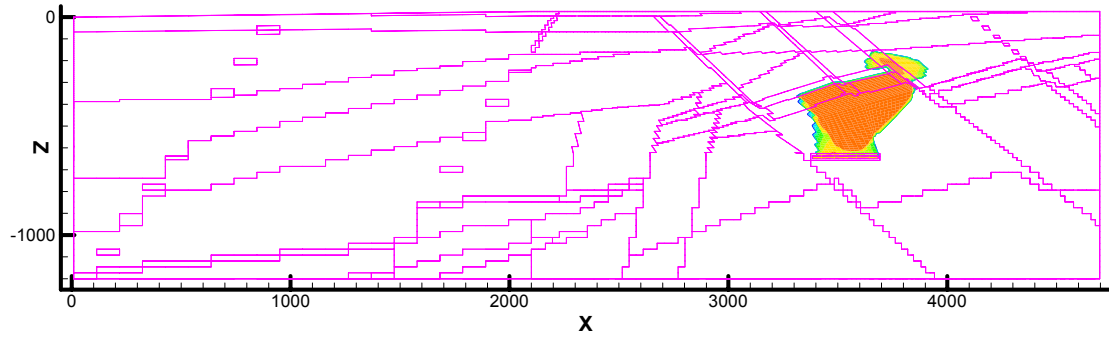


Figure 3.13 Gas saturation (top) and mass fraction of gas dissolved in liquid (bottom) 25 years post-closure.

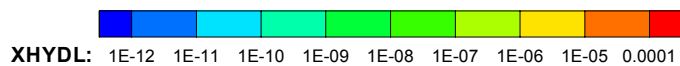
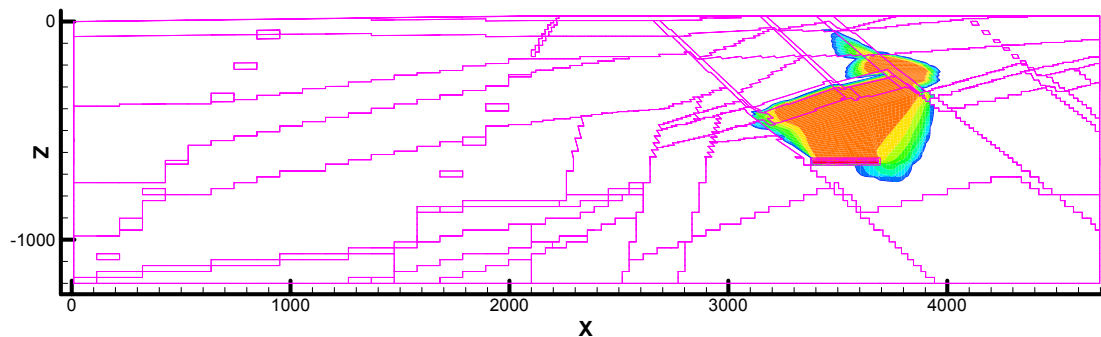
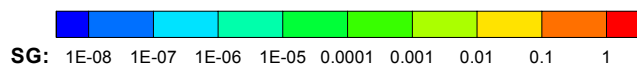
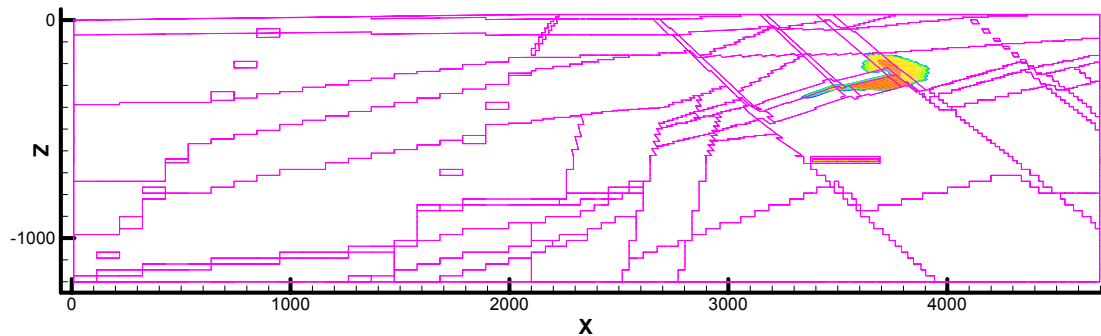


Figure 3.14 Gas saturation (top) and mass fraction of gas dissolved in liquid (bottom) 26 years post-closure.

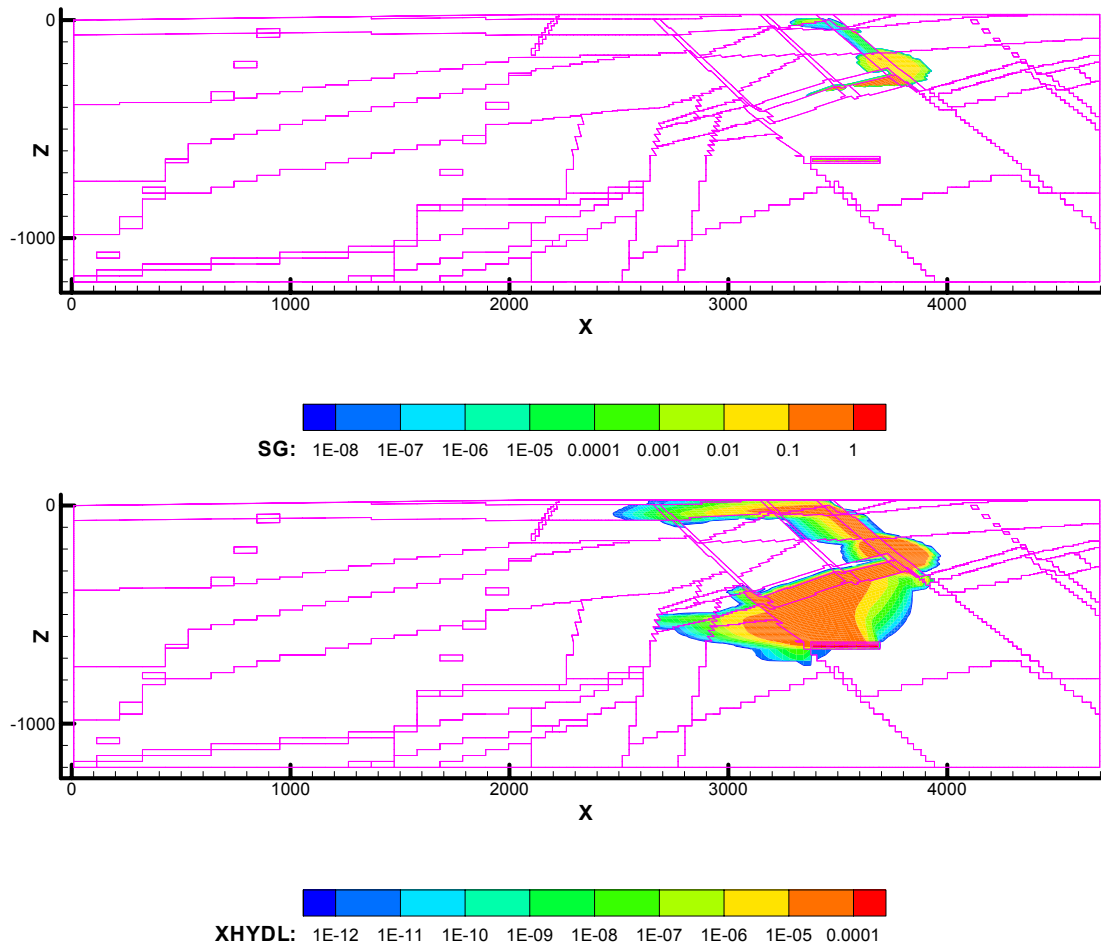


Figure 3.15 Gas saturation (top) and mass fraction of gas dissolved in liquid (bottom) 33 years post-closure.

Later, the pore water in the repository becomes saturated with gas. Dissolved gas from the repository is transported upward in the groundwater through the host rock and overlying rocks. As the groundwater rises the pressure falls, and therefore some of the gas comes out of solution and collects in another region of non-zero gas saturation below the Basal North Head Member (Figure 3.16). This region of non-zero gas saturation grows until eventually it connects back to the repository, forming a stable 'gas pathway'. Free gas from the 'gas pathway' moves into, and ultimately through, the Basal North Head Member. As this free gas continues to migrate it dissolves in the groundwater in the Faulted Undifferentiated St Bees Sandstone (Figure 3.17). The plume of dissolved gas that is formed flows at a greater depth than the original plume.

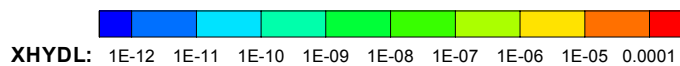
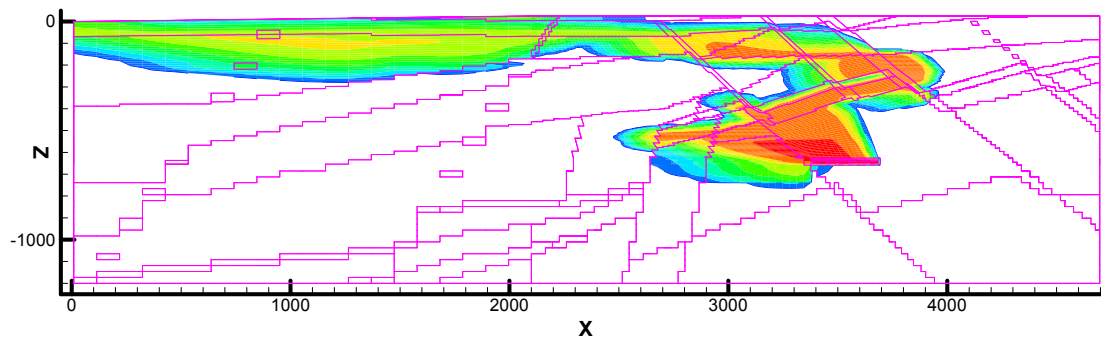
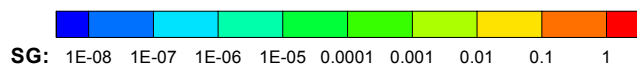
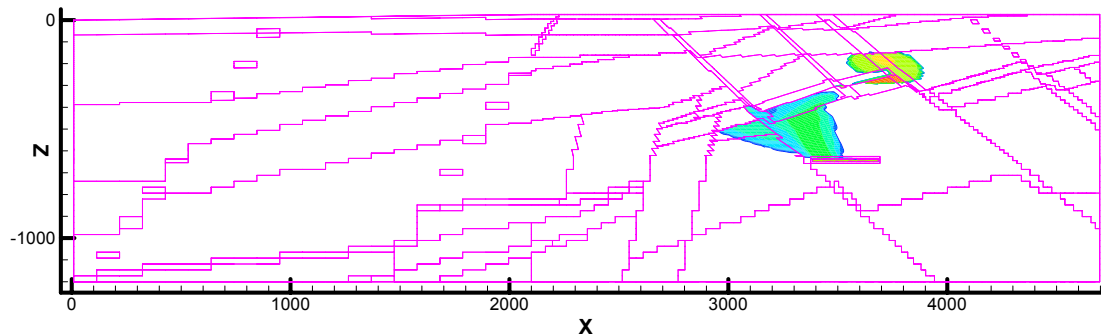


Figure 3.16 Gas saturation (top) and mass fraction of gas dissolved in liquid (bottom) 240 years post-closure.

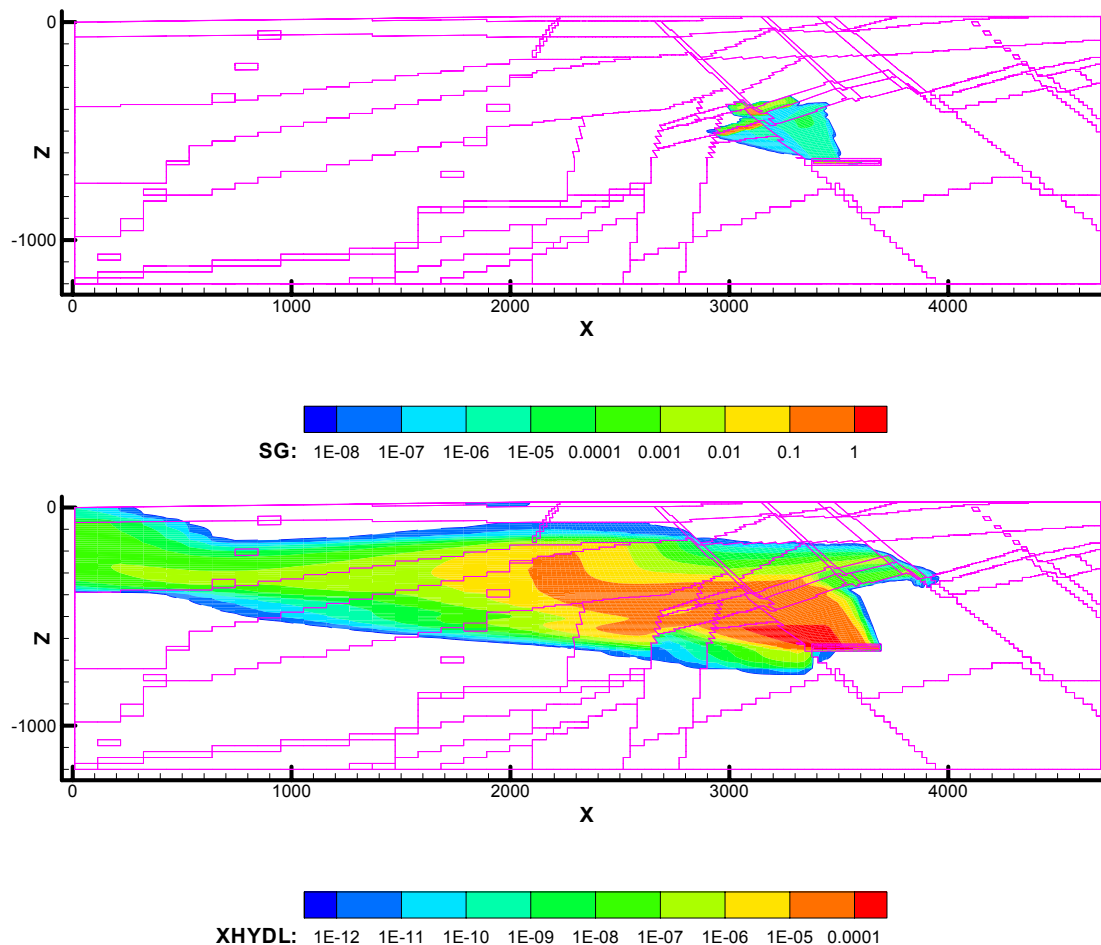


Figure 3.17 Gas saturation (top) and mass fraction of gas dissolved in liquid (bottom) 8,150 years post-closure.

To assess the consequences of the post-closure release of gas from the repository, it is necessary to have quantitative information on where the gas is going.

Over the 10,000 year duration of the simulation, about $1.2 \cdot 10^6$ kg (or $1.3 \cdot 10^7$ m³ at STP) of bulk gas (i.e. hydrogen) are injected into the model.

Figure 3.18 shows the flows of gas out of the repository as a function of time. For some time after closure, the generated gas is trapped within the repository by the pressure gradients associated with the groundwater inflow to the repository because of the drawdown. During this period, the gas pressure rises as more gas is generated and as the groundwater flowing into the repository compresses the trapped gas. The gas pressure increases to the point where free gas is able to escape from the repository. (The pressure is still below hydrostatic pressure.) The free gas then flows out of the repository and migrates upward through the BVG and Brockram to the bottom of the Basal North Head Member. About 10 years later, when much of the free gas has been released, resaturation of the repository is complete. At this point the existing free gas pathway collapses, and the dominant process for gas to escape from the repository becomes advection of dissolved gas in the groundwater. This process leads to the growth of a second region of non-zero gas saturation (see Figure 3.16), and then, at about 2320 AD, a new free gas pathway forms connecting the region to the repository. Once this new pathway has formed, free gas again starts to flow out of the repository.

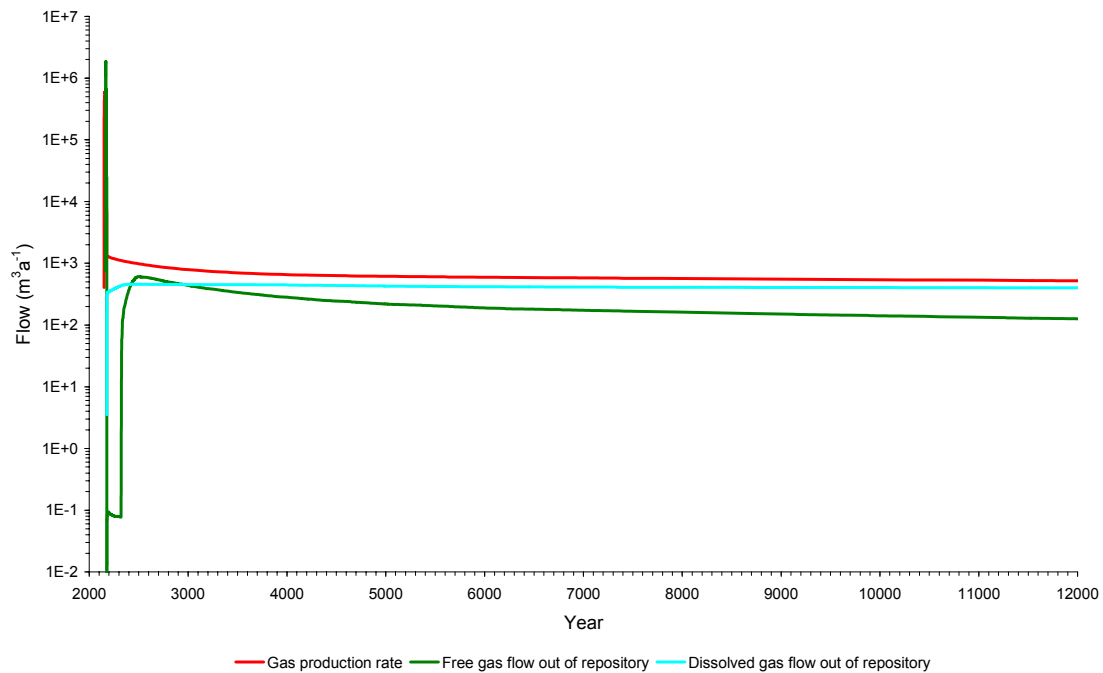
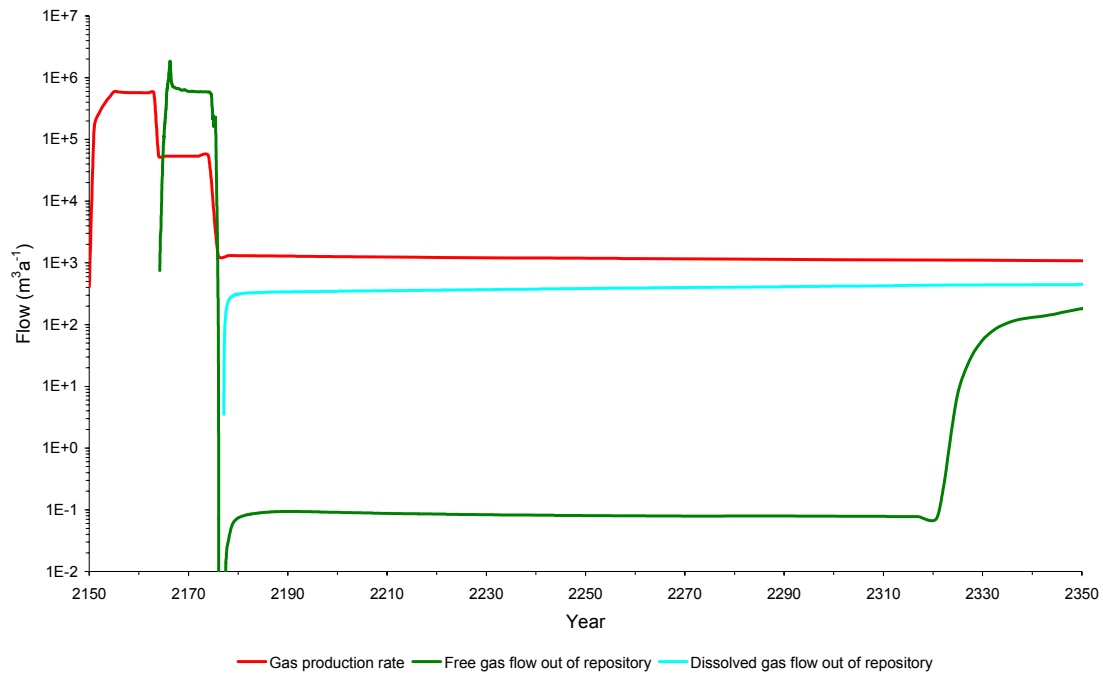


Figure 3.18 Flows of gas out of the repository as a function of time.

Of the total quantity of gas injected into the model, about $9 \cdot 10^5$ kg (or $1.0 \cdot 10^7$ m³ at STP) are stored in the geosphere. Figure 3.19 and Figure 3.20 show the variation of the mass of gas with time in the different rock units. These graphs are consistent with the existence of the two distinct routes by which gas migrates through the geosphere:

- In the first route, which persists for only a few hundred years post-closure, gas moves in the Brockram beneath the Basal North Head Member up to the location where a major fault breaks the continuity of the Basal North Head Member. A gas pocket forms, and ultimately free gas moves from

the pocket into the Faulted Undifferentiated St Bees Sandstone and then upward. As the gas migrates it dissolves in the groundwater.

- In the second route, which succeeds the first, groundwater saturated with gas rises and consequently some gas comes out of solution and collects in a region of non-zero gas saturation below the Basal North Head Member. This region grows until eventually it connects back to the repository, forming a stable 'gas pathway'. Free gas from the 'gas pathway' moves into, and ultimately through, the Basal North Head Member. As this free gas continues to migrate it dissolves in the groundwater in the Faulted Undifferentiated St Bees Sandstone.

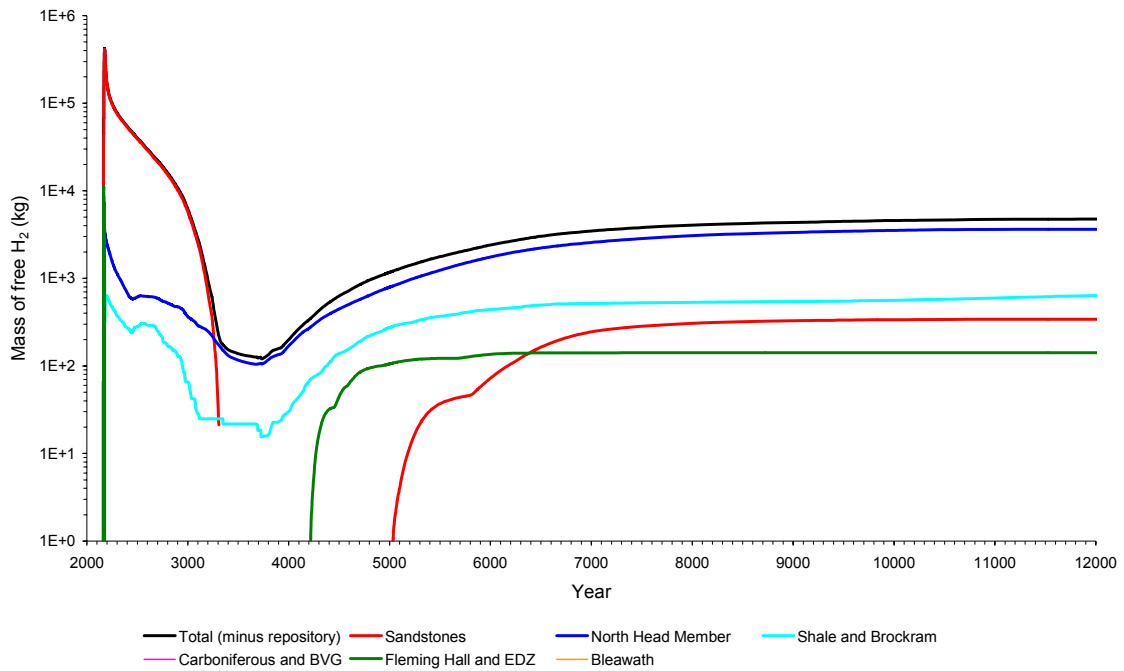


Figure 3.19 Variation of the mass of free gas with time in the different rock units (the total mass of free gas is shown by the black curve).

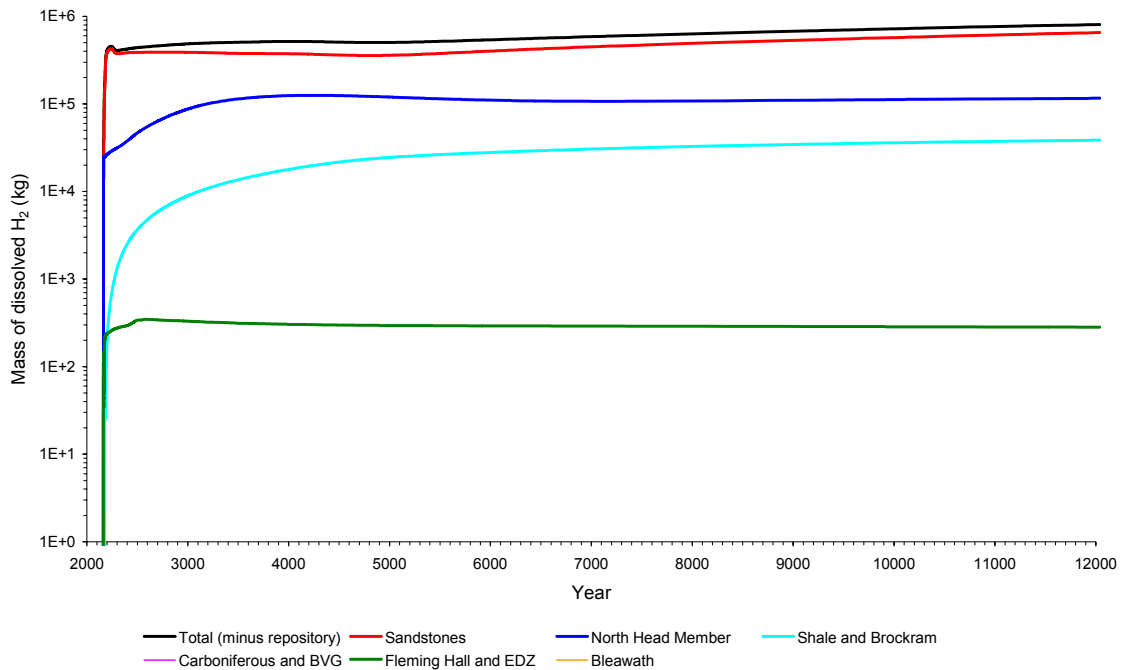


Figure 3.20 Variation of the mass of dissolved gas with time in the different rock units (the total mass of free gas is shown by the black curve).

The remainder of the gas injected into the model, that is about 3×10^5 kg (or 3×10^6 m³ at STP), flows out through the boundaries of the model (see Figure 3.21). In this case, free gas did not break through at the surface, and so only the flows of dissolved gas are shown. After the first couple of hundred years, the flow across the left-hand boundary dominates the outflow. The left-hand boundary of the model is at the coast, and therefore it is assumed that the flows across this surface are discharging to sea and can be ignored in an assessment of the consequences of the post-closure release of gas from the repository.

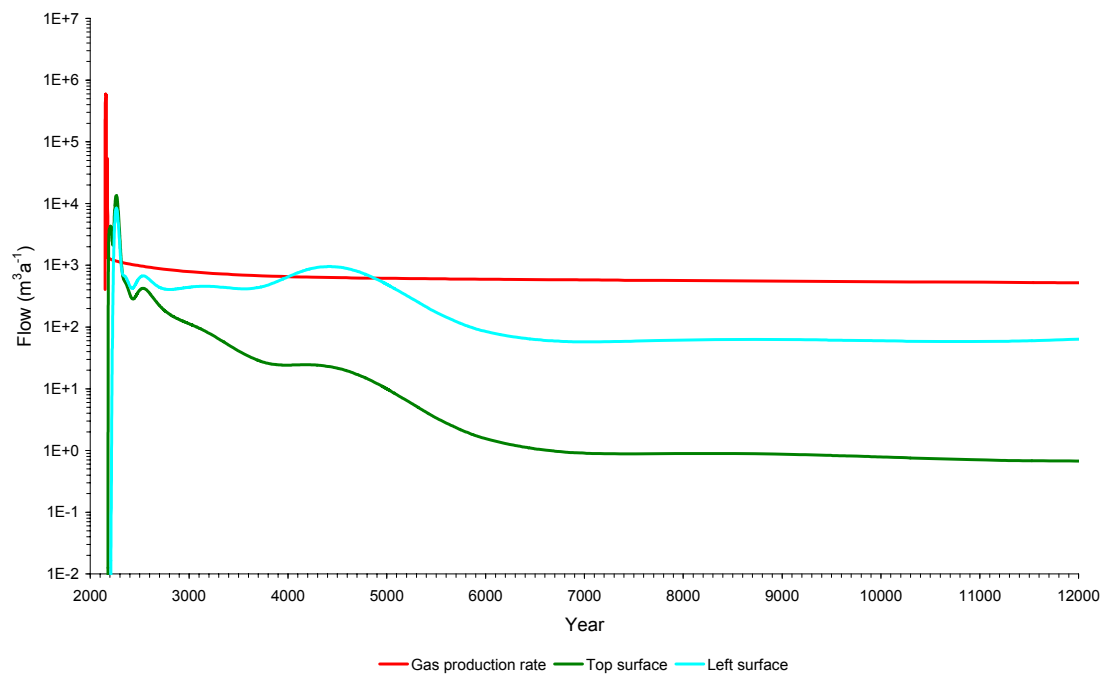
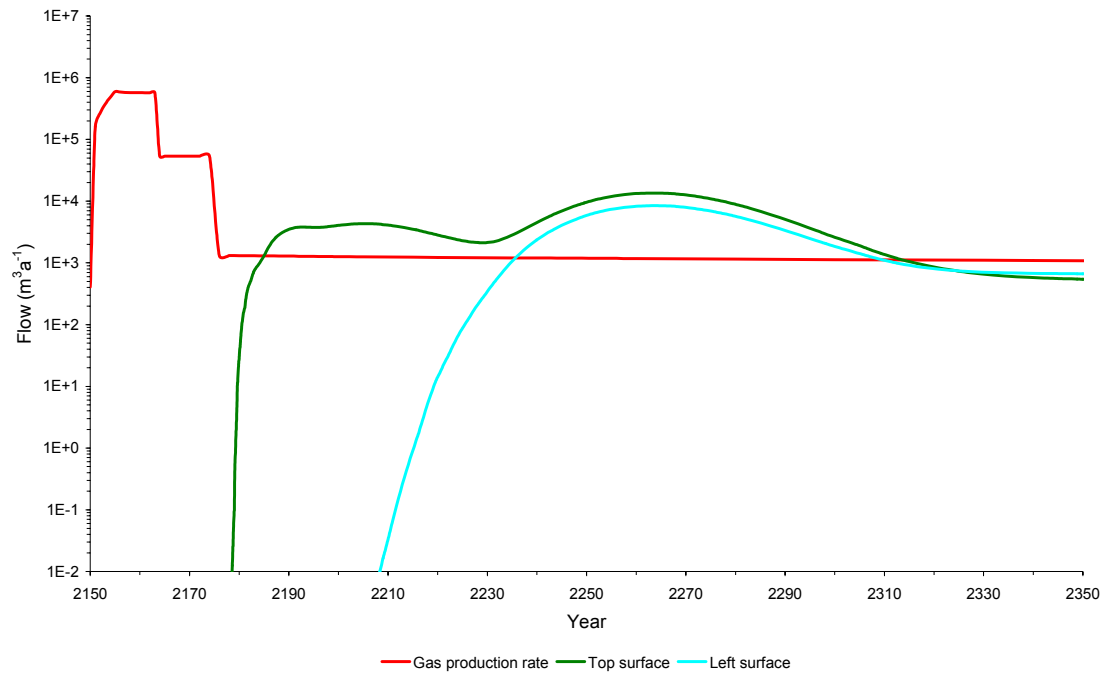


Figure 3.21 Flows of dissolved gas across the boundary of the model as a function of time.

Variant cases

One particularly important issue that will affect the migration of gas is the extent to which the gas dissolves in the groundwater. This is determined by the volume of groundwater contacted by the migrating free gas and by the gas solubility, which itself is a function of pressure, temperature and salinity. In the TOUGH2v2 calculations it is assumed that the free gas which migrates into a grid block contacts all of the groundwater within the grid block. In reality, gas may follow a number of pathways through the volume of rock represented by the block and may contact a much smaller volume of groundwater. This is a well-known phenomenon, which is referred to as ‘viscous fingering’. This could

mean that much less gas would dissolve and so more would migrate as free gas, which would have a significant effect on the gas migration.

TOUGH2v2 is based on the use of quantities that represent averages over grid blocks, and so it would be difficult to represent the possibility that gas contacts only part of the groundwater in the grid block. (This would require the use of separate variables to represent the water contacted by gas and the water not contacted by gas, which would imply a major change to TOUGH2v2.) However, the effect of the gas contacting only a fraction of the groundwater within a grid block can be mimicked to some extent by reducing the gas solubility. This required that the code be modified, but the change was small – it was simply necessary to reduce the value of Henry's constant. TOUGH2v2 therefore was modified to use a value of Henry's constant reduced by either one or two orders of magnitude and corresponding variant calculations were undertaken. It should be emphasised that the calculations are artificial, in that the gas solubility cannot be altered in reality, but nevertheless, the calculations provide a useful guide to what would happen if the gas were able to contact only a fraction of the groundwater in a grid block.

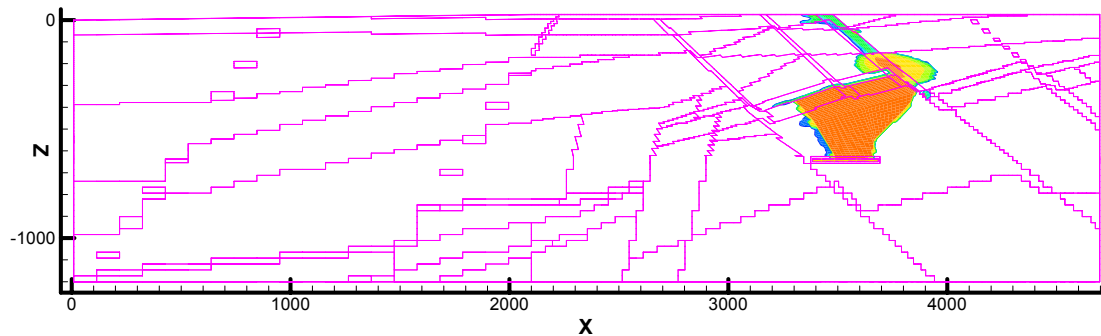
This was the only one of the variants considered in a previous gas migration study [16] for which free gas did break through at the surface.

Gas solubility reduced to 1% of its real value

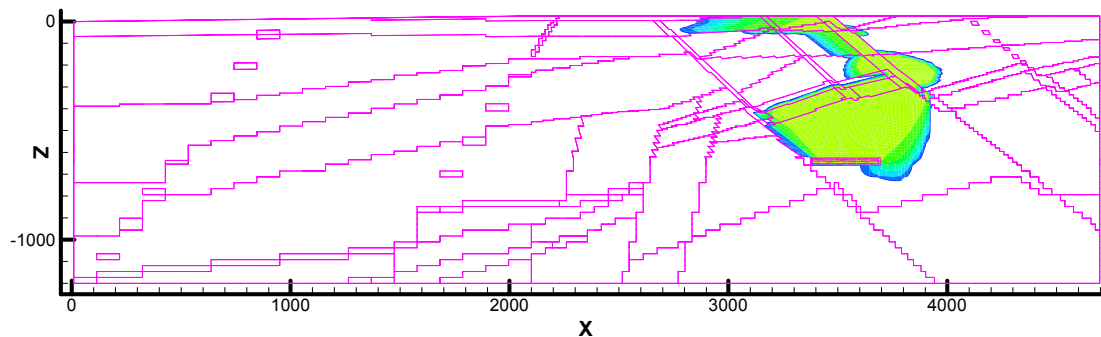
Figures 3.22–26 show the gas pathway for a variant in which Henry's constant is reduced by two orders of magnitude.

Free gas migrates out of the repository, and then moves upward through the host rock and overlying rocks until it comes to the Basal North Head Member. The gas moves in the Brockram beneath the Basal North Head Member up to the location where a major fault breaks the continuity of the Basal North Head Member. A gas pocket forms here. The pressure in the pocket increases, and ultimately the free gas moves from the pocket into the Faulted Undifferentiated St Bees Sandstone and then upward along the major fault. Free gas breaks through at the surface at 25 years post-closure (Figure 3.22).

Initially the flow of free gas is localised, but then it spreads out below the surface (Figure 3.23 and Figure 3.24) before breaking up (Figure 3.25).

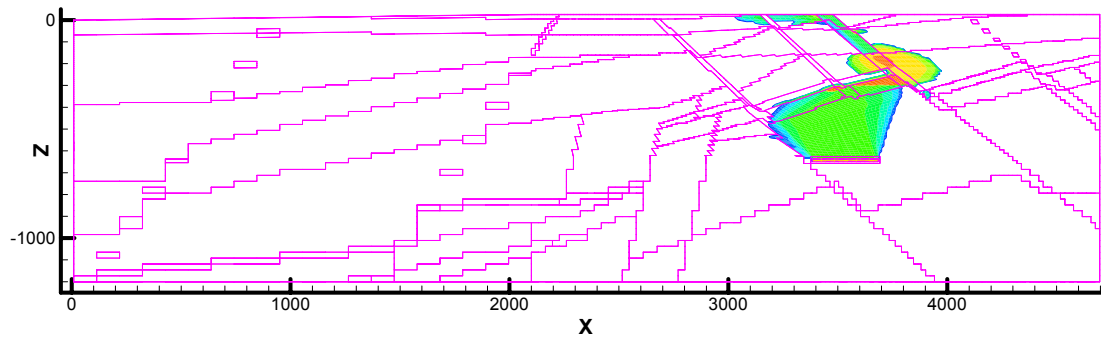


SG: 1E-08 1E-07 1E-06 1E-05 0.0001 0.001 0.01 0.1 1

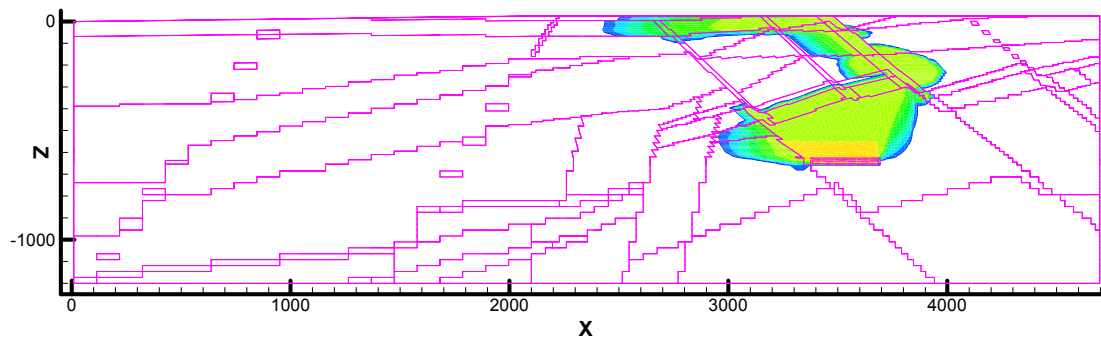


XHYDL: 1E-12 1E-11 1E-10 1E-09 1E-08 1E-07 1E-06 1E-05 0.0001

Figure 3.22 Gas saturation (top) and mass fraction of gas dissolved in liquid (bottom) 25 years post-closure. (In this variant, the gas solubility is reduced to only 1% of its true value.)

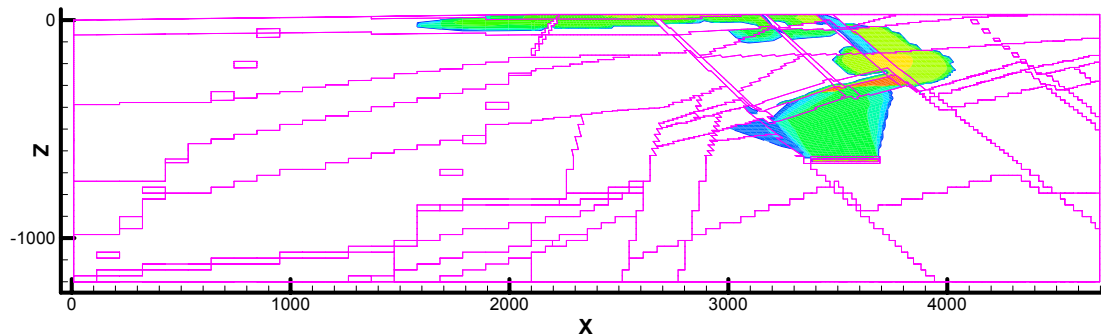


SG: 1E-08 1E-07 1E-06 1E-05 0.0001 0.001 0.01 0.1 1

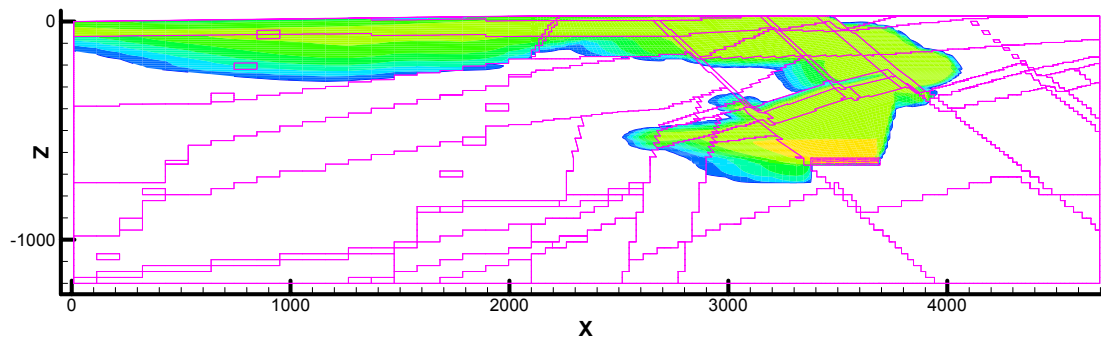


XHYDL: 1E-12 1E-11 1E-10 1E-09 1E-08 1E-07 1E-06 1E-05 0.0001

Figure 3.23 Gas saturation (top) and mass fraction of gas dissolved in liquid (bottom) 30 years post-closure. (In this variant, the gas solubility is reduced to only 1% of its true value.)

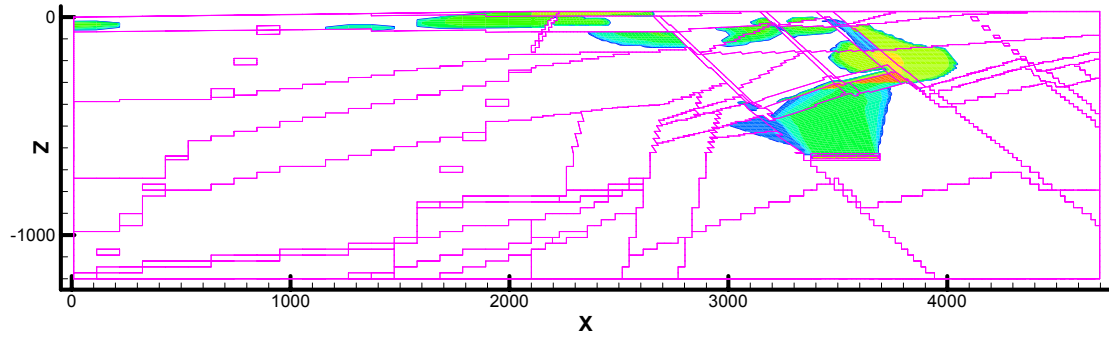


SG: 1E-08 1E-07 1E-06 1E-05 0.0001 0.001 0.01 0.1 1

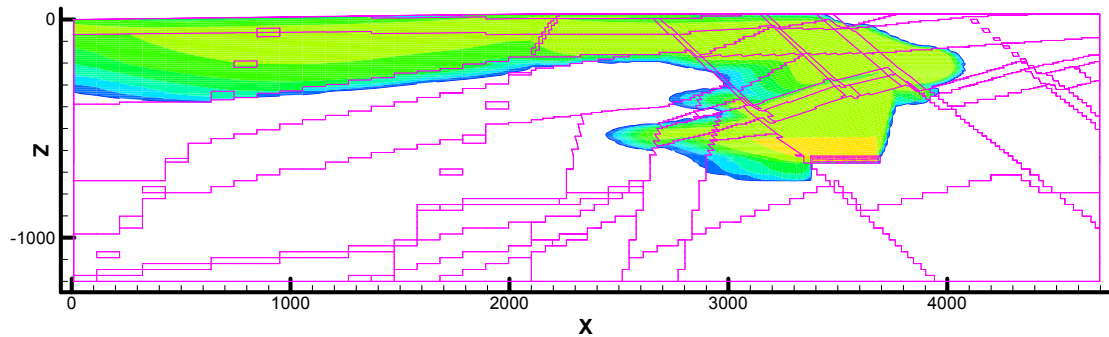


XHYDL: 1E-12 1E-11 1E-10 1E-09 1E-08 1E-07 1E-06 1E-05 0.0001

Figure 3.24 Gas saturation (top) and mass fraction of gas dissolved in liquid (bottom) 250 years post-closure. (In this variant, the gas solubility is reduced to only 1% of its true value.)



SG: 1E-08 1E-07 1E-06 1E-05 0.0001 0.001 0.01 0.1 1



XHYDL: 1E-12 1E-11 1E-10 1E-09 1E-08 1E-07 1E-06 1E-05 0.0001

Figure 3.25 Gas saturation (top) and mass fraction of gas dissolved in liquid (bottom) 710 years post-closure. (In this variant, the gas solubility is reduced to only 1% of its true value.)

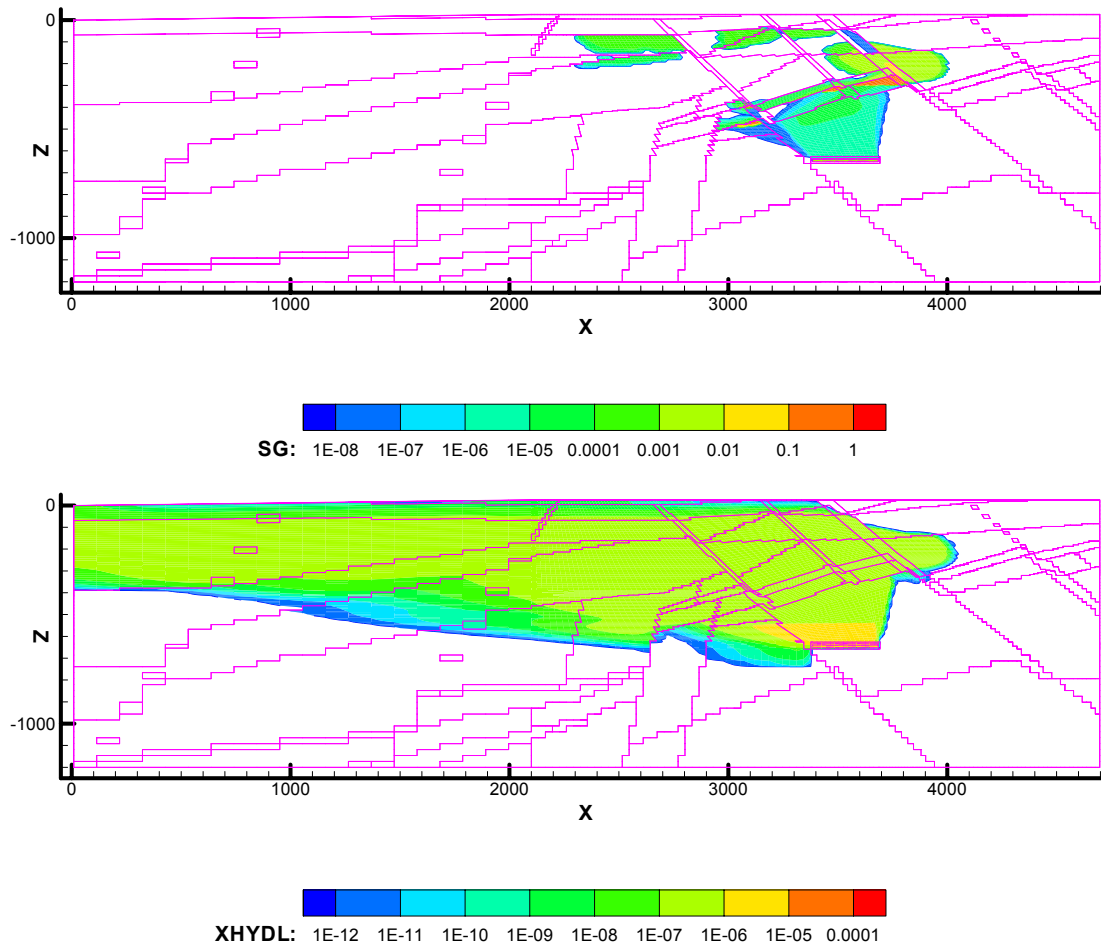


Figure 3.26 Gas saturation (top) and mass fraction of gas dissolved in liquid (bottom) 9,400 years post-closure. (In this variant, the gas solubility is reduced to only 1% of its true value.)

Figure 3.27 shows the flows of gas out of the repository as a function of time. Because Henry's constant is reduced to only 1% of its true value, little gas is able to go into solution and so the generated gas has to escape from the repository as a free gas phase.

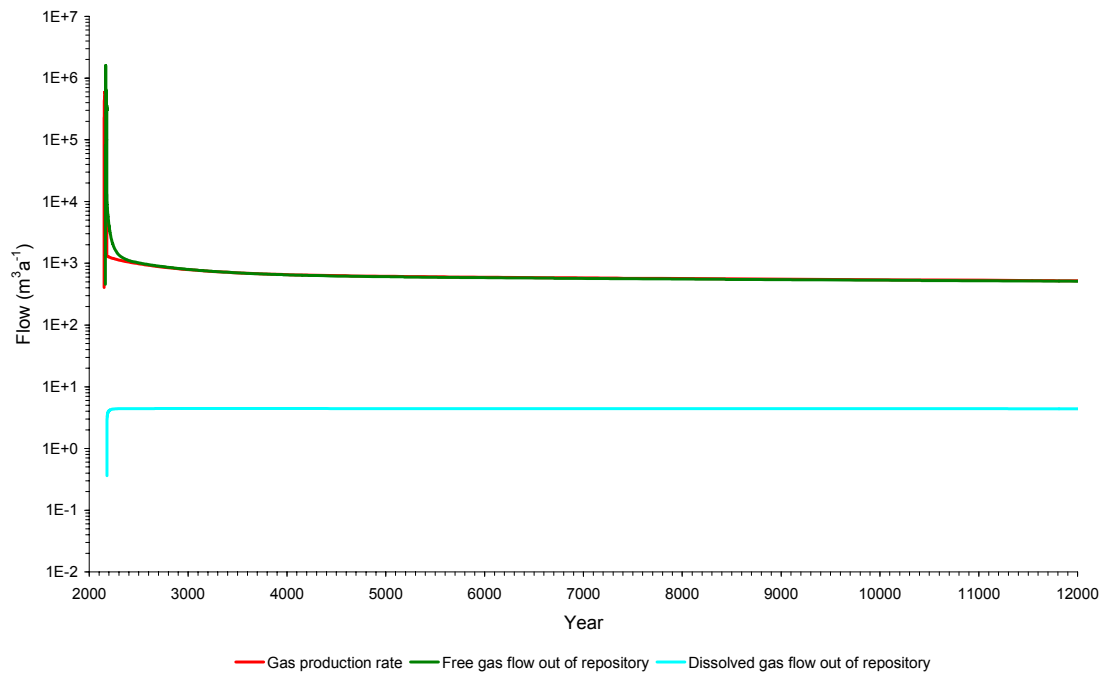
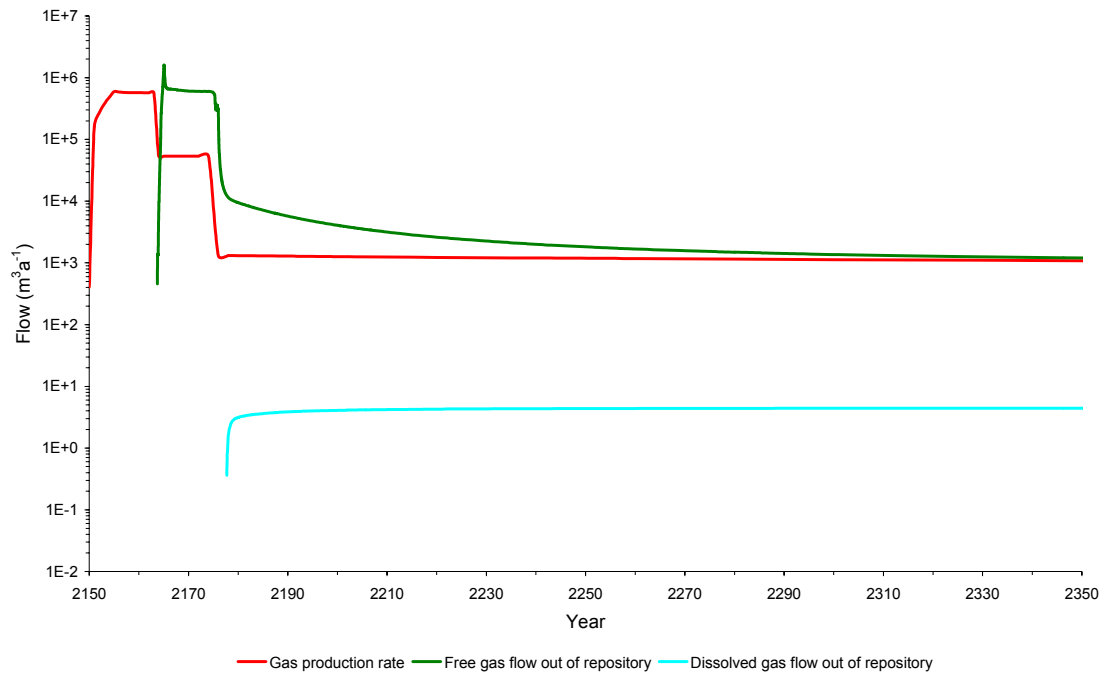


Figure 3.27 Flows of gas out of the repository as a function of time. (In this variant, the gas solubility is reduced to only 1% of its true value.)

The gas then migrates through the geosphere and flows out across the boundaries of the model, either as free gas (Figure 3.28) or as dissolved gas (Figure 3.29).

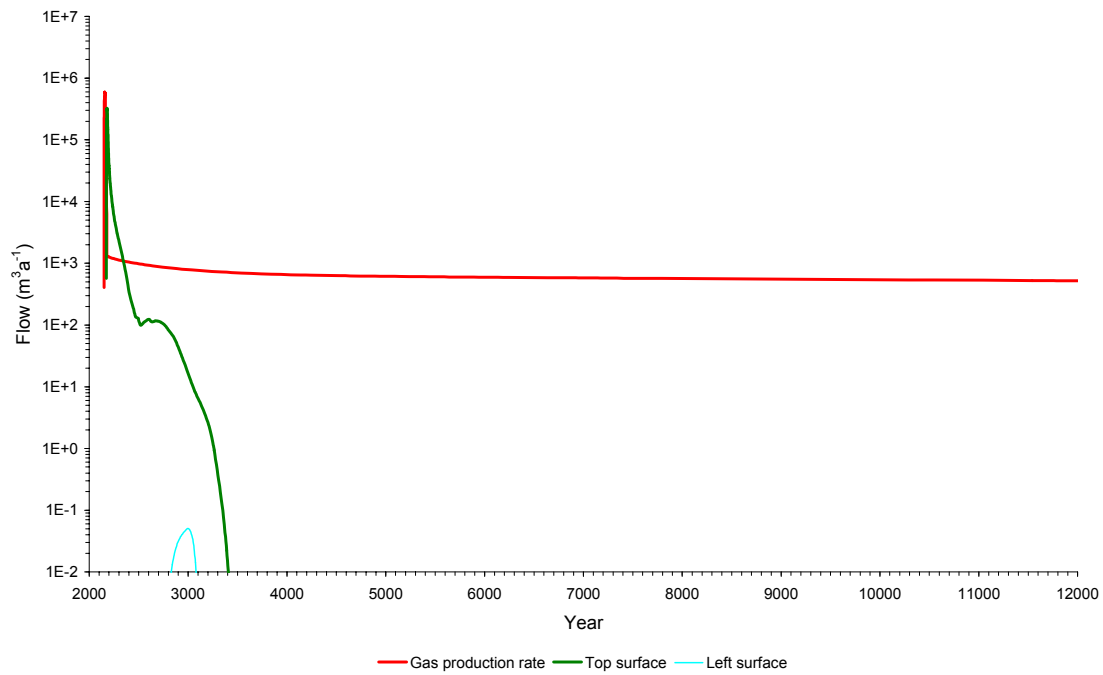
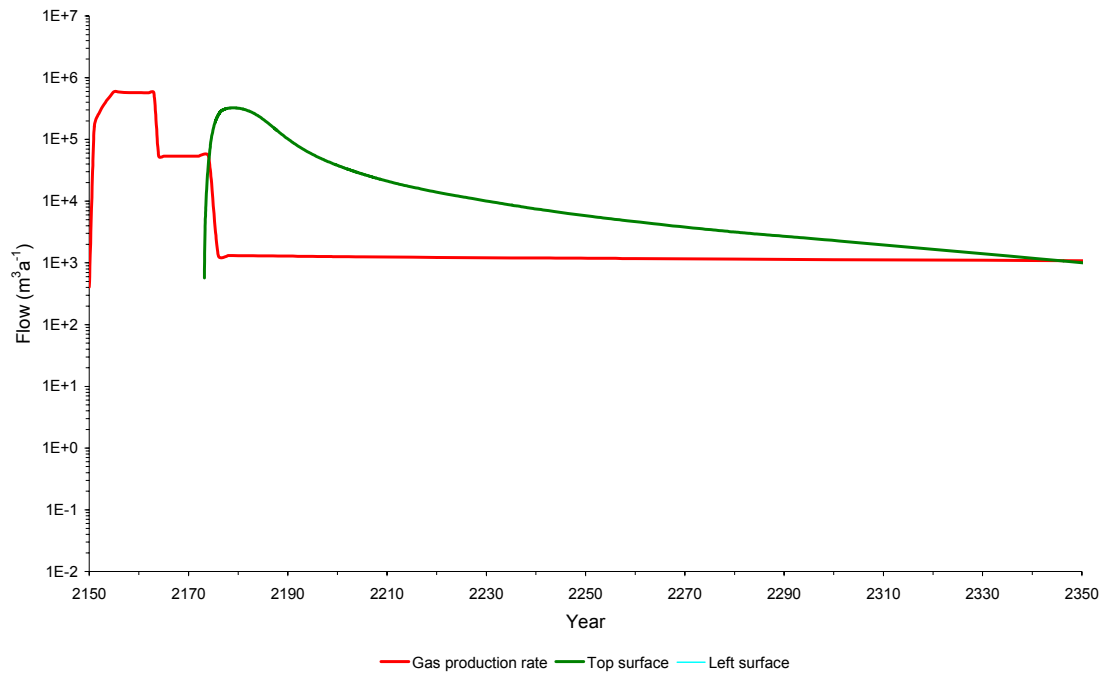


Figure 3.28 Flows of free gas across the boundary of the model as a function of time. (In this variant, the gas solubility is reduced to only 1% of its true value.)

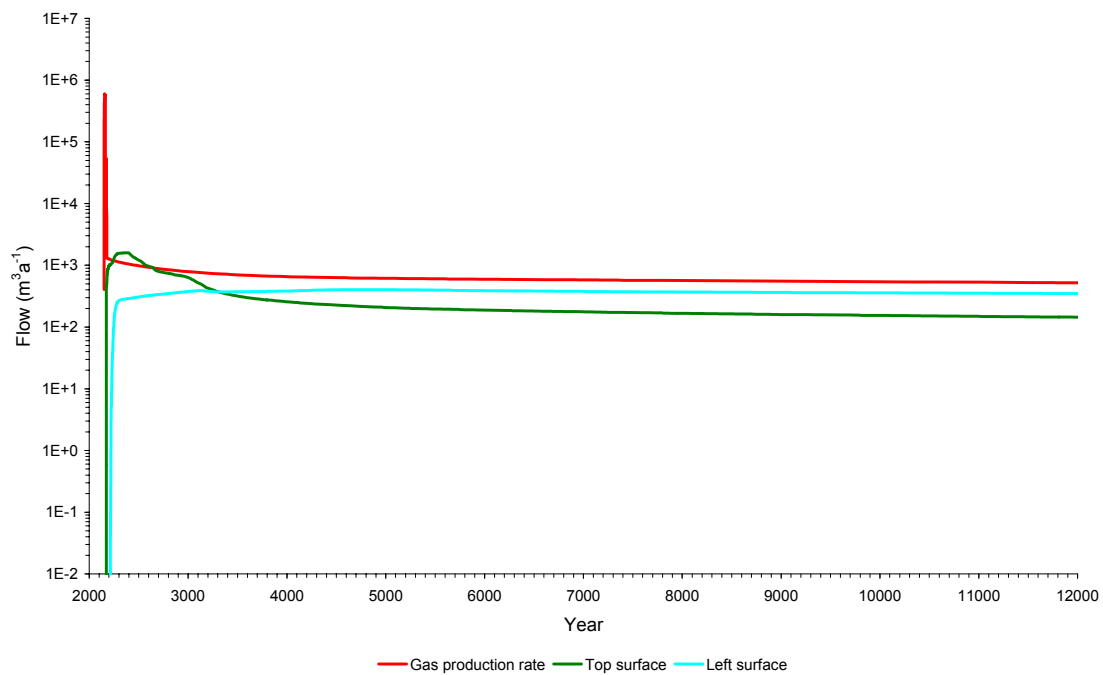
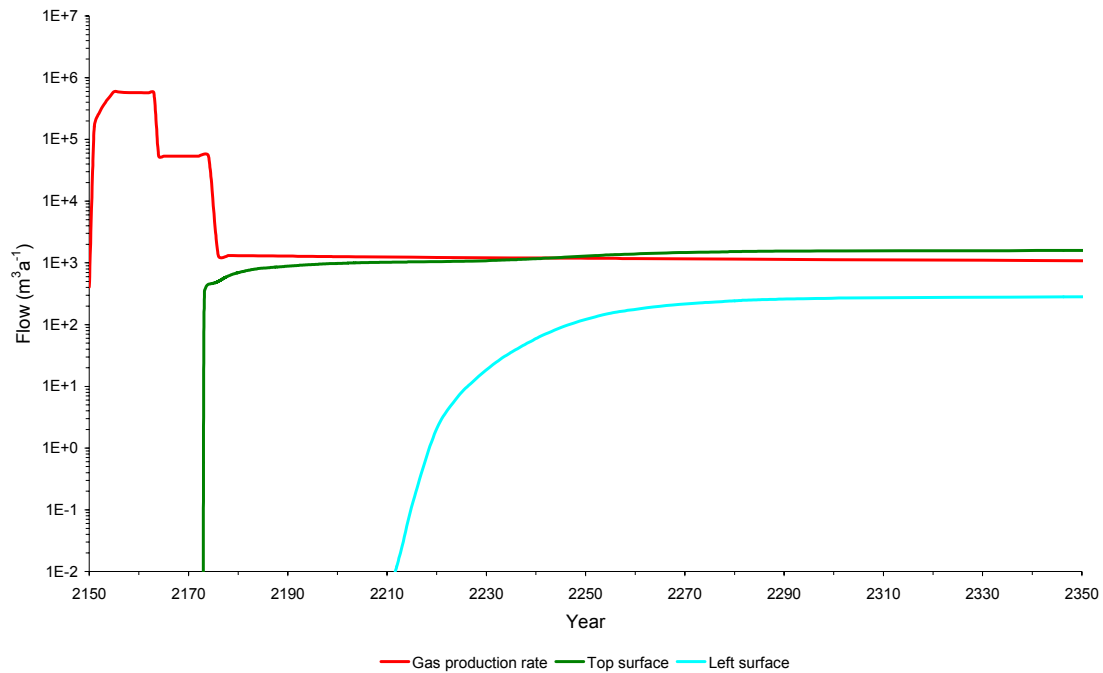


Figure 3.29 Flows of dissolved gas across the boundary of the model as a function of time. (In this variant, the gas solubility is reduced to only 1% of its true value.)

Gas solubility reduced to 10% of its real value

Figures 3.30–32 show the corresponding results for an intermediate variant in which Henry’s constant is reduced by just one order of magnitude.

Figure 3.30 shows the flows of gas out of the repository as a function of time. Because Henry’s constant is reduced by an order of magnitude from its true value, little gas is able to go into solution and so the generated gas escapes from the repository as a free gas phase.

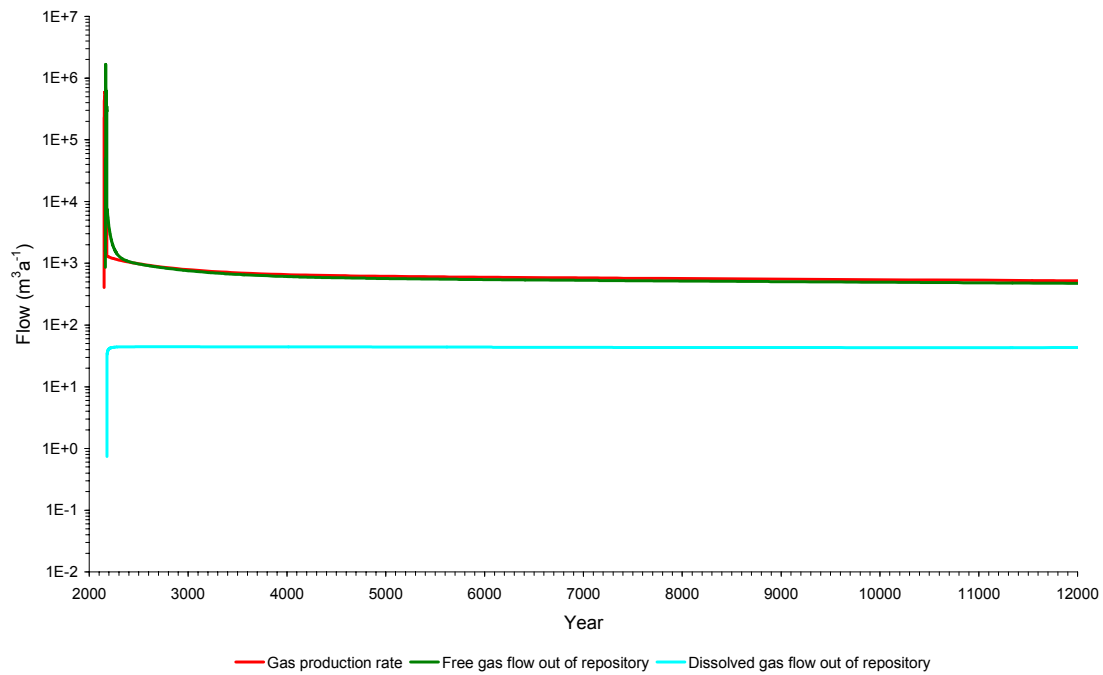
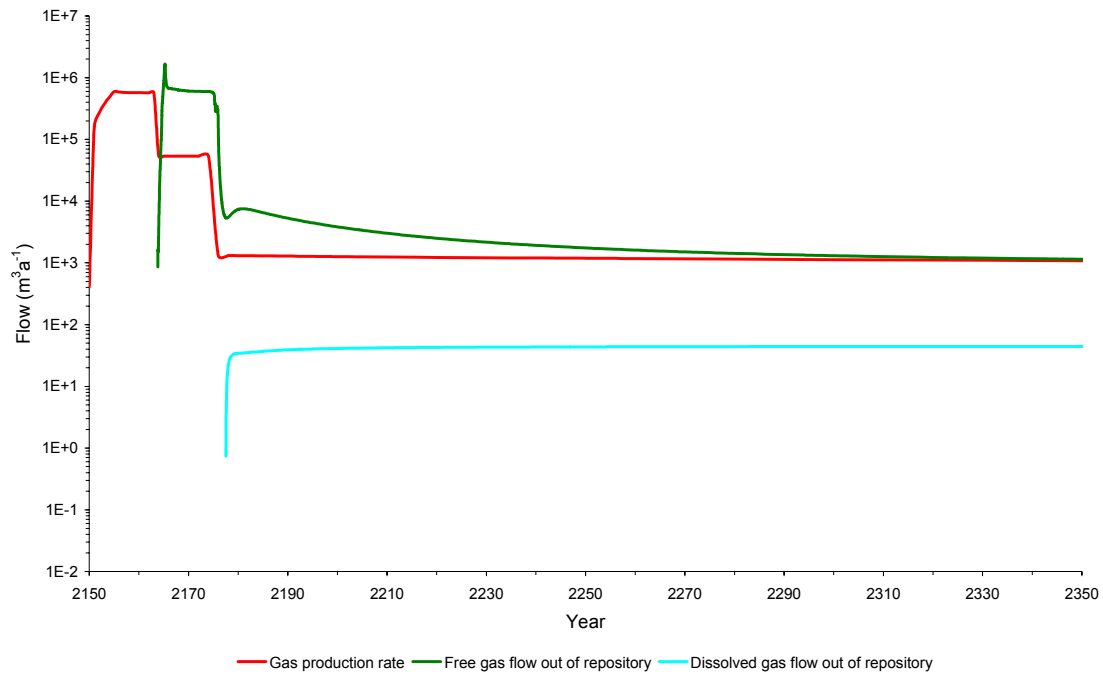


Figure 3.30 Flows of gas out of the repository as a function of time. (In this variant, the gas solubility is reduced to only 10% of its true value.)

The gas then migrates through the geosphere and flows out across the boundaries of the model, either as free gas (Figure 3.31) or as dissolved gas (Figure 3.32).

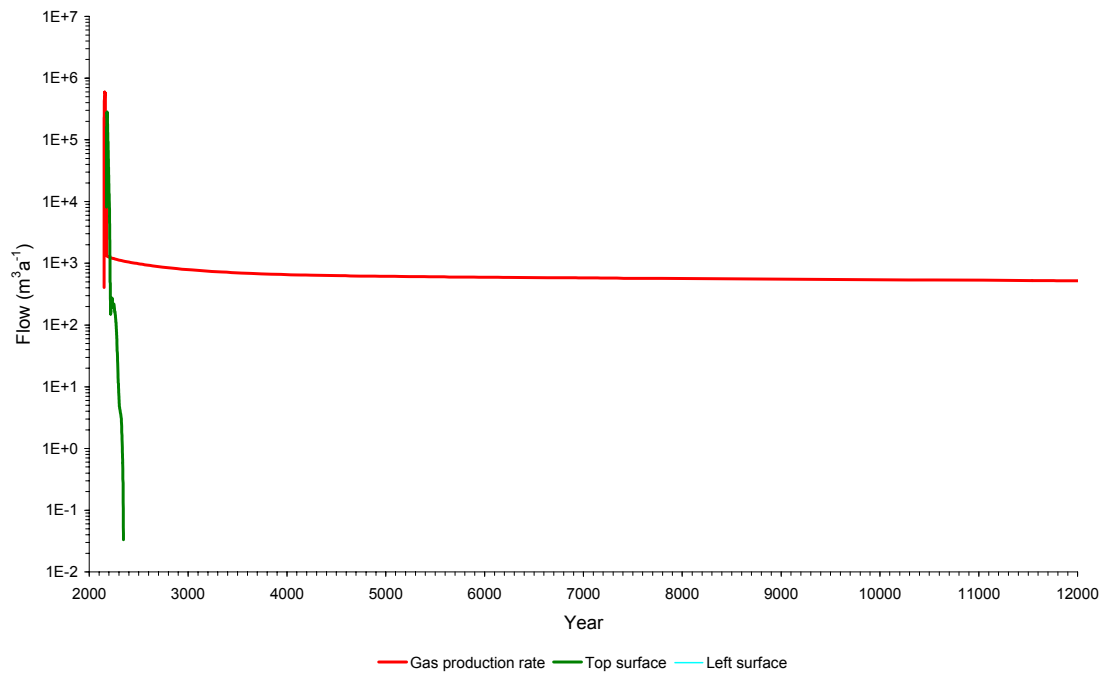
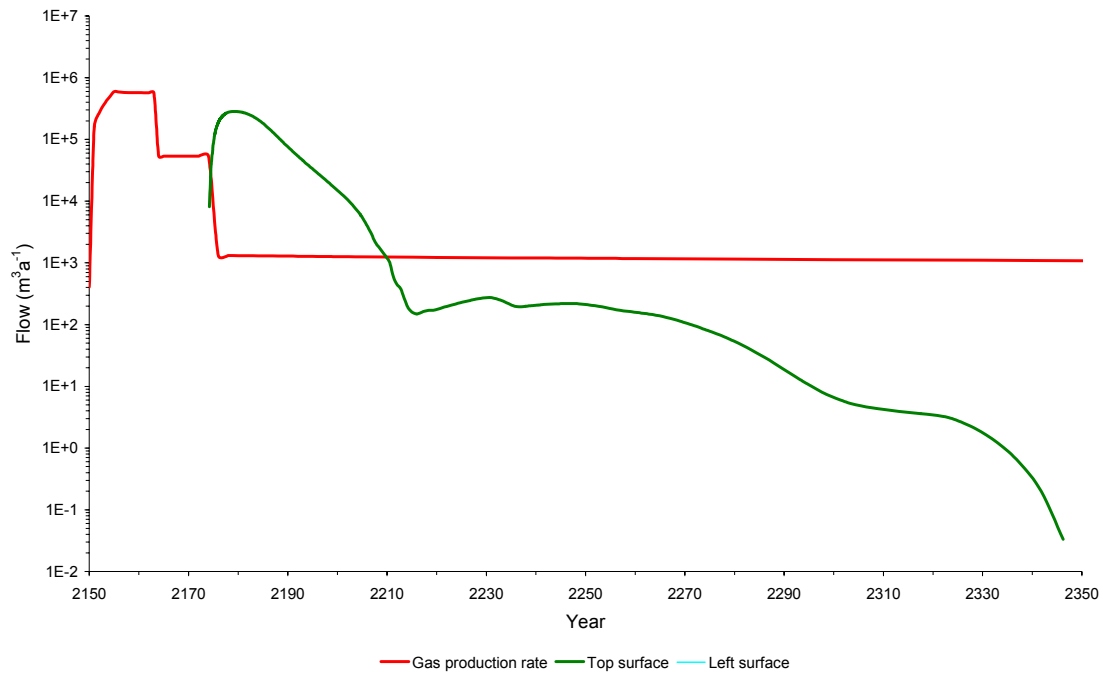


Figure 3.31 Flows of free gas across the boundary of the model as a function of time. (In this variant, the gas solubility is reduced to only 10% of its true value.)

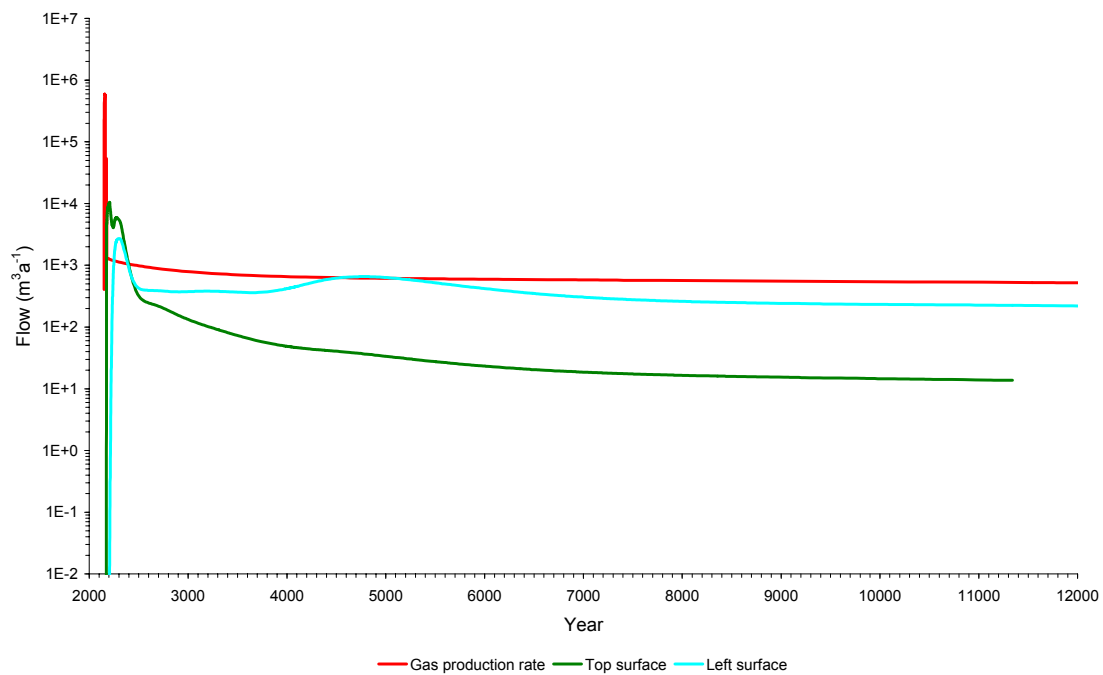
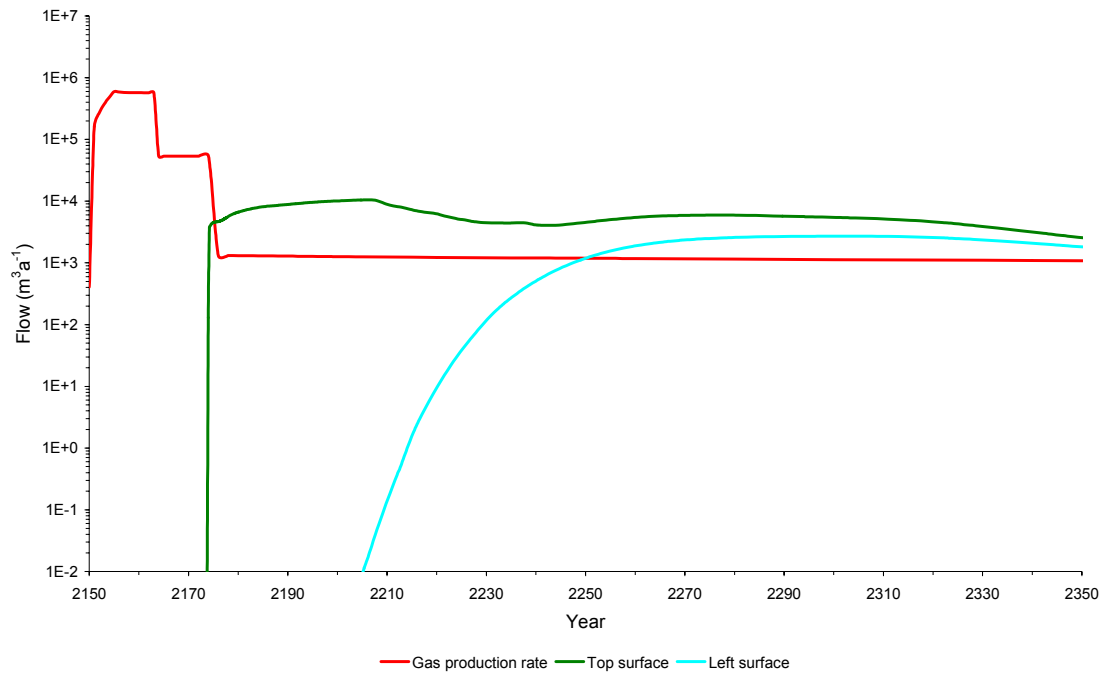


Figure 3.32 Flows of dissolved gas across the boundary of the model as a function of time. (In this variant, the gas solubility is reduced to only 10% of its true value.)

3.4 Summary of Gas Migration Calculations

Using the Reference case gas generation rate, calculations have been carried out for:

- A one-dimensional model of a generic fractured crystalline host rock;
- A one-dimensional model of a generic argillaceous host rock; and

- A two-dimensional model, based on the geology at Sellafield.

For the generic fractured crystalline host rock studied, over-pressurisation effects are predicted to be insignificant. For the argillaceous host rock, on the other hand, the pressure builds up substantially. (There is, however, uncertainty in the mechanism of gas transport in low-permeability argillaceous media, and the applicability of porous-medium flow models for simulating gas migration in these materials.)

The details of gas migration are very site-specific [16]. The path followed by free gas depends on the geometry of the various rock units and on their hydrogeological properties (e.g. permeability and saturation functions). Migrating gas will dissolve in the groundwater, and the magnitude of the groundwater flows in the more permeable rock units is important in determining whether free gas breaks through at the surface. The repository design and generation rate of gas may also play a rôle in determining whether there is breakthrough. Breakthrough does not depend linearly on these factors, but there are threshold effects.

For the specific results presented above, it is possible to make the following inferences about gas migration from the repository through the geosphere.

- Figure 3.18 suggests that a large fraction of the gas produced in the repository could dissolve in the groundwater flowing through the repository.
- Free gas might contact only part of the groundwater within the rock volume represented by a grid block. (This phenomenon is referred to as ‘viscous fingering’.) Depending on the extent to which this happens, a free gas phase could break through at the top boundary (see Figure 3.22).
 - At the time of breakthrough, the free gas flow could be larger than the gas generation rate (see Figures 3.28 and 3.31).
 - The free gas pathway could be focussed (e.g. by the presence of a fault) and so could flow across the top surface of the model through an area that is much less than that of the repository (see Figure 3.22).
 - Figures 3.23 and 3.24 suggest that a free gas pathway, if it were to form, would spread out below the top surface of the model.
 - By about 1,000 years after closure, the free gas pathway would collapse (see Figures 3.28 and 3.31).
- Thereafter, gas would migrate in solution in the groundwater (see Figures 3.16, 3.17 and 3.26).
 - Figures 3.21 and 3.32 suggest that most of the dissolved gas would flow across the left-hand boundary of the model. The left-hand boundary is at the coast, and so the flows across this surface are assumed to be discharging to sea. The flow of dissolved gas across the top boundary of the model could be substantially less than the gas generation rate.
 - Any dissolved gas that flows across the top surface of the model could be released over most of the area between the repository and the coast (see Figures 3.21 and 3.32).
- Work reported in Section 3.3.5 indicates that the Basal North Head unit could act as a low permeability barrier and that it could have a significant effect on gas migration and hence the consequences of repository-derived gas. Although this is a conclusion that can only be drawn in association with the Sellafield dataset used in this study, it emphasises a more general point: certain geosphere strata could affect gas migration, in a site-specific scenario, to a greater or lesser extent than other geosphere strata (this is relevant both to the geological disposal facility host rock and to the overburden). For strata that are considered key with regard to effects on gas migration, it is important that this is explicitly recognised in the development of a site-specific safety case, and that appropriate co-ordinated research, assessment and site characterisation studies focus on

developing an enhanced understanding of the properties of such strata in order to better understand how associated gas migration could occur. This includes the implementation of a methodical and systematic treatment of uncertainty regarding the properties of such strata, a process which should aim to identify key properties and processes, to which prioritised effort can subsequently be applied so as to reduce related uncertainties and develop a more robust understanding of strata-specific gas migration.

- Work reported in [26] considers the above points for a genericised version of the Sellafield dataset used in the current study, whereby a low permeability inclined layer can be taken as an analogue for the Basal North Head unit. Key considerations are noted in [26] to be the potential for gas migrating from depth to leak into this low permeability unit, the potential impact of capillary forces in retarding this migration, and the potential effects of a fault cutting this unit which can draw off a significant fraction of the migrating plume of free gas.

4 Conclusions

This report considers the generation of gases from waste emplaced in a deep geological disposal facility, and the consequences of such repository-derived gas. Uncertainty in gas generation and gas migration are scoped in a reference case and variant scenarios, addressing some (but not all) of the strategies for handling uncertainty noted in Section 1.1. It is noted that the treatment of uncertainty in groundwater pathway assessment studies is generally at a more mature position than the treatment of uncertainty in the assessment of the consequences of repository-derived gas. Studies such as this are therefore part of a staged approach to further develop understanding regarding the treatment of uncertainty for gas issues in the safety case, and to identify key aspects affecting the consequences of repository-derived gas to act as a focus both for further research activities, and in any future site characterisation programme.

Uncertainty in the rate of gas generation is scoped in Section 2 by the consideration of a reference case and four variant case scenarios designed to address a range of alternative assumptions that could affect gas generation in a 'real' repository environment. These scenarios all consider UK intermediate and some low-level wastes only.

In Section 3, the reference case gas generation rate from Section 2 is used as input to a series of geosphere gas migration calculations. Calculations of repository over-pressurisation and gas surface breakthrough time for two one-dimensional (generic) geologies – one corresponding to a hard fractured host rock, the other to an argillaceous host rock – are presented. Two-dimensional gas migration modelling is also reported, for an example site-specific study. This addresses both a reference case scenario, and variant scenarios to investigate the sensitivity of model output to selected variation of input parameter.

This section discusses the outcome of Sections 2 and 3, and draws some simple conclusions that could inform future assessment, research and any site characterisation studies. Key aspects affecting gas migration are noted - further study of these could benefit understanding of the consequences of repository-derived gas by enhancing the level of understanding, and by reducing uncertainty in, for example, parameter ranges to be considered in a subsequent assessment iterations.

4.1 Gas Generation

Uncertainty in the rate of gas generation has been scoped by the consideration of a reference case and four variant case scenarios designed to address a range of alternative assumptions that could affect gas generation in a 'real' repository environment. These scenarios all consider UK intermediate and some low-level wastes only.

For the different variant calculations considered, typically:

- The generation rates of both bulk and active gases have short-lived peaks due to corrosion of the reactive metals (i.e. aluminium, Magnox and uranium).
- The peak generation rate of bulk gas is about $10^6 \text{ m}^3 \text{ a}^{-1}$ at STP.
- The peak generation rates of ^3H and $^{14}\text{CH}_4$ are about 10 TBq a^{-1} .
- The long-term generation rate of bulk gas is dominated by corrosion of steel in the repository, and is in the range $10^2 - 10^3 \text{ m}^3 \text{ a}^{-1}$ at STP. The generation rate from the UILW vaults is larger than the generation rate from the SILW vaults.
- Diffusion of tritium from the steels in the waste is the dominant process for releasing this active gas.
- After the reactive metals are all corroded, corrosion of steel becomes an important source of ^{14}C in methane. In the case of the SILW/LLW vaults, ^{14}C in methane is also released as a result of the degradation of graphite.

- The rate of production of ^{222}Rn within the wastefrom can be calculated readily from the activity of ^{226}Ra present. However, the radiological consequences arising from ^{222}Rn generated in the repository are insignificant because of the short half-life of this radionuclide. The dose from ^{222}Rn arises from radon that is 'stripped' from the Quaternary sediments rather than from radon that originates in the repository.

4.2 Gas Migration

Using the Reference case gas generation rate, calculations were carried out for:

- A one-dimensional model of a generic fractured crystalline host rock;
- A one-dimensional model of a generic argillaceous host rock; and
- A two-dimensional model, based on the geology at Sellafield.

For the generic fractured crystalline host rock studied, over-pressurisation effects are predicted to be insignificant. For the argillaceous host rock, on the other hand, the pressure builds up substantially. (There is, however, uncertainty in the mechanism of gas transport in low-permeability argillaceous media, and the applicability of porous-medium flow models for simulating gas migration in these materials.)

The details of gas migration are very site-specific [16]. The path followed by free gas depends on the geometry of the various rock units and on their hydrogeological properties (e.g. permeability and saturation functions). Migrating gas will dissolve in the groundwater, and the magnitude of the groundwater flows in the more permeable rock units is important in determining whether free gas breaks through at the surface. The repository design and generation rate of gas may also play a role in determining whether there is breakthrough. Breakthrough does not depend linearly on these factors, but there are threshold effects.

In the two-dimensional model, the behaviour of the gas pathway depends on a number of assumptions. Perhaps the most important of the assumptions is the extent to which free gas will contact the groundwater within the rock volume represented by a grid block (i.e. the extent of 'viscous fingering'). If it is assumed that there is minimal contact (i.e. simulated by reducing the gas solubility to only 1% of its true value), then a free gas pathway forms. The effect of the geosphere is to introduce a time lag in, but not a reduction in the magnitude of, the initial release rate of gas compared with the release assuming instantaneous transport through the geosphere. Eventually, the free gas pathway collapses, to be replaced by dissolved gas migrating in the groundwater. If it is assumed that the free gas which migrates into a grid block contacts all of the groundwater within the grid block, then no free gas is released at the surface of the model. Only gas dissolved in the groundwater is discharged to the biosphere. The travel time for this case is longer than for the free gas pathway.

4.3 Identification of Key Processes and Model Parameters Affecting the Consequences of Repository-derived Gas

On the basis of work reported in this study, the following are recommended to be the key processes / key model parameters affecting the consequences of repository-derived gas that should be further investigated, and should be a significant focus of any future site characterisation programme. Undertaking such a programme of work would assist both in the development of understanding of gas-related processes and the reduction in associated uncertainties, and would form part of a structured programme regarding the treatment of uncertainty for gas-related phenomena and an input to the development of a safety case.

Note that these recommendations are made on the basis of this study, which itself has significant focus on the Sellafield dataset; such a study would therefore need to be repeated on a site-specific basis, as the site-specific key processes / key model parameters could differ from those noted in this study.

- The details of gas migration are very site-specific, and the path followed by free gas depends on the geometry of the various rock units and on their hydrogeological properties (e.g. permeability and saturation functions).
- Certain geosphere strata could affect gas migration, in a site-specific scenario, to a greater or lesser extent than other geosphere strata (this is relevant both to the geological disposal facility host rock and to the overburden). For strata that are considered key with regard to effects on gas migration, it is important that this is explicitly recognised in the development of a site-specific safety case, and that appropriate co-ordinated research, assessment and site characterisation studies focus on developing an enhanced understanding of the properties of such strata in order to better understand how associated gas migration could occur.
- Low permeability units may have a significant effect on site-specific gas migration. Key uncertainties to be addressed could consider the potential for gas migrating from depth to leak into this low permeability unit, the potential impact of capillary forces in retarding this migration, and the potential effects of a fault cutting this unit which can draw off a significant fraction of the migrating plume of free gas.
- Migrating gas will dissolve in the groundwater, and the magnitude of the groundwater flows in the more permeable rock units is important in determining whether free gas breaks through at the surface.
- In the two-dimensional models reported in Section 3, the behaviour of the gas pathway depends on a number of assumptions. On the basis of this study, the most important of the assumptions is suggested to be the extent to which free gas will contact the groundwater within the rock volume represented by a grid block (i.e. the extent of 'viscous fingering').
 - If it is assumed that there is minimal contact (i.e. simulated by reducing the gas solubility to only 1% of its true value), then a free gas pathway forms. In this model:
 - The effect of the presence of the geosphere is to introduce a time lag in, but not a reduction in the magnitude of, the initial release rate of gas compared with the release assuming instantaneous transport through the geosphere.
 - Eventually, the free gas pathway collapses, to be replaced by dissolved gas migrating in the groundwater.
 - If it is assumed that the free gas which migrates into a grid block contacts all of the groundwater within the grid block, then no free gas is released at the surface of the model. Only gas dissolved in the groundwater is discharged to the biosphere. The travel time for this case is longer than for the free gas pathway.
- The repository design and generation rate of gas may also play a role in determining whether there is breakthrough of free gas at the surface. Breakthrough does not depend linearly on these factors, but there are threshold effects.

5 References

- 1 Nirex, *Handling Uncertainty in the Phased Geological Repository Concept*, Nirex Technical Note, 2005.
- 2 L.D. Phillips & S.J. Wisbey, *The Elicitation of Judgmental Probability Distributions from Groups of Experts: A Description of the Methodology and Records of Seven Formal Elicitation Sessions held in 1991 and 1992*, Nirex Report NSS/B101, 1993.
- 3 Nirex, *Nirex 97: An Assessment of the Post-closure Performance of a Deep Waste Repository at Sellafield*, Nirex Science Report S/97/012, 1997.
- 4 B.T. Swift and W.R. Rodwell, *Specification for SMOGG Version 5.0: a Simplified Model of Gas Generation from Radioactive Wastes*, Serco Assurance Report SA/ENV-0452 (Version 6), 2006.
- 5 B.T. Swift, *SMOGG (Version 5.0), a Simplified Model of Gas Generation from Radioactive Wastes: User Guide*, Serco Assurance Report SA/ENV-0511 (Version 6), 2006.
- 6 *Generic Repository Studies. Generic Post-closure Performance Assessment*, Nirex Report N/080, 2003.
- 7 W.R. Rodwell and B.T. Swift, *Estimation of the Release of Radon from 500 Litre Drums of Grout-encapsulated Intermediate-level Nuclear Waste*, Serco Assurance Report Serco/ERRA-0374, Issue 2, 2003.
- 8 A.R. Hoch, S. Norris, B.T. Swift and M.M. Askarieh, *Comparison of Results from the MAGGAS and SMOGG Gas Generation Models*, Serco Assurance Report SA/ENV-0802, 2006.
- 9 A.J. Baker, D.A. Lever, J.H. Rees, M.C. Thorne, C.J. Tweed, and R.S. Wikramaratna, *Nirex 97: An Assessment of the Post-Closure Performance of a Deep Waste Repository at Sellafield, Volume 4: The Gas Pathway*, Nirex Science Report S/97/012, 1997.
- 10 J. Crank, *The Mathematics of Diffusion, Second Edition*, Oxford University Press, 1975.
- 11 A.R. Hoch and W.R. Rodwell, *Some Consequences of Gas Generation in a Nirex Repository: Estimates for the Generic Documents Update, 2003*, Serco Assurance Report SA/ENV-0542, 2003.
- 12 K. Pruess, *TOUGH User's Guide*, Nuclear Regulatory Commission Report NUREG/CR-4645 (also Lawrence Berkeley Laboratory Report LBL-20700), 1987.
- 13 K. Pruess, *TOUGH2 – A General Purpose Numerical Simulator for Multiphase Fluid and Heat Flow*, Lawrence Berkeley Laboratory Report LBL-29400, 1991.
- 14 K. Pruess, C. Oldenburg and G. Moridis, *TOUGH2 User's Guide – Version 2.0*, Lawrence Berkeley National Laboratory Report LBNL-43134, 1999.
- 15 *Generic Post-Closure Performance Assessment*, Nirex Report N/031, 2001.
- 16 F. Bate, A.R. Hoch and C.P. Jackson, *Gas Migration Calculations*, Serco Assurance Report SA/ENV-0850, Issue 2, 2006.
- 17 W.R. Rodwell, A.W. Harris, S.T. Horseman, P. Lalieux, W. Müller, L. Ortiz Amaya, and K. Pruess, *Gas Migration and Two-phase Flow through Engineered and Geological Barriers for a Deep Repository for Radioactive Waste. A Joint EC/NEA Status Report*, European Commission Report EUR 19122 EN, 1999.
- 18 C.P. Jackson and S. Watson, *Nirex 97: An Assessment of the Post-Closure Performance of a Deep Waste Repository at Sellafield, Volume 2: Hydrogeological Model Development – Effective Parameters and Calibration*, Nirex Science Report S/97/012, 1997.
- 19 L. Wei, *Evaluation of the RCF3 Pump Test Predictions and Assessment of Model F*, Golder Report 95524800/500, 1996.
- 20 R.H. Brooks, and A.T. Corey, *Hydraulic Properties of Porous Media*, Colorado State University, Hydrogeology Papers, Fort Collins, Colorado, 1964.
- 21 F. Franks, *Water, a Matrix of Life*, 2nd ed., The Royal Society of Chemistry, 2000.
- 22 E.L. Cussler, *Diffusion – Mass Transfer in Fluid Systems*, Cambridge University Press, 1984.

-
- 23 T.R. Marrero and E.A. Mason, *Gaseous Diffusion Coefficients*, Journal of Physical and Chemical Reference Data, vol. 1, nos. 1, pp. 3–118, 1972.
- 24 R.B. Bird, W.E. Stewart and E.N. Lightfoot, *Transport Phenomena*, John Wiley & Sons, 1960.
- 25 A.W. Harris and A.K. Nickerson, *The Mass-transport Properties of Cementitious Materials for Radioactive Waste Repository Construction*, Nirex Report NSS/R309, 1995.
- 26 *On Gas Migration Beneath a Dipping Low Permeability Horizon with Leakage*, Andrew Woods & Adrian Farcas, Report to NDA, BP Institute for Multiphase Flow, University of Cambridge, November 2007.